PROPERTIES AND APPLICATIONS OF ELECTROSPUN FIBERS

A Dissertation

Presented to the Faculty of the Graduate School

of Cornell University

In Partial Fulfillment of the Requirements for the Degree of

Doctor of Philosophy

by

Leon Marcel Bellan

August 2008

PROPERTIES AND APPLICATIONS OF ELECTROSPUN FIBERS

Leon Marcel Bellan, Ph. D.

Cornell University 2008

Electrospinning is the process by which an electrically forced elongational fluid jet produces solid fibers. The strong elongational flow in the jet can induce a significant degree of molecular orientation in the resulting fibers, and can also be used to orient and stretch isolated molecules and particles embedded within the jet and resulting fibers. After a brief introduction to electrospinning, I begin with a description of the direct measurement of the velocity profile in an electrospinning jet using particle image velocimetry, and then discuss measurement of the molecular orientation in individual electrospun fibers using polarized Raman micro-spectroscopy. Individual suspended fibers were also characterized using atomic force microscopy to measure their Young's moduli. I then discuss applications of electrospinning, including the use of electrospinning jets to stretch and embed isolated DNA molecules and the use of sacrificial electrospun fibers to produce nanochannels for fluidic applications. Finally, I conclude with novel electrospinning system designs, including a system that uses electric fields to steer an electrospinning jet and an automated electrospinning source using microfabricated nozzles for improved deposition.

BIOGRAPHICAL SKETCH

Leon Marcel Bellan was born in _____. He went to school at _____ and then obtained his undergraduate degree in _____ at _____.

ACKNOWLEDGMENTS

A multitude of people deserve recognition for their help with and support of my work. For the past several years I have been privileged to work in Prof. Harold Craighead's research group, a finely tuned machine of scientific production. Much like a mechanical machine, the group effort relies on the interactions of the many graduate students that form the workforce, each a gear turning towards a common goal. And Harold, like an expert mechanic, knows just how to oil and care for the gears, ensuring they continue to function without poking and prodding them to the point of interrupting their motion. I am grateful to have worked under his excellent supervision. I must also thank the past and current members of the Craighead group that have helped me. In particular, I want to thank Kevan Samiee, Sam Stavis, and Josh Cross for their antics (and help), Scott Verbridge, Grant Meyer for always being willing and able to answer my silly questions, Jose Moran-Mirabal for his knowledge and help with anything and everything biological, Haiqing Liu, Rob Reichenbach, and Elizabeth Strychalski for her continuous support and friendship. And then of course there is Rob Ilic, a scientific powerhouse, fabrication master, guitar expert, and generally fun guy to hang out with. I am truly lucky to have been able to spend time with Rob, learn from him, and call him my friend. I also want to thank Jeremiah Wala, an undergraduate working in the Craighead group, for his infinite enthusiasm and incredible research skills; he not only surpasses all expectations while working in the lab, but he is also one of the most pleasant people I've worked with.

Outside of the Craighead group, I have had many friends and collaborators who have helped me. My housemates Jacob "Jacon" Robinson and Mike Durst have been not only excellent resources for discussing work, but excellent friends who have made the often difficult road that is graduate life significantly more enjoyable. The

rest of the AEP graduate students, the APES softball team, and everyone else I know outside of the department have also contributed to my continued sanity, and I am grateful for their friendships and help. In particular, I want to thank Christopher "Kit" Umbach, Jeevak Parpia, Margaret Frey, Juan Hinestroza, Geoff Coates, Lynden Archer, Malcolm "Mick" Thomas, John Grazul, John Hunt, and the NBTC, CCMR, and CNF staff.

I am lucky to have parents willing and able to both support and advise me in my work, and I thank them for their help. I also want to thank Lynn Salmon, Glen Cass, Peter Mao, Florian Gstrein, and James Hone for their support in my early research years. Finally, I want to thank my funding sources for providing the money I get to spend on new toys; in particular I acknowledge the Cornell Nanobiotechnology Center (NBTC), a STC Program of the National Science Foundation under Agreement No. ECS- 9876771, the Cornell Center for Materials Research supported by the National Science Foundation under Award Number DMR- 0520404, 9632275 and 0079992, the National Science Foundation Grant No. HRD-0630456, the Cornell Nano-Scale Science & Technology Facility (a member of the National Nanofabrication Users Network) supported by the National Science Foundation under Grant ECS-9731293.

TABLE OF CONTENTS

LIST OF FIGURES

LIST OF TABLES

CHAPTER 1

ELECTROSPINNING OVERVIEW

Historical overview

Though the process of electrically forcing a fluid jet to make fibers, known as electrospinning, has been recognized for over 70 years, its popularity has started to increase only in the last two decades, likely due to the increased interest in nanotechnology. In 1917 Zeleny performed observational studies on the instability of electrified droplets.[1] The next relevant investigation was performed by Sir Geoffrey Taylor in the 1960s, who published articles relating to the conical shape taken by a liquid droplet to which an electric potential is applied (now known as a "Taylor cone") as well as the fluid jets expelled by electrified liquids.[2, 3] In his work, Taylor noted several intriguing instabilities of these jets; the theoretical treatment of the flow in these jets and their various instabilities is still a subject of research today. The first officially documented case of electrospinning can be found in a patent by Anton Formhals in 1934, in which he describes "an apparatus for producing artificial filaments" using "the action of an electrical field upon liquids containing solid materials dissolved in them."[4] Other early work in the field of electrospinning includes work by Baumgarten on the electrospinning of acrylic fibers[5] and by Larrondo and Manley on the electrospinning of polymer melts.[6-8]

Overview of the electrospinning process

In a standard electrospinning process, a solution of polymer dissolved in solvent is supplied to a metallic needle held a distance from a grounded collecting substrate. The solution forms a droplet at the end of the needle. Upon application of a high voltage to the needle, the droplet forms a Taylor cone under the influence of the electric field. If the voltage is increased to the point where the cone becomes unstable,

an elongational fluid jet emerges from the tip of the cone and is accelerated towards the grounded substrate. As the jet moves towards the grounded collecting substrate, it thins due to stretching and solvent evaporation. As the solvent evaporates, the fluid jet solidifies into a polymer fiber, which is deposited on the substrate. Several instabilities may arise in the jet, such as pulsing at the cone, axisymmetric breakup of the jet (Rayleigh instability), and the bending (or whipping) instability. The electrospinning process is illustrated in Figure 1.1.

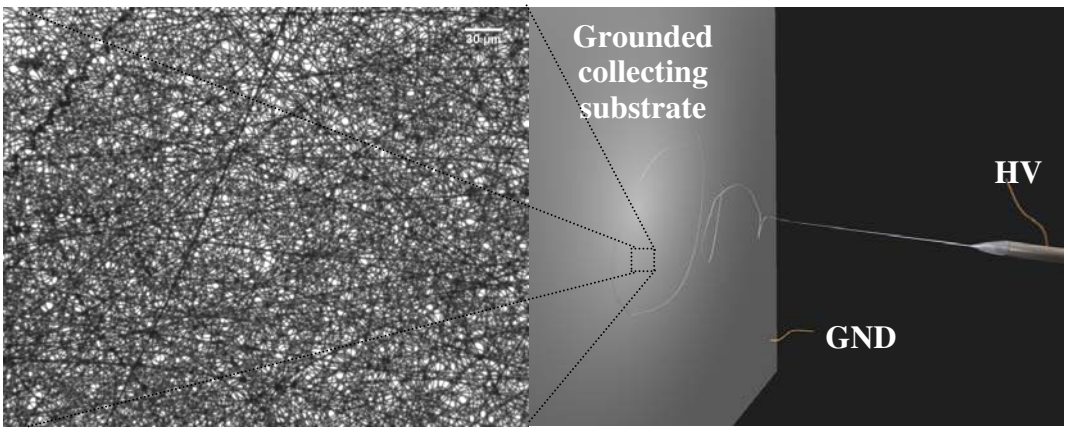

Figure 1.1- Illustration of a standard electrospinning system. A typical fiber mat is shown on the left.

Theoretical treatments of electrospinning jets

While others (including Rayleigh)[9, 10] had investigated the behavior of electrified liquid drops before him, Sir Geoffrey Taylor is often credited with the initial attempts to treat such systems theoretically.[2] In his work in 1964, Taylor presents an argument as to the critical angle formed by an electrified droplet, the Taylor cone. Taylor assumes a conducting fluid and thus that the surface of the cone must be at an equipotential. Furthermore, he argues that the force provided by the electrical potential gradient must balance that of the surface tension on the cone. From

a dimensional standpoint, the stress from the surface tension should go like γ/r, and that from the electric field should go like $\varepsilon_o E^2$, where γ is the surface tension, r is the radius along the surface of the cone, ε_o is the permittivity of free space, and E is the magnitude of the electric field (a more thorough treatment can be found in the literature[11]). This implies an $r^{-1/2}$ dependence to the electric field, and thus the electric potential can be written in a general form as

$$V = V_o + Ar^{1/2} P_{1/2}(\cos\theta) \tag{1.1}$$

where V is the electric potential, A is a constant, and $P_{1/2}(\cos\theta)$ is the Legendre polynomial of order ½ of the cosine of the exterior angle of the cone, θ. However, since the surface is an equipotential, V must be constant, and thus the requirement $P_{1/2}(\cos\theta_0)=0$ must hold. This is true for $\theta_0=130.71°$, yielding an interior opening angle of 98.57°, and a half angle of $\alpha=49.29°$. This is the angle that is commonly associated with a Taylor cone, illustrated in Figure 1.2. This conclusion, however, relies upon several assumptions, and recent work has provided more in-depth theoretical treatments of the shape of the electrified droplet and yielded the possibility of other opening angles. [12] Taylor also investigated the critical potential at which a droplet will begin to jet, using the drop stability condition provided by Rayleigh,[9, 10] $V < 4\sqrt{(\pi R_o \gamma)}$, where V is the potential of the drop, R_o is the initial radius of the drop, and γ is the surface tension of the drop.[2, 3]

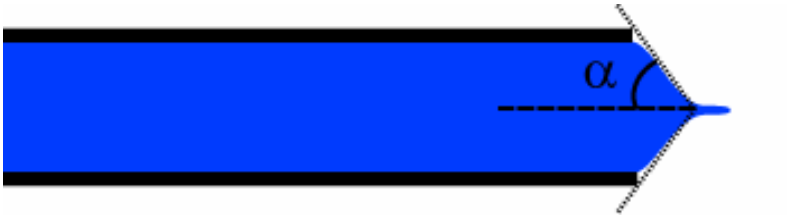

Figure 1.2- Illustration of Taylor cone.

Recent studies have attempted to derive theoretical models to predict the shape and velocity profile of electrospinning jets.[13-18] The derivation below is a simplified summary of that provided by Hohman et al.[13, 14] for Newtonian fluids. In this simplification, the only variables are the axial velocity, the jet radius, the electric field, and the surface charge density. The first equation given is a conservation of mass equation, which can be written as

$$\partial_t(\rho\pi h^2) = -\partial_z(\rho\pi h^2 v) \tag{1.2}$$

where ρ is the fluid density, $h(z)$ is the radius of the jet at an axial distance z and $v(z)$ is the axial velocity of the jet at z. The volume flow rate Q is $\pi h^2 v$. While many models assume that mass must be conserved in the system, this does not accurately reflect most electrospinning jets because a significant amount of solvent evaporates in flight. Yarin et al. show that this process dramatically alters the behavior of the jet,[19] and show that the model that accounts for evaporation agrees with experimental data much better than more simplistic models. In Chapter 3 the reader can find some discussion on direct measurements of fluid velocity in an electrospinning jet and how these measurements can indicate where along the jet solvent evaporation is significant. The charge in the system is assumed to exist mainly on the jet surface, and the conservation of charge equation is

$$\partial_t(2\pi h\sigma) = -\partial_z(2\pi h\sigma v + \pi h^2 K E_z) \tag{1.3}$$

where $\sigma(z)$ is the surface charge density, K is the fluid electrical conductivity, and $E_z(z)$ is the electric field in the axial direction. The last term is the current due to the bulk conductivity of the material. The momentum balance equation is

$$\partial_t v + \partial_z\left(\frac{v^2}{2}\right) = -\frac{1}{\rho}\partial_z p + g + \frac{2\sigma E}{\rho h} + \frac{3\mu}{\rho h^2}\partial_z(h^2\partial_z v) \tag{1.4}$$

where p is the internal pressure of the fluid, g is the acceleration of gravity, and μ is the dynamic viscosity. The third term on the right hand side is a tangential stress term

due to the electric field. The pressure is given by

$$p = \gamma \frac{R_1 + R_2}{R_1 R_2} - \frac{\varepsilon - \bar{\varepsilon}}{8\pi} E_z^2 - \frac{2\pi}{\bar{\varepsilon}} \sigma^2 \tag{1.5}$$

where R1 and R2 are the principle radii of curvature of the air-fluid interface, ε is the dielectric constant of the fluid, and $\bar{\varepsilon}$ is the dielectric constant of the surrounding medium (air). The first term is the pressure due to surface tension, the second term is the difference in axial electric field energy density across the fluid-air interface, and the last term is due to radial self-repulsion of charge on the fluid surface. The final equation necessary is the definition of the electric field,

$$E_z - \ln(\frac{1}{\chi})[\frac{\beta}{2}(h^2 E)'' - \frac{4\pi}{\bar{\varepsilon}}(h\sigma)'] = E_\infty \tag{1.6}$$

where χ is a parameter that describes the local aspect ratio of the jet, β is $(\varepsilon / \bar{\varepsilon}) - 1$ and E_∞ is the applied electric field. This relation comes from assuming an effective linear charge density on the jet $\lambda(z) = -(\beta / 4)(h^2 E)' + (2\pi h\sigma / \bar{\varepsilon})$. The reader may review Hohman et al. for a more detailed derivation of these equations and how to use them in steady-state to model the jet behavior. Theoretical treatments of the various instabilities (pulsing, Rayleigh, bending) in electrospinning jets have also been attempted.[13, 14, 19, 20]

Electrospinning technique variations

The majority of work in the field of electrospinning deals with jets of a solution of polymer dissolved in solvent that solidify in ambient air. This technique works well for polymers that are easily dissolved in volatile solvents, and can also be used to make ceramic fibers using sol gels.[21] However, there are cases when spinning from solution is either difficult or impossible and thus other techniques must be used. One popular technique is to electrospin from a melt of the desired polymer. [22, 23] In this process, a polymer melt is driven into a jet using an electric field and

the solidifying mechanism is cooling of the liquid melt into a solid fiber. Larrondo and Manley used this technique to produce relatively large (~100 micron diameter) fibers from polyethylene (PE) and polypropylene (PP).[6] More recent work by Lyons et al. has demonstrated melt electrospinning of PP fibers ranging from several hundred nanometers to several hundred microns in diameter, depending on the particular PP used.[24] In another variation, wet electrospinning, a solution is electrospun into a coagulant bath.[25-27] This technique can be used when the solvent required to dissolve the polymer is not volatile enough to fully evaporate before the jet is collected.

There are cases when it is difficult to either dissolve or melt the polymer of interest so that it can be processed. Such polymers are often processed while a polymerization reaction occurs using techniques such as reaction injection molding (RIM). The idea of using a chemical reaction to solidify the material of interest has been applied to electrospinning processes as well. Photo-induced polymerization can be used to solidify an appropriately chosen monomer/catalyst system.[28, 29] The thermoset polymer polydicyclopentadiene (PDCPD), typically shaped via RIM, was used to produce submicron fibers by electrospinning an appropriate monomer/catalyst mixture.[30]

Due to the bending instability, a typical electrospinning jet deposits fibers in a random mat. There are several application-specific reasons one might desire that the fibers be deposited in a more controlled fashion, so several techniques for influencing the layout of the fiber deposition have been developed; these can generally be grouped in two categories: mechanical and electrical.

Controlled deposition of electrospun fibers using mechanical motion is hindered by the fact that electrospinning jets typically travel at rather large velocities, approximately 1-10 m/sec. To collect straight fibers, the relative velocity between the

tip and collecting substrate must be at essentially the same velocity as the jet, or the fibers will bunch up. It is relatively straightforward to achieve linear velocities of 1-10 m/sec using rotational motion; this idea has been exploited in a variety of geometries to obtain uniaxially aligned fibers.[31-35] Another method to produce aligned bundles of fibers is to quickly oscillate the collecting substrate through the electrospinning jet.[36] However, using rotational motion or oscillatory linear motion it is only possible to control the orientation of the deposited fibers. Recently, Sun et al. developed a "near-field" electrospinning technique that allows the electrospinning jet to travel only a short distance (<1cm) before it encounters the collecting substrate.[37] The jet is accelerated for only a short time, and the jet velocity at the collecting position is low and thus standard XY linear stages can be used to move the sample and collect straight fibers.

Because the electrospinning jet is charged, it is also possible to exert some control over the deposition process using electric fields. Typically, a single grounded conducting substrate is used to collect the fibers. The grounded area can be restricted in a controlled fashion using a patterned electrode, and this causes the fibers to accumulate only on the grounded electrode, allowing patterning of the random fiber mat.[38] If two conducting collecting electrodes separated by an insulating gap are used, the jet will dance between the electrodes and produce a uniaxially aligned array of fibers.[39, 40] Utilizing an insulating substrate on which grounded metallic electrodes had been patterned, Li et al. used this effect to fabricate various geometries of electrodes connected by arrays of electrospun poly(vinyl pyrrolidone) (PVP) nanofibers.[41] Other collection techniques that rely on such behavior have been devised, such as the use of dual ring electrodes to collect a uniaxially aligned array of fibers that can be subsequently twisted into a length of yarn.[42] Another approach to manipulate the deposition of electrospun fibers is to control the electric field using

external electrodes between the tip and collecting substrate. Deitzel et al. used a series of circular electrodes as an electrostatic lens to confine the whipping mode of the electrospinning jet to a smaller radius.[43] Taking this idea one step further, we used several electrodes to apply a time-varying electric field to steer the electrospinning jet to "draw" individual fibers;[44] this work is described in Chapter 7.

The most basic electrospinning system uses a single metallic needle as the source to support to liquid droplet (the "spinneret" or tip). Other more complex systems have been developed. Multicomponent fibers have been produced using electrospinning systems with modified spinnerets. Coaxial fibers, which can in many cases be subsequently processed into hollow tubes, may be produced using a coaxial electrospinning spinneret, originally developed by Li and Xia.[45] This technique has been subsequently used to encapsulate a labeled protein, fluorescein isothiocyanate-conjugated bovine serum albumin (fitcBSA), with polyethylene glycol (PEG) within poly(ε-caprolactone) (PCL) nanofibers ,[46] and also in conjunction with melt electrospinning to encapsulate hydrocarbons.[47] Instead of using a coaxial geometry, Liu et al. used a side-by-side spinneret geometry to produce bicomponent TiO_2/SnO_2 nanofibers for photocatalysis.[48]

One aspect of typical electrospinning setups that limits commercialization is low mass throughput. Typical fiber-forming spinning systems operate at mass flow rates on the order of g/min. Electrospinning processes tend to operate at mass flow rates of order μg/min to mg/min. Several techniques have been developed to overcome this problem, all of which use an array of multiple electrospinning spinnerets operating in parallel. This technique is usually manifested in systems employing an array of needles fed by the same electrospinning solution;[49] however, other processes have also been demonstrated. For example, Yarin et al. applied a magnetic field to a ferrofluid to produce multiple spikes, each acting as an

electrospinning tip supporting a layer of electrified polymer solution.[50] Another technique to achieve high mass throughput using multiple jets is to immerse an electrified roller in the electrospinning solution.[51]

Applications of electrospun fibers

Several applications of electrospun fibers have been developed; these can be categorized into two groups: applications based on fiber mats and applications based on single fibers. Random mats of electrospun fibers are the easiest geometry to produce and offer many advantages over bulk material due to the high surface-to-volume ratio of the fiber mat. There is a vast body of literature discussing the use of electrospun fiber mats in filtration,[52, 53] tissue engineering,[25, 54-57] drug delivery,[58, 59] and sensing applications.[60-65]

Isolated electrospun nanofibers may be used as nanoscale devices, with chemical and electrical properties governed by the material, or as sacrificial structures for lithography. Direct deposition of functional materials is desirable because expensive and complicated multi-step lithography processes may then be avoided. Several studies have demonstrated devices based on single fibers. For example, Liu et al. deposited doped polyaniline (PANI) nanofibers over electrodes and used this device as a NH_3 sensor.[66] Due to the large surface-to-volume ratio of the fiber, the sensor was both highly sensitive and quick. Several groups have used electrospun fibers produced from semiconducting polymers such as PANI and regioregular poly-3-hexylthiophene (RR-P3HT) as the active component for a field effect transistor (FET).[67-69] Electrospun nanofibers may also be used as mechanical devices; Kamoeka et al. demonstrated a doubly-clamped beam resonator fabricated by depositing a silica nanofiber over a trench etched in silicon.[70] The suspended fiber was excited using a piezoelectric transducer and the resulting mechanical motion was

detected using an optical interferometric method. There are numerous other possibilities for using single electrospun fibers for device purposes, but in order to obtain significant device yield one must be able to controllably and reproducibly deposit fibers. Even when single-fiber control is not necessary, it may still be desirable to deposit the random mat in a particular pattern.

Electrospun fibers can also serve as lithographic masks or sacrificial layers. For example, Czaplewski et al. used electrospun poly(methyl methacrylate) (PMMA) fibers as etch masks to define nanoscale doubly-clamped beam resonators with widths of approximately 100nm (a feature size typically achievable only using expensive state-of-the-art photolithography or electron beam lithography).[71] Electrospun fibers may also be used as a sacrificial layer for defining fluidic channels both embedded in a bulk substrate and suspended over trenches.[72, 73]

REFERENCES

1. Zeleny, J., Instability of Electrified Liquid Surfaces. *Physical Review* **1917,** 10, (1), 1.

2. Taylor, G., Disintegration of Water Drops in an Electric Field. *Proceedings of the Royal Society of London. Series A, Mathematical and Physical Sciences* **1964,** 280, (1382), 383-397.

3. Taylor, G., Electrically Driven Jets. *Proceedings of the Royal Society of London. Series A, Mathematical and Physical Sciences* **1969,** 313, (1515), 453-475.

4. Formhals, A. Process and Apparatus for Preparing Artificial Threads. 1975504, 1934.

5. Baumgarten, P. K., Electrostatic Spinning Of Acrylic Microfibers. *Journal of Colloid and Interface Science* **1971,** 36, (1), 71-&.

6. Larrondo, L.; St John Manley, R., Electrostatic fiber spinning from polymer melts. I. Experimental observations on fiber formation and properties. *Journal of Polymer Science, Polymer Physics Edition* **1981,** 19, (6), 909.

7. Larrondo, L.; St John Manley, R., Electrostatic fiber spinning from polymer melts. II. Examination of the flow field in an electrically driven jet. *Journal of Polymer Science, Polymer Physics Edition* **1981,** 19, (6), 921.

8. Larrondo, L.; St John Manley, R., Electrostatic fiber spinning from polymer melts. III. Electrostatic deformation of a pendant drop of polymer melt. *Journal of Polymer Science, Polymer Physics Edition* **1981,** 19, (6), 933.

9. Peters, J. M. H., Rayleigh's electrified water drops. *European Journal of Physics* **1980,** 1, (3), 143-146.

10. Rayleigh, L., On the equilibrium of liquid conducting masses charged with electricity. *Philosophical Magazine* **1882,** 14, 184.

11. Wilm, M. S.; Mann, M., Electrospray and Taylor-Cone theory, Doles beam of macromolecules at last? *International Journal of Mass Spectrometry and Ion Processes* **1994,** 136, (2-3), 167-180.

12. Yarin, A. L.; Koombhongse, S.; Reneker, D. H., Taylor cone and jetting from liquid droplets in electrospinning of nanofibers. *Journal of Applied Physics* **2001,** 90, (9), 4836-4846.

13. Hohman, M. M.; Shin, M.; Rutledge, G.; Brenner, M. P., Electrospinning and electrically forced jets. II. Applications. *Physics of Fluids* **2001,** 13, (8), 2221-2236.

14. Hohman, M. M.; Shin, M.; Rutledge, G.; Brenner, M. P., Electrospinning and electrically forced jets. I. Stability theory. *Physics of Fluids* **2001,** 13, (8), 2201-2220.

15. Shin, Y. M.; Hohman, M. M.; Brenner, M. P.; Rutledge, G. C., Electrospinning: A whipping fluid jet generates submicron polymer fibers. *Applied Physics Letters* **2001,** 78, (8), 1149-1151.

16. Shin, Y. M.; Hohman, M. M.; Brenner, M. P.; Rutledge, G. C., Experimental characterization of electrospinning: the electrically forced jet and instabilities. *Polymer* **2001,** 42, (25), 9955.

17. Feng, J. J., The stretching of an electrified non-Newtonian jet: A model for electrospinning. *Physics of Fluids* **2002,** 14, (11), 3912-3926.

18. Carroll, C. P.; Joo, Y. L., Electrospinning of viscoelastic Boger fluids: Modeling and experiments. *Physics of Fluids* **2006,** 18, (5), 053102-14.

19. Yarin, A. L.; Koombhongse, S.; Reneker, D. H., Bending instability in electrospinning of nanofibers. *Journal of Applied Physics* **2001,** 89, (5), 3018-3026.

20. Reneker, D. H.; Yarin, A. L.; Hao, F.; Koombhongse, S., Bending instability of electrically charged liquid jets of polymer solutions in electrospinning. *Journal of Applied Physics* **2000,** 87, (9, pt.1-3), 4531-4547.

21. Li, D.; Xia, Y., Fabrication of titania nanofibers by electrospinning. *Nano*

Letters **2003,** 3, (4), 555-560.

22. Zhou, H.; Kim, K. W.; Giannelis, E. P.; Joo, Y. L., Polymeric Nanofibers. In *ACS Symposium*, Reneker, D. H.; Fong, H., Eds. American Chemical Society 2006; Vol. 918, pp 217-230.

23. Reneker, D. H.; Chun, I., Nanometre diameter fibres of polymer, produced by electrospinning. *Nanotechnology* **1996,** 7, (3), 216-223.

24. Lyons, J.; Li, C.; Ko, F., Melt-electrospinning part I: processing parameters and geometric properties. *Polymer* **2004,** 45, (22), 7597-7603.

25. Khil, M.-S.; Bhattarai, S. R.; Kim, H.-Y.; Kim, S.-Z.; Lee, K.-H., Novel fabricated matrix via electrospinning for tissue engineering. *Journal of Biomedical Materials Research* **2005,** 72B, (1), 117-124.

26. Wen, Y.; Hao, Y.; Meifang, Z.; Hongwei, B.; Yanmo, C., Poly(m-Phenylene Isophthalamide) Ultrafine Fibers from an Ionic Liquid Solution by Dry-Jet-Wet-Electrospinning. *Journal of Macromolecular Science: Physics* **2006,** 45, (4), 573-579.

27. Piotr, K., Cellulose nanofibers prepared by the N-methylmorpholine-N-oxide method. *Journal of Applied Polymer Science* **2005,** 98, (4), 1855-1859.

28. Gupta, P.; Trenor, S. R.; Long, T. E.; Wilkes, G. L., In situ photo-cross-linking of cinnamate functionalized poly(methyl methacrylate-co-2-hydroxyethyl acrylate) fibers during electrospinning. *Macromolecules* **2004,** 37, (24), 9211-9218.

29. Kim, S. H.; Kim, S.-H.; Nair, S.; Moore, E., Reactive Electrospinning of Cross-Linked Poly(2-hydroxyethyl methacrylate) Nanofibers and Elastic Properties of Individual Hydrogel Nanofibers in Aqueous Solutions. *Macromolecules* **2005,** 38, (9), 3719 - 3723.

30. Bellan, L. M.; Coates, G. W.; Craighead, H. G., Poly(dicyclopentadiene) Submicron Fibers Produced by Electrospinning. *Macromolecular Rapid Communications* **2006,** 27, (7), 511-515.

31. Theron, A.; Zussman, E.; Yarin, A. L., Electrostatic field-assisted alignment of electrospun nanofibres. *Nanotechnology* **2001,** 12, (3), 384-390.

32. Czaplewski, D.; Kameoka, J.; Craighead, H. G., Nonlithographic approach to nanostructure fabrication using a scanned electrospinning source. *Journal Of Vacuum Science & Technology B* **2003,** 21, (6), 2994-2997.

33. Kameoka, J.; Craighead, H. G., Fabrication of oriented polymeric nanofibers on planar surfaces by electrospinning. *Applied Physics Letters* **2003,** 83, (2), 371-373.

34. Kameoka, J.; Czaplewski, D.; Liu, H. Q.; Craighead, H. G., Polymeric nanowire architecture. *Journal Of Materials Chemistry* **2004,** 14, (10), 1503-1505.

35. Kameoka, J.; Orth, R.; Yang, Y. N.; Czaplewski, D.; Mathers, R.; Coates, G. W.; Craighead, H. G., A scanning tip electrospinning source for deposition of oriented nanofibres. *Nanotechnology* **2003,** 14, (10), 1124-1129.

36. Fong, H.; Liu, W.; Wang, C.-S.; Vaia, R. A., Generation of electrospun fibers of nylon 6 and nylon 6-montmorillonite nanocomposite. *Polymer* **2002,** 43, (3), 775-780.

37. Sun, D.; Chang, C.; Li, S.; Lin, L., Near-Field Electrospinning. *Nano Letters* **2006,** 6, (4), 839 -842.

38. Teo, W. E.; Ramakrishna, S., A review on electrospinning design and nanofibre assemblies. *Nanotechnology* **2006,** 17, (14), R89-R106.

39. Li, D.; Wang, Y.; Xia, Y., Electrospinning of polymeric and ceramic nanofibers as uniaxially aligned arrays. *Nano Letters* **2003,** 3, (8), 1167-1171.

40. Li, D.; Wang, Y. L.; Xia, Y. N., Electrospinning nanofibers as uniaxially aligned arrays and layer-by-layer stacked films. *Advanced Materials* **2004,** 16, (4), 361-366.

41. Li, D.; Ouyang, G.; McCann, J. T.; Xia, Y. N., Collecting electrospun nanofibers with patterned electrodes. *Nano Letters* **2005,** 5, (5), 913-916.

42. Dalton, P. D.; Klee, D.; Moller, M., Electrospinning with dual collection rings. *Polymer* **2005,** 46, (3), 611-614.

43. Deitzel, J. M.; Kleinmeyer, J. D.; Hirvonen, J. K.; Beck Tan, N. C., Controlled deposition of electrospun poly(ethylene oxide) fibers. *Polymer* **2001,** 42, (19), 8163-8170.

44. Bellan, L. M.; Craighead, H. G., Control of an electrospinning jet using electric focusing and jet-steering fields. *Journal of Vacuum Science & Technology B* **2006,** 24, (6), 3179-3183.

45. Li, D.; Xia, Y., Direct fabrication of composite and ceramic hollow nanofibers by electrospinning. *Nano Letters* **2004,** 4, (5), 933-938.

46. Zhang, Y. Z.; Wang, X.; Feng, Y.; Li, J.; Lim, C. T.; Ramakrishna, S., Coaxial Electrospinning of (Fluorescein Isothiocyanate-Conjugated Bovine Serum Albumin)-Encapsulated Poly(ε-caprolactone) Nanofibers for Sustained Release. *Biomacromolecules* **2006,** 7, (4), 1049-1057.

47. McCann, J. T.; Marquez, M.; Xia, Y., Melt Coaxial Electrospinning: A Versatile Method for the Encapsulation of Solid Materials and Fabrication of Phase Change Nanofibers. *Nano Lett.* **2006,** 6, (12), 2868-2872.

48. Liu, Z.; Sun, D. D.; Guo, P.; Leckie, J. O., An Efficient Bicomponent TiO_2/SnO_2 Nanofiber Photocatalyst Fabricated by Electrospinning with a Side-by-Side Dual Spinneret Method. *Nano Lett.* **2006**.

49. Theron, S. A.; Yarin, A. L.; Zussman, E.; Kroll, E., Multiple jets in electrospinning: experiment and modeling. *Polymer* **2005,** 46, (9), 2889-2899.

50. Yarin, A. L.; Zussman, E., Upward needleless electrospinning of multiple nanofibers. *Polymer* **2004,** 45, (9), 2977-2980.

51. Jirsak, O.; Sanetrnik, F.; Lukas, D.; Kotek, V.; Martinova, L.; Chaloupek, J. A Method of Nanofibres Production from a Polymer Solution Using Electrostatic

Spinning and a Device for Carrying out the Method. WO 2005/024101 A1, 17 March, 2005.

52. Yun, K. M.; Hogan Jr, C. J.; Matsubayashi, Y.; Kawabe, M.; Iskandar, F.; Okuyama, K., Nanoparticle filtration by electrospun polymer fibers. *Chemical Engineering Science* **2007,** 62, (17), 4751-4759.

53. Gopal, R.; Kaur, S.; Feng, C. Y.; Chan, C.; Ramakrishna, S.; Tabe, S.; Matsuura, T., Electrospun nanofibrous polysulfone membranes as pre-filters: Particulate removal. *Journal of Membrane Science* **2007,** 289, (1-2), 210-219.

54. Boudriot, U.; Dersch, R.; Greiner, A.; Wendorff, J. H., Electrospinning Approaches Toward Scaffold Engineering-A Brief Overview. *Artificial Organs* **2006,** 30, (10), 785-792.

55. Li, W. J.; Laurencin, C. T.; Caterson, E. J.; Tuan, R. S.; Ko, F. K., Electrospun nanofibrous structure: A novel scaffold for tissue engineering. *Journal Of Biomedical Materials Research* **2002,** 60, (4), 613-621.

56. Yoshimoto, H.; Shin, Y. M.; Terai, H.; Vacanti, J. P., A biodegradable nanofiber scaffold by electrospinning and its potential for bone tissue engineering. *Biomaterials* **2003,** 24, (12), 2077-2082.

57. Shin, M.; Yoshimoto, H.; Vacanti, J. P., In vivo bone tissue engineering using mesenchymal stem cells on a novel electrospun nanofibrous scaffold. *Tissue Engineering* **2004,** 10, (1-2), 33-41.

58. Jing, Z.; Xu, X. Y.; Chen, X. S.; Liang, Q. Z.; Bian, X. C.; Yang, L. X.; Jing, X. B., Biodegradable electrospun fibers for drug delivery. *Journal Of Controlled Release* **2003,** 92, (3), 227-231.

59. Zeng, J.; Yang, L. X.; Liang, Q. Z.; Zhang, X. F.; Guan, H. L.; Xu, X. L.; Chen, X. S.; Jing, X. B., Influence of the drug compatibility with polymer solution on the release kinetics of electrospun fiber formulation. *Journal Of Controlled Release*

2005, 105, (1-2), 43-51.

60. Patel, A. C.; Li, S.; Yuan, J. M.; Wei, Y., In Situ Encapsulation of Horseradish Peroxidase in Electrospun Porous Silica Fibers for Potential Biosensor Applications. *Nano Lett.* **2006,** 6, (5), 1042-1046.

61. Li, D.; Frey, M. W.; Baeumner, A. J., Electrospun polylactic acid nanofiber membranes as substrates for biosensor assemblies. *Journal of Membrane Science* **2006,** 279, (1-2), 354-363.

62. Ding, B.; Kim, J.; Miyazaki, Y.; Shiratori, S., Electrospun nanofibrous membranes coated quartz crystal microbalance as gas sensor for NH3 detection. *Sensors and Actuators B: Chemical* **2004,** 101, (3), 373-380.

63. Ding, B.; Yamazaki, M.; Shiratori, S., Electrospun fibrous polyacrylic acid membrane-based gas sensors. *Sensors and Actuators B: Chemical* **2005,** 106, (1), 477-483.

64. Kessick, R.; Tepper, G., Electrospun polymer composite fiber arrays for the detection and identification of volatile organic compounds. *Sensors and Actuators B: Chemical* **2006,** 117, (1), 205-210.

65. Tao, S.; Li, G.; Yin, J., Fluorescent nanofibrous membranes for trace detection of TNT vapor. *Journal of Materials Chemistry* **2007,** 17, (26), 2730-2736.

66. Liu, H. Q.; Kameoka, J.; Czaplewski, D. A.; Craighead, H. G., Polymeric nanowire chemical sensor. *Nano Letters* **2004,** 4, (4), 671-675.

67. Liu, H. Q.; Reccius, C. H.; Craighead, H. G., Single electrospun regioregular poly(3-hexylthiophene) nanofiber field-effect transistor. *Applied Physics Letters* **2005,** 87, (25), 253106.

68. Pinto, N. J.; Johnson, A. T.; MacDiarmid, A. G.; Mueller, C. H.; Theofylaktos, N.; Robinson, D. C.; Miranda, F. A., Electrospun polyaniline/polyethylene oxide nanofiber field-effect transistor. *Applied Physics Letters* **2003,** 83, (20), 4244-4246.

69. Gonzalez, R.; Pinto, N. J., Electrospun poly (3-hexylthiophene-2,5-diyl) fiber field effect transistor. *Synthetic Metals* **2005,** 151, (3), 275-278.

70. Kameoka, J.; Verbridge, S. S.; Liu, H. Q.; Czaplewski, D. A.; Craighead, H. G., Fabrication of suspended silica glass nanofibers from polymeric materials using a scanned electrospinning source. *Nano Letters* **2004,** 4, (11), 2105-2108.

71. Czaplewski, D. A.; Verbridge, S. S.; Kameoka, J.; Craighead, H. G., Nanomechanical oscillators fabricated using polymeric nanofiber templates. *Nano Letters* **2004,** 4, (3), 437-439.

72. Czaplewski, D. A.; Kameoka, J.; Mathers, R.; Coates, G. W.; Craighead, H. G., Nanofluidic channels with elliptical cross sections formed using a nonlithographic process. *Applied Physics Letters* **2003,** 83, (23), 4836-4838.

73. Verbridge, S. S.; Edel, J. B.; Stavis, S. M.; Moran-Mirabal, J. M.; Allen, S. D.; Coates, G.; Craighead, H. G., Suspended glass nanochannels coupled with microstructures for single molecule detection. *Journal Of Applied Physics* **2005,** 97, (12), 124317.

CHAPTER 2

DIRECT MEASUREMENT OF FLUID VELOCITY IN AN ELECTROSPINNING JET[1]

Introduction

There has been a great deal of theoretical work devoted to modeling the dynamic behavior of electrospinning jets in order to understand the interplay between the parameters that influence the jet.[1-9] Often, these studies compare their models to measurements of the jet behavior. The majority of these measurements are static images of the jet profile taken with brightfield microscopy.[7, 10] Dynamic studies of jet behavior have the potential to reveal information regarding how the polymer microstructure forms in the jet and resulting fibers; but such studies are nontrivial because the jets have radii that taper from a fraction of a millimeter to less than a micron, velocities that range from zero to over 5 meters/second, and complex motions in three dimensions. Because of the strong electric fields in the vicinity of the jet (due to the high voltage on the electrospinning tip) and the charged jet's susceptibility to any external field, it is difficult to place any measurement apparatus close to the jet without affecting its behavior or causing arcing. Thus, most jet characterization techniques are optical and involve imaging optics relatively far from the jet itself.[7, 10] Electrical measurements of the jet current have also been conducted;[4, 10] however, these measurements can be ambiguous due to background current from corona formed at the electrospinning tip.

Several optical methods have been used to characterize electrospinning jets, ranging from simple low-speed or static white light imaging of the jet profile near the tip to more complex techniques such as high-speed brightfield imaging of unique

[1] Reproduced in part from with permission from Bellan, L. M.; Craighead, H. G.; Hinestroza, J. P., Direct measurement of fluid velocity in an electrospinning jet using particle image velocimetry. *Journal of Applied Physics* **2007,** 102, (9), 094308.

formations in the jet[1, 3] and laser Doppler velocimetery.[11] These techniques can be limited by the resolving power of the optical system, a requirement for large sample volume to produce measurable signal, or the assumption that nonuniformities in the macroscopic jet are traveling at the same speed as the fluid. An early study used tracer particles to image eddy currents in the Taylor cone region.[12] Often jet velocity and strain rate are not measured directly but simply estimated from other measurements.[1]

In this study we used fluorescence microscopy to track individual fluorescent particles in the Taylor cone and in the fluid jet. The measured velocities can then be compared to calculated velocities from other, less direct measurement techniques in order to determine whether the assumptions upon which these techniques rely are correct. Because the electrospinning jet is relatively thin, the tracer particles must be small and thus give off low levels of light. This necessitates an objective of reasonable numerical aperture to collect enough light, and a highly sensitive camera. Moreover, the field of view must be of dimensions similar to those of the jet, and thus high velocity particles will only appear to the imaging system for a short period of time, necessitating a high speed (i.e. high frame rate) video camera.

Methods and Materials

The optical system used to observe the fluorescent particles consisted of several parts, discussed below. An argon ion laser (Ion Laser Technology 5425A-OOC-2) was used as the fluorescence excitation source. The laser beam first passed through a beam expander (Edmund Optics 10x beam expander), and then into a standard fluorescence microscope filter cube. The excitation light then entered a 4x objective (PlanC 4x/0.1 NA), which focused the light on the electrospinning jet. The emission light was collected using a high speed intensified camera (Ultracam 3,

Videoscope Intl, gated 250 µs) operating at 1000 fps or video rate intensified camera (ICCD-350F, Videoscope Intl). The fields of view of the cameras were calibrated using a microscope stage micrometer with 10 µm marks. The video signal from the ICCD-350F camera was captured on a computer using a PCTV USB2 video capture device (Pinnacle Systems). A schematic of the optical system is shown in Figure 2.1. This system was also able to operate in a pseudo-brightfield mode using white light from a flashlight to illuminate the jet from behind. An image of the electrospinning jet profile taken in this white light mode is shown in Figure 2.2. We used Matlab to convert this image into a quantitative jet profile dataset and to further process the data. The entire experimental setup was mounted on a vibration isolation table.

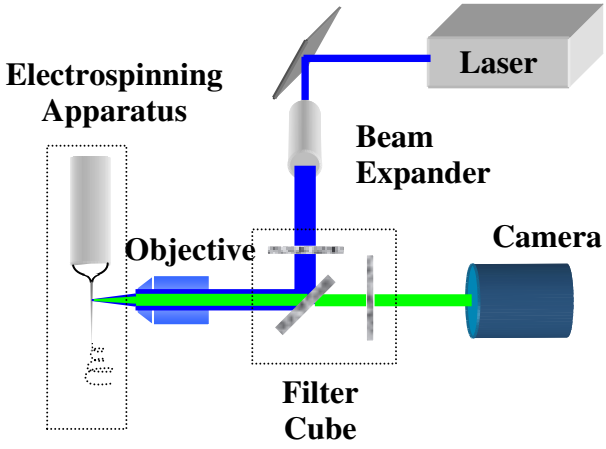

Figure 2.1- Schematic of optical measurement setup.

The polymer solution used in this experiment consisted of 1 g of polyethylene oxide (Acros organics, Mw 100,000) dissolved in a mixture of 5mL of deionized water and 25 µL of 2µm FluoSphere solution (Invitrogen F8888 size kit, 2µm bead solution, 2% solids) that had been diluted with water 1000-fold. Because the FluoSpheres are made of polystyrene with a density of 1.05 g/mL (as stated by the manufacturer), they are essentially the same density as the solution and can accurately indicate flow

characteristics.[13] This solution was fed into a blunt 22 gauge metal needle using a syringe pump (Harvard Apparatus 22) at a rate of 0.11 μL/sec. Using a high voltage power supply (Bertan series 230), we applied a voltage of 4 kV to the metal needle held at a distance of 17.5 mm above a grounded water bath. The grounded water bath was used as a collector to avoid an accumulation of charged polymer. The electrospinning system was mounted on an XYZ stage so that it could be moved within the field of view of the optical system.

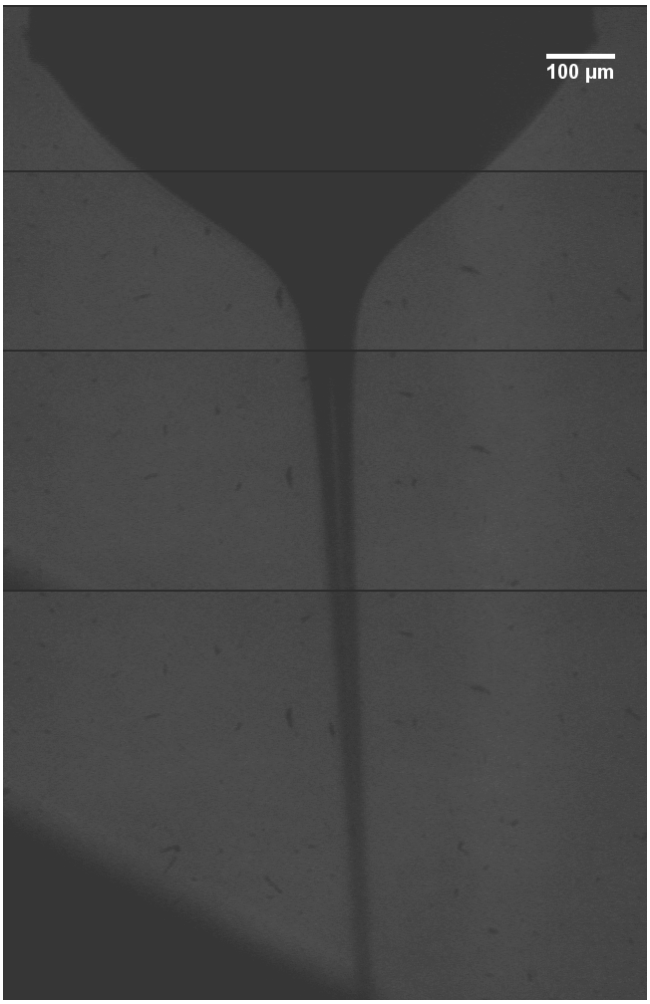

Figure 2.2- Image of electrospinning jet as illuminated from the rear with white light. The measured jet profile was extracted from this image. Several frames at different jet positions from a video were combined to make the image

The rheological properties of the electrospinning solution were characterized to provide information on the transient response of the material to stress and strain fields. We used an AR2000 rheometer (TA Instruments) operating with a concentric Couette cylinder fixture to measure the storage and loss moduli as a function of frequency using a small angle oscillatory procedure. The point at which these curves cross is usually considered to correspond to the average relaxation time of the solution. As the rheometer was unable to operate at a high enough frequency to reach a crossing point, we determined the longest relaxation time using time-temperature superposition (TTS) measuring mode to construct an extended master curve at 298K (Figure 2.3). The rheological data exhibits terminal behavior at lower frequencies similar to that of a single Maxwell fluid.[14] Therefore, a single relaxation time, small amplitude oscillatory shear Maxwell model (equations shown below) was used to obtain the relaxation time τ.[15]

$$G'(\omega) = G_o \frac{(\omega\tau)^2}{1+(\omega\tau)^2} \qquad G''(\omega) = G_o \frac{\omega\tau}{1+(\omega\tau)^2} \qquad (2.1ab)$$

The resulting value of 1651 rad/sec is then taken to be the point at which the extrapolated moduli data curves would intersect, and thus the longest relaxation time of the material is 0.61 ms.

Results and Discussion

Using the high speed intensified camera, we were able to track fluorescent particles moving at velocities faster than 200 mm/sec in regions of the jet exhibiting strain rates varying from 0 to over 400 sec^{-1}. Images from videos of these particles traveling in the jet are shown in Figure 2.4. Sometimes multiple spots appeared due to ghosting on the intensifier phosphor screen, but this did not cause any problems when measuring the particle velocity. The velocity in the vertical direction was determined by manually measuring the y-position of the particle in two subsequent video frames,

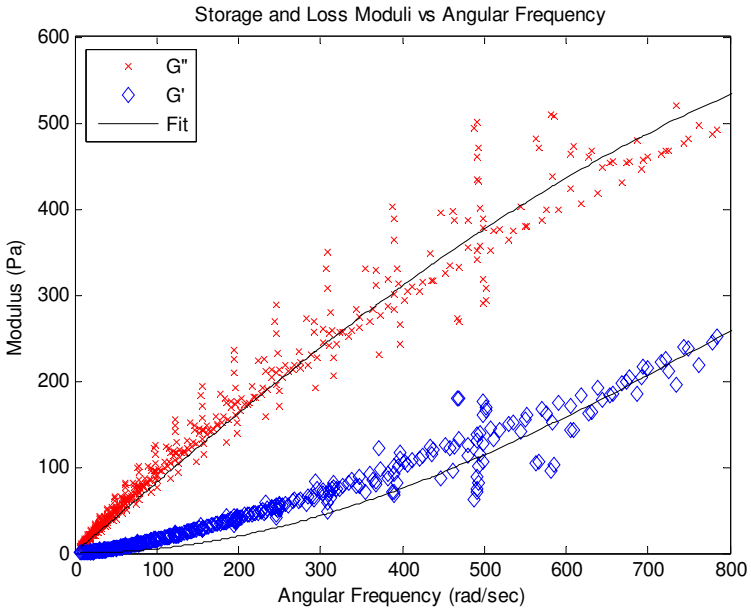

Figure 2.3- Storage modulus and loss modulus as a function of angular frequency. The longest relaxation time was calculated to be 0.61 ms using a single relaxation time Maxwell fluid model (fit parameters G_o = 1360 Pa and τ = 0.61 ms).

and multiplying this separation by the frame rate. The y-position ascribed to a given velocity measurement was halfway between the two points measured. The velocities of several particles, at several different positions along the jet, were measured and plotted as a function of their position along the jet (Figure 2.5). The fluid velocity can also be calculated from the jet profile using the volume conservation relation $\pi R^2 v = Q$ where R is the jet radius, v is the jet velocity, and Q is the volume flow rate. This relation is true only when solvent evaporation is negligible. Previous studies have shown that solvent evaporation is significant in many cases,[3] and thus this relation cannot be assumed for all jets at all positions. This is expected since at some position along the jet the fibers are solid (essentially no solvent is left), and the solvent fraction of the initial solution is large. On the same chart, we also plotted the velocity

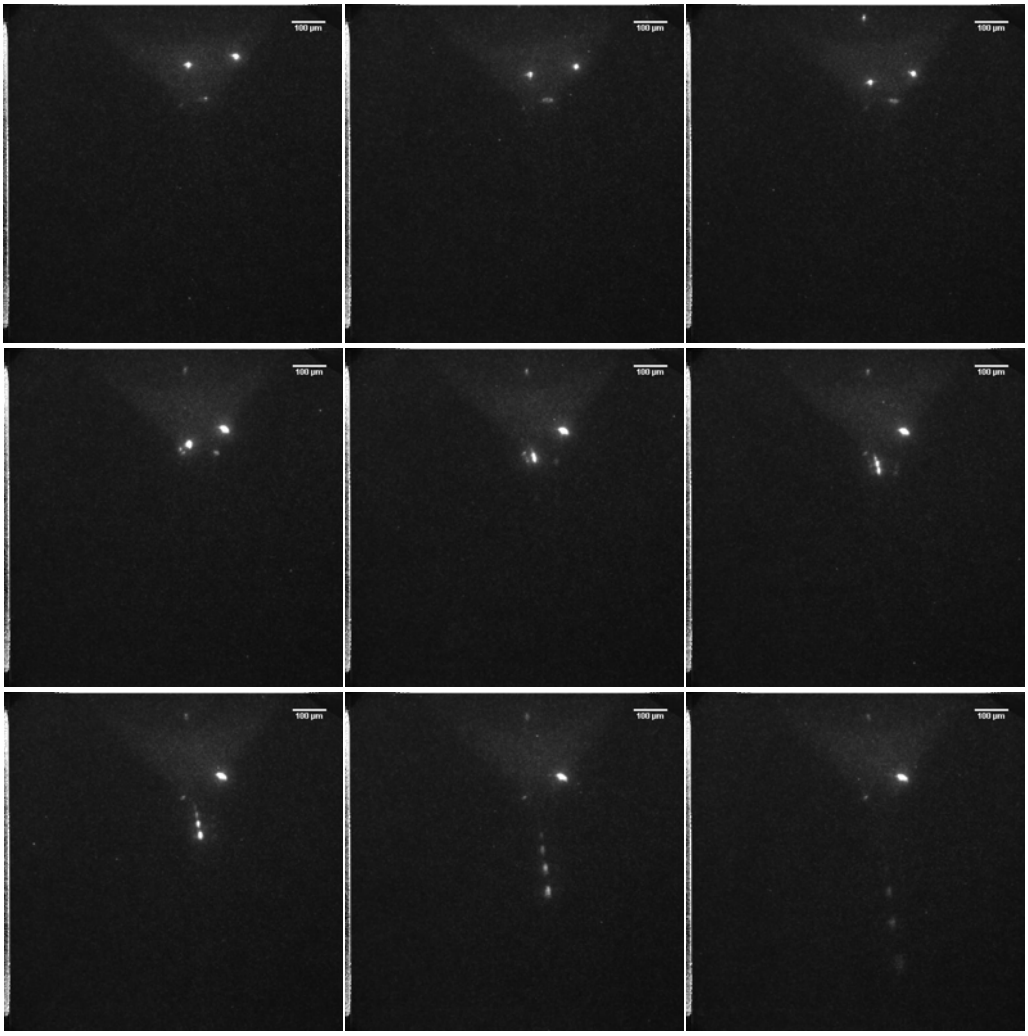

Figure 2.4- Individual images from a high speed video indicating particle movement. The combination of ghosting on the phosphor and the 250 μs intensifier gating time used causes a single particle to appear as multiple spots (temporally separated by 1ms) in the high velocity regimes.

calculated from the jet radius measured from both the autofluorescence of the jet observed in the high speed video and the jet profile imaged using white light illumination (Figure 2.2). Finally, we calculated the jet radius from the velocity data and plotted this calculated profile along with the two measured profiles (Figure 2.5).

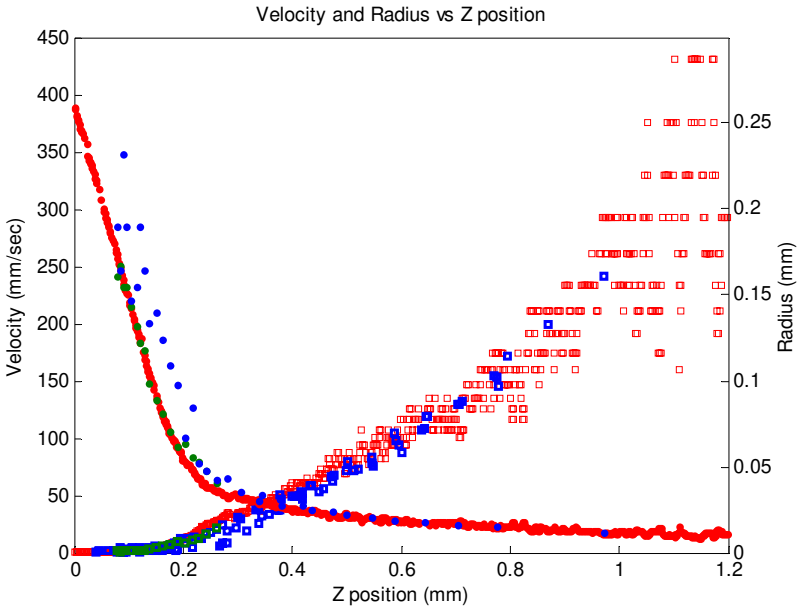

Figure 2.5- Velocity and jet radius plotted as a function of Z position (length along the jet). Legend: •-Radius calculated from velocity data •-Radius measured via white light illumination, •-Radius measured from fluid autofluorescence, □-Velocity measured from particle, □-Velocity calculated from white light-measured radius □-Velocity calculated from autofluorescence-measured radius

The data measured and calculated from the white light illumination experiment required an arbitrary constant offset to be added to the x-axis due to small shifts in the experimental setup.

In several cases we observed transverse oscillatory movement of the tracer particle at the beginning of the fluid jet (Figure 2.6). This movement, which would not be obvious using other measurement techniques, appears to occur with a frequency of approximately 250-350Hz and an amplitude of ~10 μm. This transverse movement is intriguing because it could be the precursor to the bending instability that often manifests itself macroscopically at some distance down the jet. Moreover, at least one

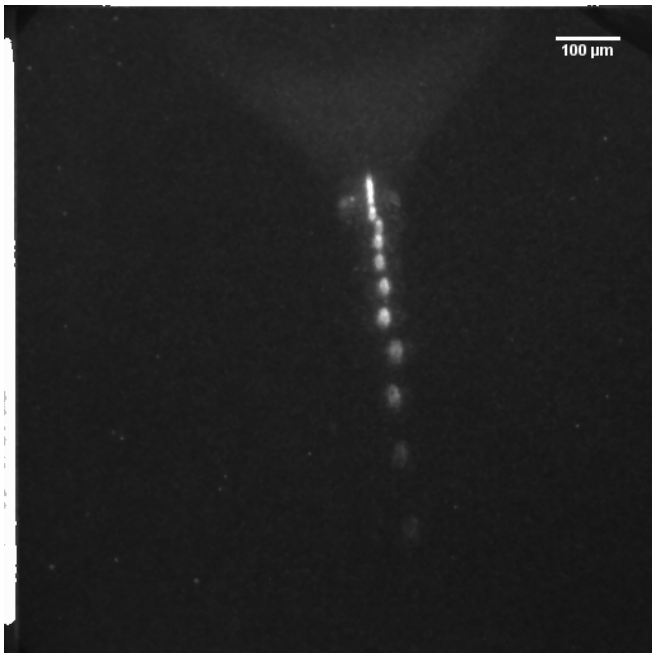

Figure 2.6- Several frames of high speed video combined to illustrate the oscillatory transverse motion of the tracer particle.

theoretical treatment of the bending motion[1] assumes, arbitrarily, an initial small transverse oscillatory perturbation at the top of the jet that is amplified along the jet and eventually becomes visible bending. These high speed images are experimental evidence that this initial transverse oscillation does, in fact, occur. Future studies with faster cameras may be able to follow this oscillation further down the jet to observe whether it truly correlates with the bending instability. An improved imaging system could also enable observation of more subtle phenomena such as higher-frequency oscillations or motion in and out of the focal plane.

In order to analyze the behavior of the polymer jet system, we plot the Deborah number *De* of the jet as a function of Z position (Figure 2.7). The Deborah number is given by $De = \dot{\varepsilon}\tau$ where $\dot{\varepsilon}(z) = \partial v(z)/\partial z$ is the strain rate of the jet, v is the axial velocity, z is the axial position and τ is the relaxation time of the polymer solution.

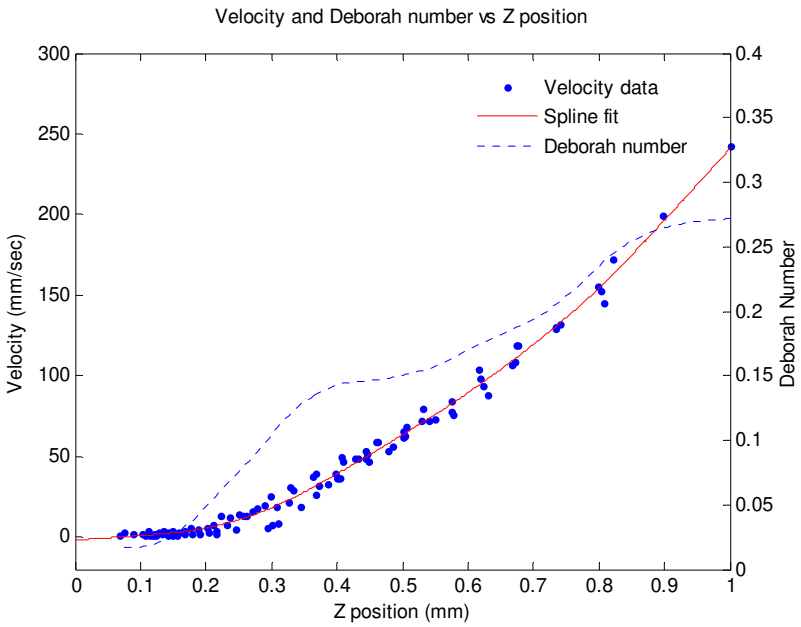

Figure 2.7- Velocity and Deborah number plotted as a function of Z position. A spline curve was fit to the velocity data, and subsequently differentiated to obtain a strain rate curve. The Deborah number is the product of the strain rate and relaxation time of the polymer system.

This dimensionless parameter describes the fluidity of the system and the extent to which the polymer molecules are stretched.[16] A polymer molecule will undergo a coil-stretch transition at $De \approx 0.5$.[17, 18] To determine *De*, we first fit the measured velocity data using a spline curve. The resulting fit data is numerically differentiated with respect to jet position to determine the strain rate as a function of position. This strain rate is then multiplied by the longest relaxation time of the polymer system as measured via rheometry. Because the region of the jet in which we have performed our measurements appears to be one in which solvent evaporation is not playing a dramatic role (as indicated by the agreement between the measured velocity and that calculated from volume conservation), the relaxation time of the polymer solution may

be taken to be essentially constant throughout the experiment. Future experiments will need to consider that, as the solvent evaporates, the relaxation time of the system will change. The resulting Deborah numbers indicate that the system is closely approaching the point at which the polymer chains are stretched (i.e. a Deborah number > 0.5) at a position of just ~1/18 the total jet length. A previous study, discussed in Chapter 5, has demonstrated that an electrospinning jet of a carrier polymer can be used to isolate and elongate a dilute concentration of others molecules such as DNA.[19] Using the relaxation time for the longer DNA molecule calculated in this study, we can calculate the Deborah number for the DNA molecules at the high speed end of the velocity data. These value ranges from 900 to 8500, indicating that, at least for the jet analyzed in the current studies, such DNA molecules would experience strong elongation even in this initial region of the jet.

Conclusion

We have demonstrated direct imaging of the fluid motion in an electrospinning jet using fluorescent tracking particles. Unlike other less direct methods, this technique allows us to measure both the axial and transverse jet velocity at various positions along the jet length. This allowed us to observe transverse oscillatory motion in the region where the Taylor cone starts to form a fluid jet. We were also able to map out the velocity as a function of axial position, and thereby calculate the strain rate as a function of position. This allowed us to plot Deborah number as a function of position, demonstrating the elongational properties of the system. The limitations of this measurement technique are determined by the camera hardware (imaging speed and sensitivity) and optical system (field of view and depth of focus). By measuring the velocity directly and comparing the actual value to that predicted by the volume conservation relation, it is possible to determine where along the jet

evaporation of the solvent begins to play an important role in the jet dynamics. More recent work by Helgeson et al. used a variant of this measurement technique to measure fluid properties of a PEO electrospinning jet and fit the resulting jet profile to an empirical model.[20]

REFERENCES

1. Reneker, D. H.; Yarin, A. L.; Hao, F.; Koombhongse, S., Bending instability of electrically charged liquid jets of polymer solutions in electrospinning. *Journal of Applied Physics* **2000,** 87, (9, pt.1-3), 4531-4547.

2. Yarin, A. L.; Koombhongse, S.; Reneker, D. H., Taylor cone and jetting from liquid droplets in electrospinning of nanofibers. *Journal of Applied Physics* **2001,** 90, (9), 4836-4846.

3. Yarin, A. L.; Koombhongse, S.; Reneker, D. H., Bending instability in electrospinning of nanofibers. *Journal of Applied Physics* **2001,** 89, (5), 3018-3026.

4. Hohman, M. M.; Shin, M.; Rutledge, G.; Brenner, M. P., Electrospinning and electrically forced jets. II. Applications. *Physics of Fluids* **2001,** 13, (8), 2221-2236.

5. Hohman, M. M.; Shin, M.; Rutledge, G.; Brenner, M. P., Electrospinning and electrically forced jets. I. Stability theory. *Physics of Fluids* **2001,** 13, (8), 2201-2220.

6. Shin, Y. M.; Hohman, M. M.; Brenner, M. P.; Rutledge, G. C., Electrospinning: A whipping fluid jet generates submicron polymer fibers. *Applied Physics Letters* **2001,** 78, (8), 1149-1151.

7. Shin, Y. M.; Hohman, M. M.; Brenner, M. P.; Rutledge, G. C., Experimental characterization of electrospinning: the electrically forced jet and instabilities. *Polymer* **2001,** 42, (25), 9955.

8. Feng, J. J., The stretching of an electrified non-Newtonian jet: A model for electrospinning. *Physics of Fluids* **2002,** 14, (11), 3912-3926.

9. Carroll, C. P.; Joo, Y. L., Electrospinning of viscoelastic Boger fluids: Modeling and experiments. *Physics of Fluids* **2006,** 18, (5), 053102-14.

10. Yu, J. H.; Fridrikh, S. V.; Rutledge, G. C., The role of elasticity in the formation of electrospun fibers. *Polymer* **2006,** 47, (13), 4789-4797.

11. Warner, S. B.; Buer, A.; Ugbolue, S. C.; Rutledge, G. C.; Shin, M. Y. *A Fundamental Investigation of the Formation and Properties of Electrospun Fibers*; National Textile Center Annual Report: 1998; pp 83-90.

12. Hayati, I., Eddies inside a liquid cone stressed by interfacial electrical shear. *Colloids and Surfaces* **1992,** 65, (1), 77-84.

13. Melling, A., Tracer particles and seeding for particle image velocimetry. *Measurement Science and Technology* **1997,** 8, (12), 1406-1416.

14. Vinogradov, G. V., Critical regimes of deformation of liquid polymeric systems. *Rheologica Acta* **1973,** 12, (3-4), 357-73.

15. Bird, R. B., *Dynamics of polymeric liquids*. Wiley: New York, 1977; p 2 v. (773 p. in various pagings).

16. Smith, D. E.; Chu, S., Response of Flexible Polymers to a Sudden Elongational Flow. *Science* **1998,** 281, (5381), 1335-1340.

17. Larson, R. G.; Magda, J. J., Coil-stretch transitions in mixed shear and extensional flows of dilute polymer solutions. *Macromolecules* **1989,** 22, (7), 3004-3010.

18. Perkins, T. T.; Smith, D. E.; Chu, S., Single Polymer Dynamics in an Elongational Flow. *Science* **1997,** 276, (5321), 2016-2021.

19. Bellan, L. M.; Cross, J. D.; Strychalski, E. A.; Moran-Mirabal, J.; Craighead, H. G., Individually Resolved DNA Molecules Stretched and Embedded in Electrospun Polymer Nanofibers. *Nano Letters* **2006,** 6, (11), 2526-2530.

20. Helgeson, M. E.; Grammatikos, K. N.; Deitzel, J. M.; Wagner, N. J., Theory and kinematic measurements of the mechanics of stable electrospun polymer jets. *Polymer* **2008,** 49, (12), 2924-2936.

CHAPTER 3

MEASUREMENT OF MOLECULAR ORIENTATION IN INDIVIDUAL ELECTROSPUN FIBERS USING POLARIZED RAMAN SPECTRSCOPY[2]

Introduction

In most electrospinning systems, the strong elongational flow of the fluid jet results in fibers with high degrees of molecular orientation. The extent of this orientation, as well as its uniformity over the length of the fiber, will have an impact on the material properties of the fiber. Several previous studies have observed molecular orientation in large bundles of fibers using X-ray scattering and diffraction techniques,[1-4] polarized Raman spectroscopy,[2] and birefringence analysis.[5] Other studies have measured mechanical properties of both electrospun fiber mats [6, 7] and individual electrospun fibers. [3, 6, 8] Transmission electron diffraction techniques have been used to attempt to characterize the microstructure of single fibers,[1, 4, 9] but because of problems due to sample thickness and damage to the fiber caused by the incident beam, the resulting data is either non-existent or has a very poor signal-to-noise ratio; thus quantitative molecular orientation measurements using this method have yet to be published. While measurements of molecular orientation performed on large bundles of fibers provide information about the average molecular orientation over several fibers (or, from a different point of view, over several distantly spaced positions of material deposited from the same jet), these measurements cannot provide much information about the uniformity of this orientation. Electrospinning jets exhibit complex fluid behavior and various types of instabilities, [10-12] resulting in fibers with properties with a wide distribution. For

[2] Reproduced in part from with permission from Bellan, L. M.; Craighead, H. G., Molecular orientation in individual electrospun nanofibers measured via polarized Raman spectroscopy. *Polymer* **2008,** 49, (13-14), 3125-3129. Copyright 2008 Elsevier.

example, a single electrospinning jet depositing fibers from a single solution will form fibers with a wide range of diameters. [6, 13] It is likely that other parameters, such as density, crystallinity, and molecular orientation, would exhibit a similarly wide distribution; this has been suggested by transmission electron microscopy (TEM) studies.[4] Moreover, it would be useful to compare mechanical measurements taken from a single, short (tens of microns) section of fiber to a measurement of molecular orientation taken from the same fiber section.

In this chapter we describe the measurement of molecular orientation from polarized Raman spectra from an individual electrospun Nylon-6 fiber. We acquire spectra using four polarization geometries (X|X, Y|Y, X|Y, Y|X using the notation "incident polarization | analyzed polarization" and the axes shown in Figure 3.1). We qualitatively compare these spectra to those from unoriented and oriented Nylon-6 film, as well as to spectra taken from large bundles of Nylon-6 fibers. [14] We also present results from quantitative analysis of the single-fiber spectra, yielding the P2 (sometimes called the Herman's function) and P4 orientation functions.

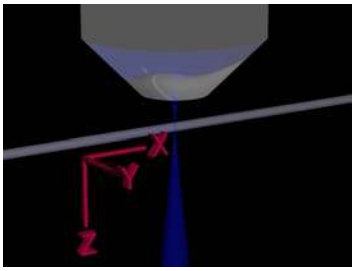

Figure 3.1-Geometry of polarized Raman experiments. A laser beam passes through a microscope objective and is focused on an isolated fiber. The backscattered light is collected with the same objective, and passes to the Raman spectrometer.

Experimental Methods

Raman spectra were acquired using a Renishaw inVia micro-Raman system using incident light at 488nm from a Melles Griot laser (Melles Griot 543-AP-A01, incident power 4-5 mW) focused on the sample using a 50x 0.75 NA objective (Leica). A λ/2 waveplate (Thorlabs) was sometimes inserted in the beam path prior to the microscope entrance to allow rotation of the polarization of the incident radiation. A λ/2 waveplate and polarizer (part of the micro-Raman system) were at times inserted after the notch filter to select the appropriate polarization of the analyzed light. Using this setup, we were able to take spectra in four geometries (X|X, X|Y, Y|X, and Y|Y) from any sample. For the purposes of this article, we define Z as the axis of incident radiation, X as the axis of orientation in the sample, and Y as the axis transverse to the sample orientation (Figure 3.1). A backscattering geometry was used in all cases. The spot diameter of the incident radiation was approximately 4 μm.

Control experiments were performed using unoriented Nylon-6 film (Kenylon 6250, KNF Corporation). Spectra were taken from the unoriented film and from film that had been stretched on a homebuilt system. For the experiments with film, the λ/2 waveplate for the incident beam was not used and the film was rotated with respect to the incident polarization. Nanofibers were electrospun from a solution of 30% Nylon-6 (Aldrich) in formic acid (Mallinckrodt) using the scanned electrospinning technique.[15] In this technique (illustrated in Figure 3.2), a droplet of solution is placed on an electrified (6-10kV) microfabricated silicon tip held a distance of 2-4 cm from a grounded substrate. The droplet forms a fluid jet which is accelerated towards a grounded substrate. As the solvent in the fluid evaporates from the jet, a solid fiber is formed and deposited on the grounded substrate. We used a chopper motor to rotate the substrate through the jet to isolate and orient the fibers. A transmission electron microscopy (TEM) grid was used as the collecting substrate so that regions of the

fibers would be freely suspended, but over relatively small holes to reduce fiber drift. The grid was glued to a metal washer for ease of handling. The washer was placed on a stack of washers sitting on an XY piezo stage system (Physik Instrumente M662.4) mounted on a rotation stage. This rotation stage was centered using the manual microscope stage on the micro-Raman system.

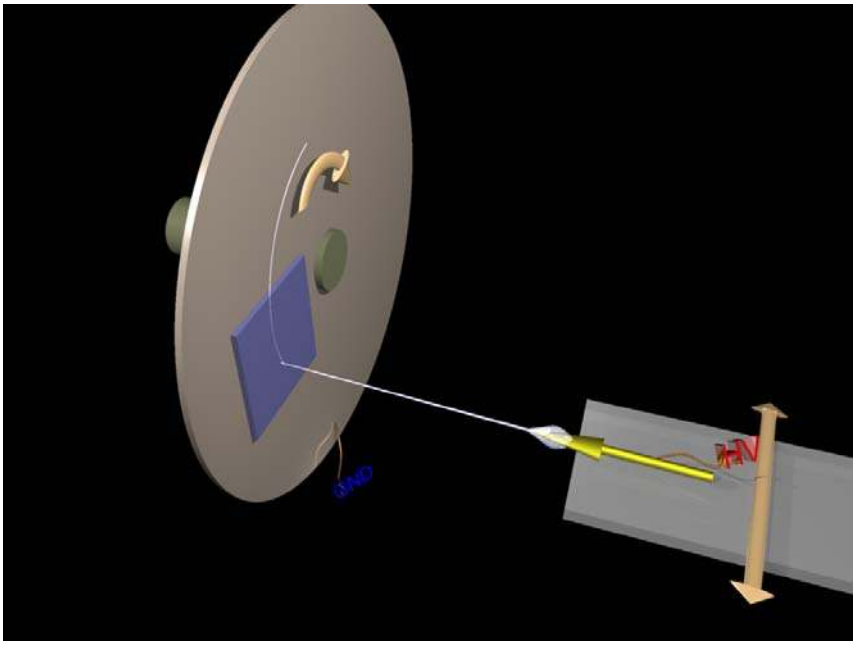

Figure 3.2- Illustration of the scanned electrospinning apparatus.

Results and Discussion

Spectra over the 800-1800 cm^{-1} range from control experiments performed on unoriented and oriented Nylon-6 film are shown in Figure 3.3. By observing the changes in the spectra from the X|X and Y|Y geometries one can qualitatively determine that stretching the film induces anisotropy, as expected. We were able to identify the peaks expected in Nylon-6: the s(C-CO) peak at 934 cm^{-1}, the s(C-C) peaks at 1001, 1040, 1063, 1078, 1127, and 1168 cm^{-1}, the w(CH_2)+t(CH_2) peaks at 1204 and 1230 cm^{-1}, the Amide III peak at 1278 cm^{-1}, the t(CH_2) peak at 1306 cm^{-1}, the w(CH_2) peak at 1379 cm^{-1}, the b(CH_2) peak at 1443 cm^{-1}, the Amide II peak at

1555 cm^{-1}, and the Amide I peak at 1635 cm^{-1} [14, 16] (where *s* indicates stretching, *w* indicates wagging, *t* indicates twist and *b* indicates bending). The chemical structure of Nylon-6 is illustrated in Figure 3.4 for reference.

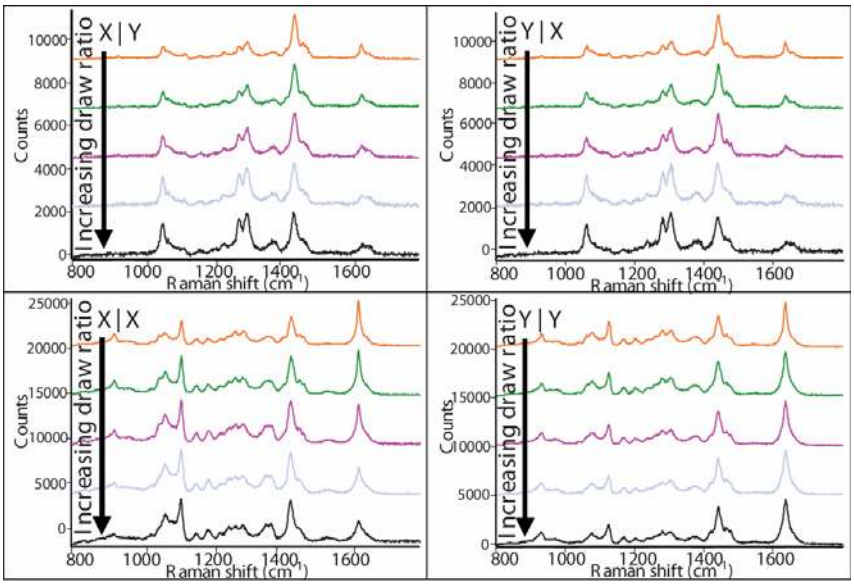

Figure 3.3- Spectra from unoriented and oriented Nylon-6 film with four polarization geometries. As the draw ratio increases, the material becomes more anisotropic, manifested by differences between the X|X and Y|Y spectra.

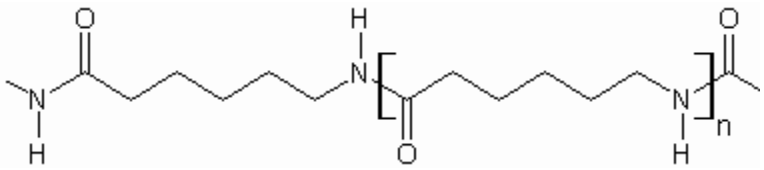

Figure 3.4- Illustration of Nylon-6 chemical structure.

We were also able to obtain Raman spectra from individual electrospun Nylon-6 nanofibers. Figure 3.5 shows a single fiber as observed using the brightfield illumination on the micro-Raman system (Figure 3.5a) and the same fiber imaged using a scanning electron microscope (SEM) (Figure 3.5b) after Raman spectra were obtained. From SEM imaging, the diameter of this fiber was determined to be 280 nm. The fiber was oriented horizontally using a rotation stage and then positioned in

the beam using linear piezo stages. Due to the difficulty in perfectly centering the rotation stage, the polarization of the incident light with respect to the sample orientation was rotated using the incident beam λ/2 waveplate as opposed to rotating the sample. Raman spectra from the four geometries for this fiber (over the 800-1700 cm^{-1} range) are shown in Figure 3.6. Spectra were taken at three places along the fiber; these are indicated by different colors. Each spectrum corresponds to a single "SynchroScan" extended scan acquisition of 200 seconds and a binning value of 3. Variations between the spectra at the three positions may be due to actual variations in the fiber, variations in the fiber position in the laser spot (in the X, Y, and Z (focus) directions), and noise in the system. The background in the spectra may be due to noise inherent to the Raman system, fluorescence of the fiber, and background from the air surrounding the fiber (note that the strong peak at 1555 cm^{-1} in the X|X and Y|Y spectra is likely due to the oxygen in the air,[17] as the Amide II peak at the same wavenumber should be weak for all geometries [14, 16] and the 1555 cm^{-1} peak is seen in spectra taken without any fiber under the microscope objective). By noting the significant qualitative differences between the X|X and Y|Y spectra, we observe that there is significant molecular orientation in the fiber.

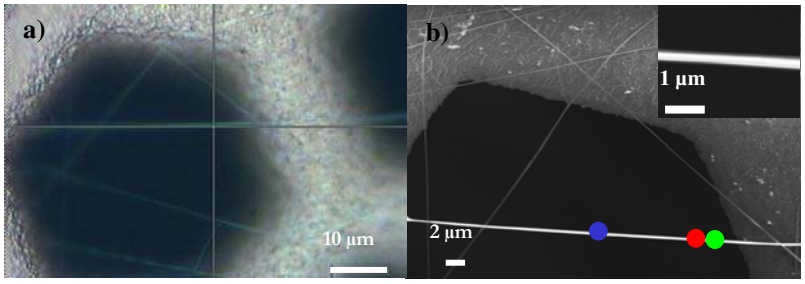

Figure 3.5-a) Brightfield image of individual electrospun Nylon-6 fiber (under crosshairs) from micro-Raman system and b) SEM image of the same fiber. Higher magnification SEM images (inset) indicate a fiber diameter of approximately 280 nm. The colored dots indicate approximate positions corresponding to the spectra in Figure 3.6.

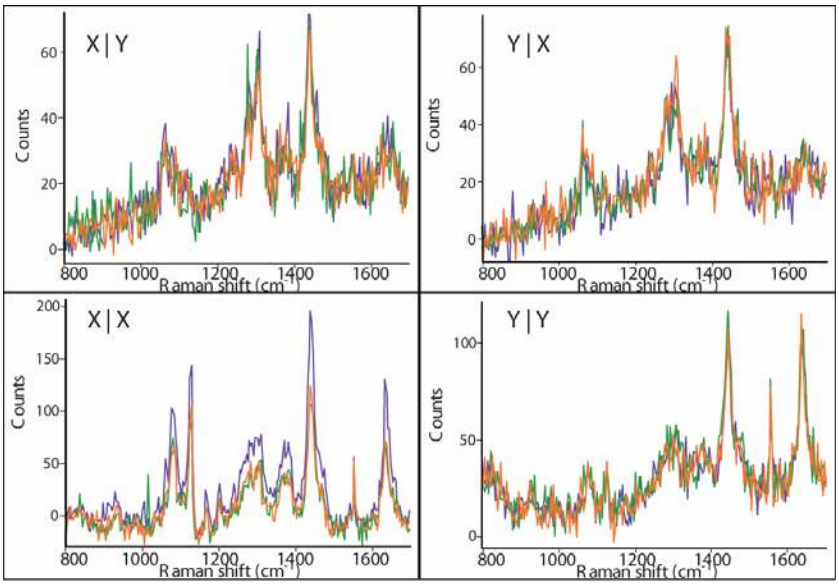

Figure 3.6-Polarized Raman spectra from the isolated electrospun Nylon-6 nanofiber shown in Figure 3.5. The differences between the X|X and Y|Y spectra indicate significant anisotropy.

Previous studies using Raman spectroscopy to analyze Nylon-6 bundles indicate that electrospinning Nylon-6 results in the γ crystalline form of the material;[14] this is in agreement with studies employing X-ray diffraction to analyze electrospun Nylon-6 nanofibers.[18] This crystalline form, unlike the α form typically observed in bulk and solution-cast films, is observed in high-speed melt-spun Nylon-6 filament and is the dominant crystalline form for fibers formed under high stress.[19] In electrospun Nylon-6 fibers, the chain axis of the γ crystalline form is parallel to the fiber axis.[20] Upon comparison to spectra in reference 12, some regions (the orange spectrum in Figure 3.7) showed spectra strongly indicative of a γ form, while others (the blue spectrum in Figure 3.7) appeared to posses shapes slightly different from the pure γ form. While all regions demonstrate significant molecular orientation, the

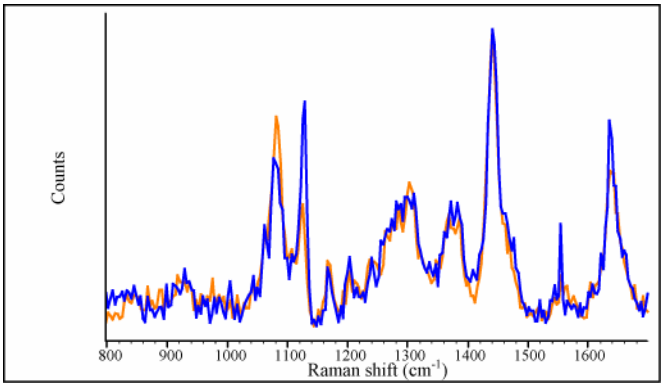

Figure 3.7- X|X spectra from two different fibers, demonstrating the difference in shape. The spectra were scaled to fit in the same window. The blue spectrum is from the fiber indicated in Figure 3.5, and the orange spectrum is from the fiber referred to at the bottom of Table 3.1.

crystallinity and orientation of crystals may vary significantly,[4] which may account for the variation in spectrum shape.

Polarized Raman spectroscopy may be used as a tool to quantitatively measure molecular orientation by calculating the P2 and P4 orientation functions: [21-26]

$$P2 = \frac{1}{2}(3 < \cos^2\theta > -1) \quad (3.1)$$

$$P4 = \frac{1}{8}(35 < \cos^4\theta > -30 < \cos^2\theta > +3) \quad (3.2)$$

We have chosen to analyze the s(C-C) peak at ~1120-1130 cm^{-1} as it has a low depolarization ratio but a measurable peak height in all spectra, indicates a vibration along the molecular backbone, and is easily isolated from other peaks. Peaks were fit using the WiRE software from Renishaw, and the resulting values (along with the depolarization ratio, 0.075, measured from the unoriented film) were used to solve a series of equations for P2 and P4 according to two slightly different treatments. [21] [25] We also calculate a qualitative orientation parameter, $P_{qual}=1-(I_{yy}/I_{xx})$, where I_{xx}

and I_{yy} are the intensities of the peak in the X|X and Y|Y spectra, respectively.[24] The results for the unoriented film, the most highly oriented film, and several positions along an individual electrospun fiber are shown in Table 3.1. In order to determine the standard deviation of this measurement technique, ten sets of four spectra were obtained from a single position on another fiber deposited from the same solution at a different time. The resulting orientation function values, along with the standard deviations, are reported in Table 3.1. For this set of data, the $\langle\cos^2\theta\rangle$ and $\langle\cos^4\theta\rangle$ values were 0.67 ± 0.04 and 0.07 ± 0.09, respectively (using the method outlined in ref. 21). We observed no correlation between the calculated orientation values and the set number, indicating that the incident radiation was not measurably altering the microstructure over this timescale.

Table 3.1-P2 and P4 values calculated using two methods and a qualitative orientation parameter from polarized Raman spectra from several samples

Sample	P2 (ref 21, ref 25)	P4 (ref 21, ref 25)	P_{qual}
Unoriented film	0.03, 0.03	0.08, 0.06	0.08
Highly oriented film	0.20, 0.14	0.31, 0.33	0.35
Red position	0.88, 0.88	-1.7, -0.91	0.78
Blue position	0.87, 1.1	-0.53, -.55	0.86
Green position	0.66, 0.83	-0.92, -1.0	0.75
Another fiber (not shown)	0.59 ± 0.06, 0.65 ± 0.07	-2.2 ± 0.4, -2.1 ± 0.3	0.65 ± 0.06

Though the quantitative analysis described above yields reproducible values, the quantitative results for the electrospun nanofiber samples fall outside the allowed range for the P4 function. For a distribution in which all molecules point along the same angle, $\langle\cos^4\theta\rangle = \langle\cos^2\theta\rangle^2$ and thus $P4=(1/18)(35P2^2-10P2-7)$. In the other extreme, a randomly oriented sample will have both P2 and P4 equaling 0. It can be shown using Schwartz's inequality that $|\langle\cos^2\theta\rangle|^2 \leq \langle\cos^4\theta\rangle \leq \langle\cos^2\theta\rangle$, which imposes a range on the value of P4 for a given value of P2.[27] Though the film samples yield proper P2 and P4 values, the P4 values in Table 3.1 for the electrospun nanofiber samples all fall outside the allowed range. We believe that this is due to the high background and poor signal-to-noise ratio (SNR) in the electrospun nanofiber spectra, especially in the X|Y and Y|X spectra where the peak is difficult to resolve over the background. This may also explain the anomalous P2 value of 1.1 obtained for the blue position. It is also possible that birefringence effects may be altering the relative intensities in the spectra so as to cause the calculations to yield anomalous results.

The values in Table 1 can be compared to orientation function values measured in other Nylon-6 systems, such as highly drawn fibers produced using conventional spinning techniques. Previous work investigating orientation in both Nylon-6,6 and Nylon-6 fibers that were drawn at room temperature post-spinning indicates that the P2 orientation function rapidly approaches its maximum value of 1 at draw ratios less than 10.[28-30] Estimates of the draw ratio in electrospinning jets are of the order of ~10,000,[10] and the Deborah numbers in these systems are quite high,[31] suggesting that the molecular orientation in electrospun fibers should be similar to, if not exceed that of highly drawn melt-spun fibers.

Conclusion

We have obtained polarized Raman spectra for a single electrospun Nylon-6 nanofiber which indicate a significant degree of molecular orientation. These spectra qualitatively agree with those taken from drawn Nylon-6 film, and show features similar to those in previous studies on bundles of electrospun Nylon-6 (known to be in the γ crystalline form). We calculated the P2 and P4 orientation functions with the data we have obtained from individual fibers. The quality of the current quantitative results is limited by the spectra quality, and thus we sometimes obtain anomalous values for the orientation functions P2 and P4. Future work will focus on optimizing the experimental setup and acquiring spectra from a larger set of fibers in order to allow comparison between deposition parameters (take-up velocity, driving voltage, electrospinning solution, etc.). We have observed reproducible differences in the spectra taken from different fibers suggesting that this technique allows molecular orientation measurement from isolated, micron-length areas of individual nanofibers and may give insight into the uniformity of both the electrospinning process and the properties of the resulting nanofibers.

REFERENCES

1. Dror, Y.; Salalha, W.; Khalfin, R. L.; Cohen, Y.; Yarin, A. L.; Zussman, E., Carbon nanotubes embedded in oriented polymer nanofibers by electrospinning. *Langmuir* **2003,** 19, (17), 7012-7020.

2. Kakade, M. V.; Givens, S.; Gardner, K.; Lee, K. H.; Chase, D. B.; Rabolt, J. F., Electric Field Induced Orientation of Polymer Chains in Macroscopically Aligned Electrospun Polymer Nanofibers. *J. Am. Chem. Soc.* **2007,** 129, (10), 2777-2782.

3. Zussman, E.; Burman, M.; Yarin, A. L.; Khalfin, R.; Cohen, Y., Tensile deformation of electrospun nylon-6,6 nanofibers. *Journal of Polymer Science Part B: Polymer Physics* **2006,** 44, (10), 1482-1489.

4. Dersch, R.; Liu, T.; Schaper, A. K.; Greiner, A.; Wendorff, J. H., Electrospun nanofibers: Internal structure and intrinsic orientation. *Journal of Polymer Science Part A: Polymer Chemistry* **2003,** 41, (4), 545-553.

5. Catalani, L. H.; Collins, G.; Jaffe, M., Evidence for Molecular Orientation and Residual Charge in the Electrospinning of Poly(butylene terephthalate) Nanofibers. *Macromolecules* **2007,** 40, (5), 1693-1697.

6. Li, L.; Bellan, L. M.; Craighead, H. G.; Frey, M. W., Formation and properties of nylon-6 and nylon-6/montmorillonite composite nanofibers. *Polymer* **2006,** 47, (17), 6208.

7. Li, M.; Mondrinos, M. J.; Gandhi, M. R.; Ko, F. K.; Weiss, A. S.; Lelkes, P. I., Electrospun protein fibers as matrices for tissue engineering. *Biomaterials* **2005,** 26, (30), 5999-6008.

8. Bellan, L. M.; Kameoka, J.; Craighead, H. G., Measurement of the Young's moduli of individual polyethylene oxide and glass nanofibres. *Nanotechnology* **2005,** 16, (8), 1095-1099.

9. Huang, C.; Chen, S.; Lai, C.; Reneker, D.; H; Qiu, H.; Ye, Y.; Hou, H., Electrospun polymer nanofibres with small diameters. *Nanotechnology* **2006,** 17, (6), 1558-1563.

10. Reneker, D. H.; Yarin, A. L.; Hao, F.; Koombhongse, S., Bending instability of electrically charged liquid jets of polymer solutions in electrospinning. *Journal of Applied Physics* **2000,** 87, (9, pt.1-3), 4531-4547.

11. Shin, Y. M.; Hohman, M. M.; Brenner, M. P.; Rutledge, G. C., Electrospinning: A whipping fluid jet generates submicron polymer fibers. *Applied Physics Letters* **2001,** 78, (8), 1149-1151.

12. Shin, Y. M.; Hohman, M. M.; Brenner, M. P.; Rutledge, G. C., Experimental characterization of electrospinning: the electrically forced jet and instabilities. *Polymer* **2001,** 42, (25), 9955.

13. Li, D.; Xia, Y., Fabrication of titania nanofibers by electrospinning. *Nano Letters* **2003,** 3, (4), 555-560.

14. Stephens, J. S.; Chase, D. B.; Rabolt, J. F., Effect of the Electrospinning Process on Polymer Crystallization Chain Conformation in Nylon-6 and Nylon-12. *Macromolecules* **2004,** 37, (3), 877-881.

15. Kameoka, J.; Orth, R.; Yang, Y. N.; Czaplewski, D.; Mathers, R.; Coates, G. W.; Craighead, H. G., A scanning tip electrospinning source for deposition of oriented nanofibres. *Nanotechnology* **2003,** 14, (10), 1124-1129.

16. Song, K.; Rabolt, J. F., Polarized Raman Measurements of Uniaxially Oriented Poly(ε-caprolactam). *Macromolecules* **2001,** 34, (6), 1650-1654.

17. *Raman spectroscopy of gases and liquids*. Springer-Verlag: Berlin ; New York, 1979; p x, 318 p.

18. Fong, H.; Liu, W.; Wang, C.-S.; Vaia, R. A., Generation of electrospun fibers of nylon 6 and nylon 6-montmorillonite nanocomposite. *Polymer* **2002,** 43, (3), 775-

780.

19. Samon, J. M.; Schultz, J. M.; Wu, J.; Hsiao, B.; Yeh, F.; Kolb, R., Study of the structure development during the melt spinning of nylon 6 fiber by on-line wide-angle synchrotron X-ray scattering techniques. *Journal of Polymer Science Part B: Polymer Physics* **1999,** 37, (12), 1277-1287.

20. Liu, Y.; Cui, L.; Guan, F.; Gao, Y.; Hedin, N. E.; Zhu, L.; Fong, H., Crystalline Morphology and Polymorphic Phase Transitions in Electrospun Nylon-6 Nanofibers. *Macromolecules* **2007,** 40, (17), 6283-6290.

21. Huang, K.; Archer, L. A.; Fuller, G. G., Polarization-modulated Raman scattering measurements of nematic liquid crystal orientation. *Review of Scientific Instruments* **1996,** 67, (11), 3924-3930.

22. Purvis, J.; Bower, D. I., Molecular orientation in poly(ethylene terephthalate) by means of laser-raman spectroscopy. *Journal of Polymer Science: Polymer Physics Edition* **1976,** 14, (8), 1461-1484.

23. Jen, S.; Clark, N. A.; Pershan, P. S.; Priestley, E. B., Polarized Raman scattering studies of orientational order in uniaxial liquid crystalline phases. *The Journal of Chemical Physics* **1977,** 66, (10), 4635-4661.

24. Lefevre, T.; Rousseau, M. E.; Pezolet, M., Determination of molecular orientation in protein films and fibres by Raman microspectroscopy. *Canadian Journal of Analytical Sciences and Spectroscopy* **2005,** 50, (1), 41-48.

25. Rousseau, M. E.; Lefevre, T.; Beaulieu, L.; Asakura, T.; Pezolet, M., Study of Protein Conformation and Orientation in Silkworm and Spider Silk Fibers Using Raman Microspectroscopy. *Biomacromolecules* **2004,** 5, (6), 2247-2257.

26. George, T., Analysis of polarization measurements in Raman microspectroscopy. *Journal of Raman Spectroscopy* **1984,** 15, (2), 103-108.

27. Samori, B.; Thulstrup, E. W.; North Atlantic Treaty Organization. Scientific

Affairs Division., *Polarized spectroscopy of ordered systems*. Kluwer Academic Publishers: Dordrecht ; Boston, 1988; p vii, 578 p.

28. Salem, D. R.; Moore, R. A. F.; Weigmann, H. D., Macromolecular Order In Spin-Oriented Nylon-6 (Polycaproamide) Fibers. *Journal of Polymer Science Part B-Polymer Physics* **1987,** 25, (3), 567-589.

29. Salem, D. R., *Structure formation in polymeric fibers*. Hanser Gardner Publications: Cincinnati, 2001; p xiii, 578 p.

30. Vasanthan, N.; Ruetsch, S. B.; Salem, D. R., Structure development of polyamide-66 fibers during drawing and their microstructure characterization. *Journal of Polymer Science Part B-Polymer Physics* **2002,** 40, (17), 1940-1948.

31. Bellan, L. M.; Craighead, H. G.; Hinestroza, J. P., Direct measurement of fluid velocity in an electrospinning jet using particle image velocimetry. *Journal of Applied Physics* **2007,** 102, (9), 094308.

CHAPTER 4

MECHANICAL PROPERTIES OF SINGLE ELECTROSPUN FIBERS[3]

Introduction

Due to the strong elongational flow in an electrospinning jet, the resulting fibers may exhibit significant molecular orientation, which can cause their mechanical properties to differ from those of unoriented bulk material. We have determined the Young's moduli of suspended polyethylene oxide (PEO), polysiloxane, polydicyclopentadiene (PDCPD), DNA, and glass nanofibers by depressing them with an atomic force microscope (AFM) probe (Figure 4.1), a method previously used to measure Young's moduli of carbon nanotubes .[1-4] This method has also been used to determine mechanical properties of short suspended poly (L-lactic) acid (PLLA) fibers [5] and various biological materials.[6] In our study, the resulting force-displacement curves yield the Young's moduli if the additional tension in the fiber due to the electrospinning process is not large.

Methods

The polyethylene oxide nanofibers were extracted from a solution composed of PEO (MW 100,000) dissolved in a 50-50 mixture of water and ethanol. We used

[3] Reproduced in part with permission from Bellan, L. M.; Kameoka, J.; Craighead, H. G., Measurement of the Young's moduli of individual polyethylene oxide and glass nanofibres. *Nanotechnology* **2005,** 16, (8), 1095-1099. Copyright 2005 Institute of Physics.
Reproduced in part with permission from Bellan, L. M.; Coates, G. W.; Craighead, H. G., Poly(dicyclopentadiene) Submicron Fibers Produced by Electrospinning. *Macromolecular Rapid Communications* **2006,** 27, (7), 511-515. Copyright 2006 Wiley-VCH.
Reproduced in part with permission from Bellan, L. M.; Strychalski, E. A.; Craighead, H. G., Electrospun DNA nanofibers. *Journal of Vacuum Science & Technology B* **2007,** 25, 2255-2257. Copyright 2007 American Vacuum Society.

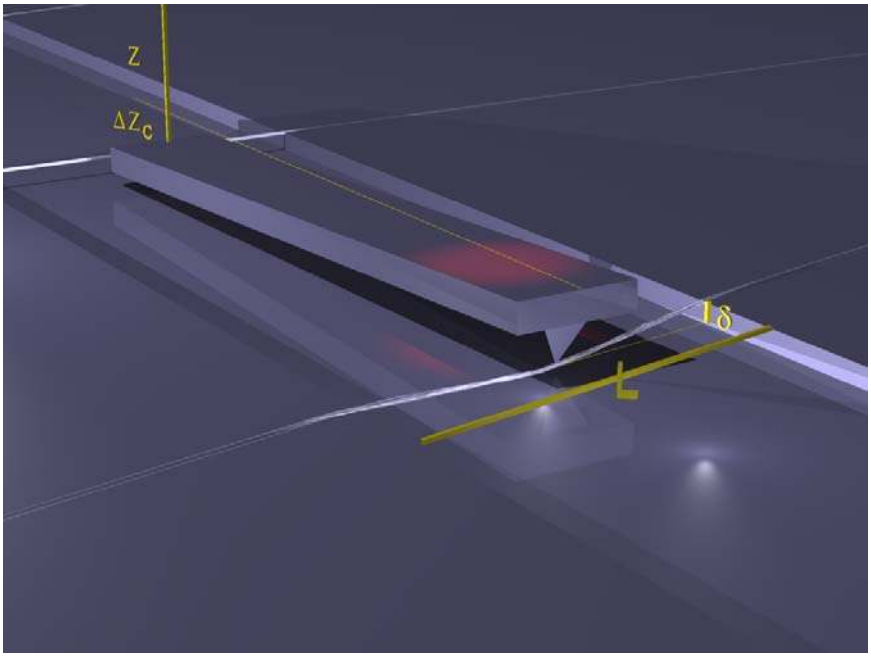

Figure 4.1-Schematic of an AFM tip depressing a suspended fiber

concentrations of 10%-20% PEO by weight. The PDCPD fibers were deposited using an electrospinning jet in which a ring opening metathesis polymerization reaction was occurring (Figure 4.2). In this system, the solidification of the jet was due to a chemical reaction, as opposed to the typical solidification process of solvent evaporation. The solution used for electrospinning the PDCPD fibers consisted of 1-2 mg of Grubbs 2nd generation catalyst (Materia) dissolved in 250 μL dichloromethane (Aldrich) mixed with 1 mL DCPD (Aldrich). These solution parameters were chosen so that the polymerization progressed slowly enough to allow for adequate processing time, but quickly enough to produce solidified fibers from the electrospinning jet. After approximately 5-10 minutes, drops of the solution were placed on the microfabricated Si tip used for electrospinning. DNA electrospinning solutions were made by mixing stock λ bacteriophage DNA solution (500 μg/mL, New England BioLabs) with the intercalating fluorescent dye YOYO-1 (Molecular Probes). In some

cases, the anti-photobleaching agent 2-Mercaptoethanol (Sigma) was added. The solution was gently mixed and then purified using a spin column (P-6 or P-30, Biorad Bio-Spin column). Polysiloxane and glass fibers were formed from a polysiloxane solution (Futurrex IC1-200) mixed with 6% (by weight) polyvinylpyrrolidone (PVP) (MW 1,300,000). Measurements were performed on these fibers both directly after deposition (polysiloxane fibers) and after baking in air at 850° C for 6 hours (glass fibers).

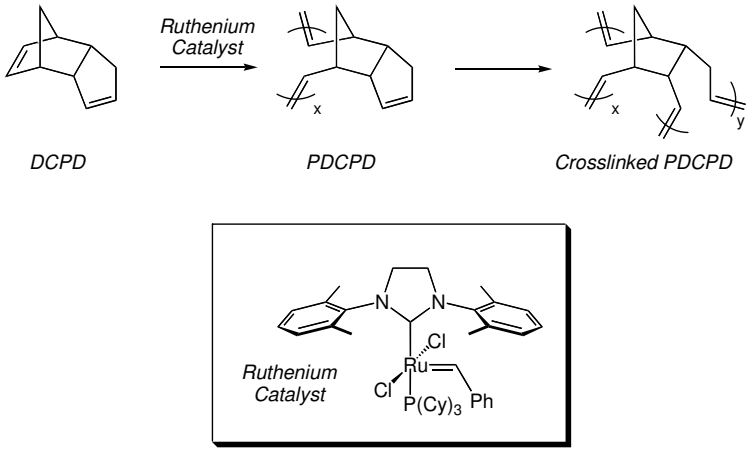

Figure 4.2-Polymerization of DCPD and crosslinking of PDCPD using ruthenium catalyst.

To form the fibers, a drop of solution was placed on a gold-coated microfabricated silicon tip that was kept at a high voltage (5-10 kV) relative to a grounded plate behind the substrate. In this experiment, the substrate consisted of a silicon or fused silica chip in which several trenches had been etched. The trenches were 10-80 μm wide and 5-10 μm deep. We used the scanned electrospinning technique[7] (Figure 3.2), whereby the substrate and plate are rotated, allowing us to orient the fibers relative to the trenches in the substrate (Figure 4.3a). Scanning electron microscope (SEM) imaging of the resulting fibers indicated that some fibers were fully suspended over the trench while others sagged into the trench and touched

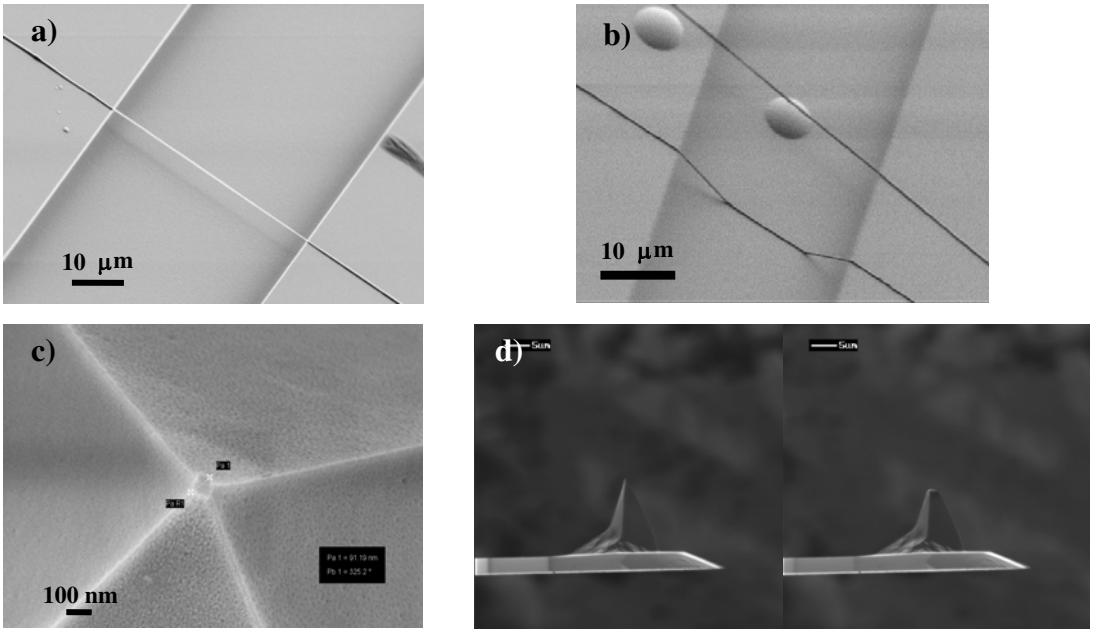

Figure 4.3- a) SEM image of a suspended PEO fiber, b) SEM image of suspended and drooping PEO fibers, c) SEM image of AFM probe tip. The flat surface at the tip is approximately 100nm wide. Since the diameters of the fibers were in the 100-300 nm range, it is unlikely that the AFM tip penetrated the fiber during the force curve measurement, d) FIB images of an AFM probe before and after milling (scale bar is 5 μm).

the bottom (Figure 4.3b). These variations are due to changes in electrospinning conditions during the deposition process.

Force curves were obtained using an AFM (Dimension 3000, Digital Instruments (DI)) operated in contact mode. Because we measured fibers with different suspended lengths, the resulting restoring forces experienced by the AFM probe varied significantly among fibers. We had to choose the AFM probe spring constants to translate the restoring forces to deflections in the AFM measurement range. We used a DI DNP-S probe with a nominal spring constant of 0.58 N/m, a DI TESP probe with a spring constant of approximately 50 N/m, NanoSensors FM probes

with calculated spring constants of ~1.7 N/m, and NanoSensors EFM probes with calculated spring constants of ~3.8 N/m. The tips were dulled by strongly tapping them with the AFM against a hard Si substrate for more than 20 minutes or by using a focused ion beam (FIB) (FEI 611 Focused Ion Beam System) to mill away the sharper section of the AFM probe. The resulting radii of curvature of the tips were comparable to the fiber diameters, and thus it was unlikely that they would penetrate the fiber (Figures 4.3c and 4.3d).

Variations in the geometry and material properties of the probe can cause the actual spring constant to be larger or smaller than the manufacturer's specification by an order of magnitude. Thus, it is important to calibrate the spring constant of the cantilever each time an AFM probe is put on the AFM scanner head. Several methods for calibrating AFM probe spring constants exist in the literature.[8] If the material properties and geometry of the cantilever are known (and the probe of interest is a rectangular cantilever), one can use the standard expression for the spring constant of a rectangular cantilever from Euler-Bernoulli theory, $k = Ewt^3 / 4L^3$, where k is the spring constant, E is the Young's modulus, and w, t, and L are the cantilever width, thickness, and length, respectively. One can also use the resonant frequency of the cantilever, $f \approx (t / 2\pi L^2)\sqrt{(E / \rho)}$ where ρ is the density of the cantilever material, to avoid having the measure the thickness of the cantilever; this yields the relation $k \approx 2w(f\pi L\sqrt{\rho})^3 / \sqrt{E}$.[9] If one does not want to rely upon measurements of the cantilever material properties, several other calibration techniques are possible. A known static force can be applied to the cantilever (often using a reference cantilever), and the deflection measured, yielding the spring constant of the cantilever.[10] Using the equipartition theory, one can extract the spring constant of a cantilever from the power spectrum of the thermal motion using $k < z_c^2 >= k_b T$ where $< z_c^2 >$ is the mean square displacement of the cantilever, k_b is Boltzman's constant, and T is the

temperature.[11] Recent AFM hardware and software now has the ability to perform this calibration automatically. The cantilever can also be driven at resonance, and by observing how the frequency shifts as test masses are added to the cantilever (for example, by gluing small reference spheres to the end of the probe), one can calculate the spring constant; this method is often called the "Cleveland method."[9] Finally, using the "Sader method", one can calculate the spring constant knowing the cantilever geometry, resonance frequency and quality factor, and the density and viscosity of the fluid in which the cantilever is resonating.[12]

We calibrated the spring constants of our AFM probes using reference cantilevers from Digital Instruments (model CLFC-NOBO). Each calibration yielded spring constant values with a statistical error of less than 10% and as small as 2%. The resulting values for the spring constant varied for the same probe used in different sittings. The calibrated spring constant values varied by up to 80% from the manufacturers specifications. Moreover, due to drift of the position of the laser spot on the cantilever, we observed the effective spring constant vary by 10% during a 1 hour sitting. Unfortunately, recent discussions with collaborators who have had the opportunity to compare different sets of CLFC-NOBO reference cantilevers have indicated that the numbers provided by the manufacturer for the spring constants of the reference cantilevers are incorrect, sometime by up to a factor of two.[4] For all the data presented in this work, the probe spring constants were calibrated with the same reference cantilever, and so it is possible to compare the datasets to each other. However, since the provided spring constant for the reference cantilever may be incorrect, comparisons to data from other sources must be taken with a grain of salt. The reader is advised to avoid using these reference cantilevers for any future work and to use another spring constant calibration method.

[4] Personal correspondence with Prof. David Tannenbaum at Pomona College.

In order to determine the cross-sectional area of the fibers, we assumed that the fibers had a circular cross-section and used the maximum height of the fiber above the substrate as measured by the AFM as the diameter. All fibers measured appeared to have a roughly constant diameter when imaged by a SEM, and we have verified that the cross sections of several fibers are approximately circular by cleaving them and imaging the cross section with a SEM. Because the fibers were not necessarily oriented perfectly perpendicular to the trenches, to calculate the length of the fiber suspended across the trench we assumed that the fiber did not sag and measured both the width of the trench (using the AFM) and the angle of the fiber with respect to the trench walls (using the vision system of the AFM). The AFM probe was aligned to the center of the suspended fiber (L/2) using the vision system. To check that the fibers were firmly anchored at the trench edges, several fibers were laterally displaced with the AFM tip distances of at least 5 microns while watching for slipping with the AFM vision system. No movement was observed.

Raw AFM data were translated to force-displacement curves by converting tip deflection ΔZ_c to force using the cantilever spring constant and converting the height of the AFM probe, Z, to fiber displacement δ using $\delta(Z)=(Z-Z_0)-\Delta Z_c$ where Z_0 is the AFM Z position of initial contact point.[3] The shape of the resulting force curve depends on the initial tension in the suspended fibers. If no tension is assumed, we may use the standard cubic equation for the displacement of a suspended elastic string with fixed ends (in the small deflection approximation)

$$F = 8AE(\delta/L)^3 \tag{4.1}$$

where A is the cross sectional area of the fiber, E is the Young's modulus of the fiber, and L is the suspended length of the fiber. [13] This equation describes the force due to elongation of the string caused by displacement at L/2. In this model we assume that the material is linearly elastic. If there is an additional initial tension in the fiber

T_0 (e.g. stretching due to the motion of the substrate being faster than the polymer jet velocity), then there is an additional linear term yielding

$$F = 8AE(\delta/L)^3 + 4T_0(\delta/L) \tag{4.2}$$

Thus, the force curve may be predominantly linear or cubic, depending on the relative contributions of the initial tension and the tension produced by the AFM tip displacement. If the linear tension term is too strong, the data will reach the AFM's deflection limit before the cubic dependence can manifest itself enough to get a well-defined value for the 3rd order term. Another linear term will arise due to bending of the fiber at the point of contact with the AFM tip, but for our fiber diameters and deflection ranges the forces caused by elongation dominate those caused by bending for the majority of the data range. Because there may be a variety of contributions to terms lower than 3rd order (e.g. additional tension, errors in setting the initial contact point appropriately, forces due to bending), we find it is safest to extract the Young's modulus from the cubic term. All data were fit to 3rd order polynomials so as to account for lower order terms. Sources of error among results for different fibers include variation in fiber cross sectional area, inaccuracies in the measurement of the suspended length L (including the possibility of sagging fibers), possible slipping of fibers during depression, and any difference between the center of the trench and the point of contact between the AFM tip and the fiber. Due to the aspect ratio of the suspended fiber, and given the contact area between the AFM probe and fiber and the resulting forces, transverse deformation of the suspended fiber is not likely to have a significant effect in these measurements.

Results

Figure 4.4a shows an example of measured PEO force curves when the additional tension term is negligible. The data fit well to the predicted 3rd order

polynomial model, and yielded a Young's modulus of ~7.6 GPa from the cubic term. It is interesting to note that the cubic dependence is seen not only when the fiber is depressed ($Z<Z_0$), but also in the region of the curve corresponding to the fiber sticking to the AFM tip as the tip retracts from the surface. Figure 4.4b shows an example of a measured force curve for a glass fiber with Young's modulus ~186 GPa. The TESP tip used stuck to the fibers only slightly during the retracting cycle of the curve. The glass fibers were found to sag several hundred nanometers in the center of the trench. While this does not affect the fiber length measurement significantly, it does change the shape of the force-displacement curve. The flat region in the retracting curve shown corresponds to the AFM tip motion taking up the slack in the fiber. Because of this flat region a piecewise model, consisting of two third order polynomials separated by a line, was used to fit the data. The fit parameters included the position of intervals.

Discussion

PEO fibers

Several force curves were generated for each fiber. Our data for PEO fibers indicate no significant dependence of Young's modulus on fiber diameter, though recent experiments with other materials systems sometimes do show a dependence on diameter.[14] The average value of Young's modulus for the PEO fibers is 7.0 ± 0.5 GPa, which is larger than what has been previously seen in PEO thin films (0.2-5.0 GPa) [15] and in highly crystalline bulk material (0.29 GPa) .[16] The chain modulus of PEO has been measured using several techniques including Raman and X-ray experiments and yielded ~13 GPa .[17] Some of the PEO fibers have Young's moduli of up to ~20 GPa, which is above the theoretical limit of the chain modulus. This may

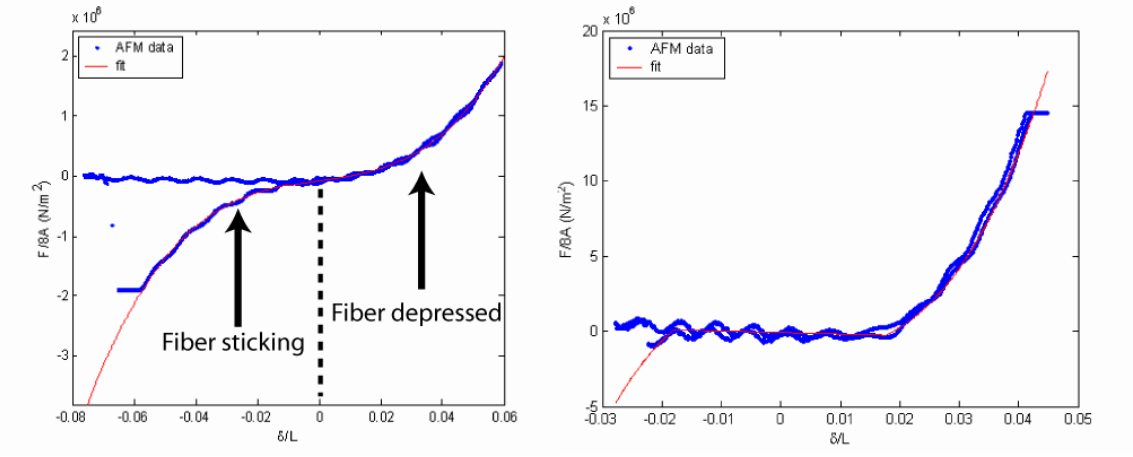

Figure 4.4- a) Typical force-displacement curve for suspended polymeric nanofiber with no significant additional tension. The displacement is arbitrarily set to zero at the contact point. The slight oscillation in the signal is an artifact produced by the AFM due to changes in the optical path length traveled by the laser. b) Typical force-displacement curve for suspended spin-on glass nanofiber. The fit is a piecewise function consisting of two 3rd order polynomials separated by a line to take into account the zero-deflection region due to the fiber sagging.

be due to any difference between the contact position of the AFM tip on the fiber and the center of the trench. Since we assumed that the contact position was at L/2, an offset of 10% from center will cause the Young's modulus to appear 25% larger, and an offset of 20% will cause it to appear 150% larger. An error of 15% was used in the error analysis. The fact that the average Young's modulus of the PEO fibers is significantly larger than bulk and film values suggests that the molecules in the fibers are oriented parallel to the fiber axis. This hypothesis is supported by previous X-ray diffraction studies on bundles of electrospun nanofibers which also show a high degree of molecular orientation ,[18] as well as the results of chapter 3.

Polysiloxane and glass fibers

The resulting average value of Young's modulus for the glass fibers was 240 ± 90 GPa, which agrees with previously published data on the resonant frequency of suspended glass nanofibers produced by electrospinning [19] if we assume negligible tension and use

$$E = (\frac{16\rho}{d^2})(\frac{2\pi f L^2}{4.73^2})^2 \quad (4.3)$$

where E is the Young's modulus, ρ is the density of the material, d is the diameter of the fiber, f is the resonant frequency, and L is the suspended length of the fiber.[20] The average Young's modulus of fibers formed from polysiloxane appears to increase by about a factor of 10 during the baking process. Previous studies observed that the resonant frequency of similar structures roughly doubled after a similar curing process, though the scaling behavior in that study implied that tension was not negligible for those structures.[21] If we again use the model that assumes negligible tension, the relation $f \propto \sqrt{E/\rho}$ implies that the density of the glass fibers must increase slightly during the curing process. This increase has been observed in HSQ thin films.[22]

PDCPD fibers

Images of suspended PDCPD fibers are shown in Figure 4.5. The Young's moduli were measured for several different PDCPD fibers, yielding an average value of 11±5 GPa. Values of the Young's modulus for bulk PDCPD range from 2-3 GPa in the manufacturer's literature.[23] We conducted a tensile test on a bulk PDCPD sample (0.1004" x 0.1892" x 0.638") using an Instron 1125 mechanical test system, which yielded a Young's modulus of 768 MPa.

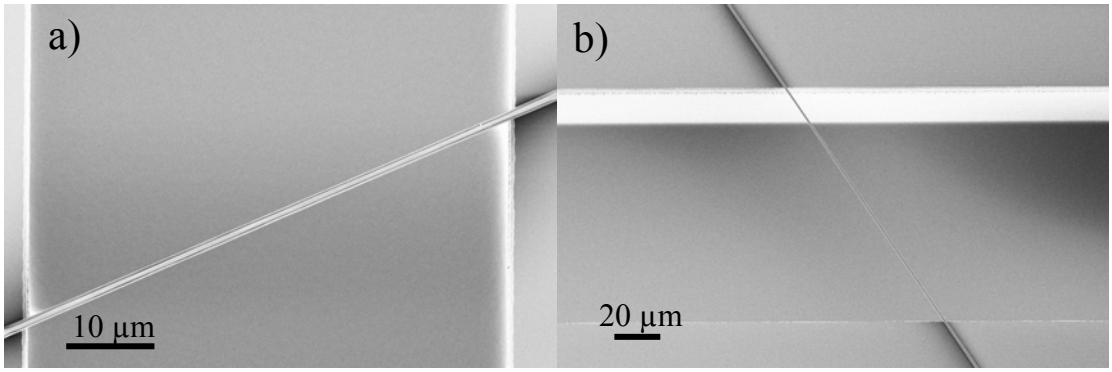

Figure 4.5- SEM images of suspended PDCPD fibers

DNA fibers

Images of a typical DNA nanofiber are shown in Figure 4.6. To measure force curves on electrospun DNA nanofibers, we had to use a combined AFM/fluorescence microscope system (Digital Instruments Bioscope AFM mounted on Olympus IX-70 microscope with a Photometrics Cascade 512b camera), as the fibers were too small to see (~30 nm diameter) with the standard brightfield imaging system. From this data (19 curves from the same fiber) we calculate a Young's modulus of 15 ± 2 GPa. Previous studies investigating mechanical properties of single DNA molecules in solution have concluded that the Young's modulus of native λ DNA is of the order of 10^8 Pa, about two orders of magnitude less than the values we calculate.[24, 25] However, our material is not a single molecule of pure DNA but bulk DNA labeled with the intercalating dye YOYO-1, and is not dissolved in solution but in a solid fiber formed from an elongational flow. It is known that the binding of an intercalating molecule such as YOYO-1 affects the contour length of the DNA molecule and can change the molecule's response to external forces.[26-29] The elastic behavior of DNA in solution is complex and dependent on solution properties such as ionic strength and type of ion (monovalent or multivalent) present.[29, 30] This complexity

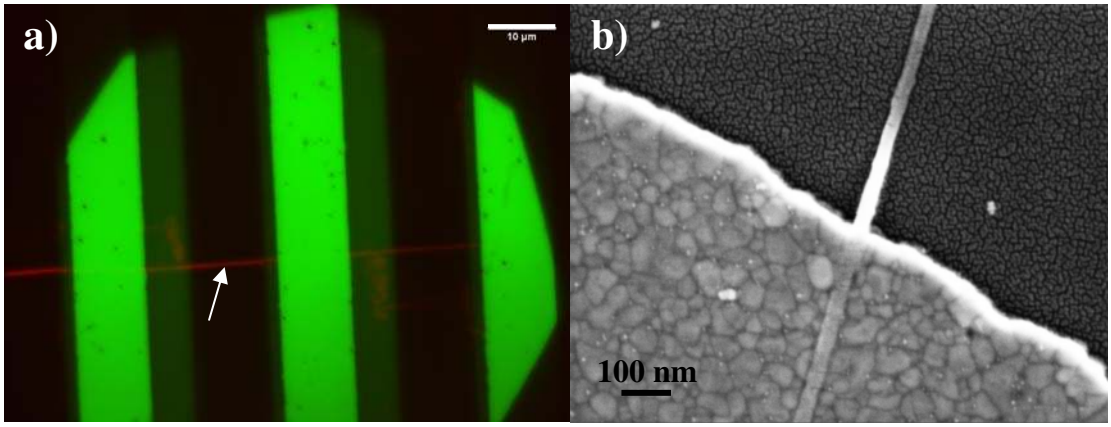

Figure 4.6- a) False color image of DNA nanofiber (red) over Au electrodes (bright green) and trenches (black). The green color channel is from a brightfield image, and the red color channel is from a fluorescence image. The white arrow points to the fiber. b) SEM image of DNA nanofiber on Au electrode (bottom left) and oxide (upper right)

even in solution suggests that comparison of the elastic behavior of single molecules in solution and bundles of molecules in air is not at all straightforward, and the behaviors of the two systems need not necessarily agree. Indeed, for the structure we have measured we assume a linear elastic response, whereas studies of single molecules of DNA reveal much more complex behavior.[30]

Conclusion

We measured the Young's moduli of suspended PEO, PDCPD, DNA, polysiloxane, and glass nanofibers by depressing them with an AFM tip and recording the force vs. displacement data. The shape of the resulting force curves will depend significantly on any sagging of the fiber as well as the relative forces due to tension caused by the AFM tip and initial tension in the fiber. The Young's moduli of PEO

fibers with little additional tension on average exceed values given in previous studies of the Young's moduli of PEO thin films. The Young's moduli of glass fibers agreed with previously measured values for resonant frequencies of similar structures.

REFERENCES

1. Salvetat, J. P.; Briggs, G. A. D.; Bonard, J. M.; Bacsa, R. R.; Kulik, A. J.; Stockli, T.; Burnham, N. A.; Forro, L., Elastic and shear moduli of single-walled carbon nanotube ropes. *Physical Review Letters* **1999,** 82, (5), 944-947.

2. Salvetat, J. P.; Kulik, A. J.; Bonard, J. M.; Briggs, G. A. D.; Stockli, T.; Metenier, K.; Bonnamy, S.; Beguin, F.; Burnham, N. A.; Forro, L., Elastic modulus of ordered and disordered multiwalled carbon nanotubes. *Advanced Materials* **1999,** 11, (2), 161-165.

3. Tombler, T. W.; Zhou, C. W.; Alexseyev, L.; Kong, J.; Dai, H. J.; Lei, L.; Jayanthi, C. S.; Tang, M. J.; Wu, S. Y., Reversible electromechanical characteristics of carbon nanotubes under local-probe manipulation. *Nature* **2000,** 405, (6788), 769-772.

4. Walters, D. A.; Ericson, L. M.; Casavant, M. J.; Liu, J.; Colbert, D. T.; Smith, K. A.; Smalley, R. E., Elastic strain of freely suspended single-wall carbon nanotube ropes. *Applied Physics Letters* **1999,** 74, (25), 3803-3805.

5. Tan, E. P. S.; Lim, C. T., Physical properties of a single polymeric nanofiber. *Applied Physics Letters* **2004,** 84, (9), 1603-1605.

6. Xu, W.; Mulhern, P. J.; Blackford, B. L.; Jericho, M. H.; Templeton, I., A New Atomic-Force Microscopy Technique For The Measurement Of The Elastic Properties Of Biological-Materials. *Scanning Microscopy* **1994,** 8, (3), 499-506.

7. Kameoka, J.; Orth, R.; Yang, Y. N.; Czaplewski, D.; Mathers, R.; Coates, G. W.; Craighead, H. G., A scanning tip electrospinning source for deposition of oriented nanofibres. *Nanotechnology* **2003,** 14, (10), 1124-1129.

8. Ohler, B., Practical Advice on the Determination of Cantilever Spring Constants. In *Veeco Applications Note AN94*, 2007; pp 1-12.

9. Cleveland, J. P.; Manne, S.; Bocek, D.; Hansma, P. K., A nondestructive

method for determining the spring constant of cantilevers for scanning force microscopy. *Review of Scientific Instruments* **1993,** 64, (2), 403-405.

10. Tortonese, M.; Kirk, M. In *Characterization of application specific probes for SPMs*, San Jose, CA, USA, 1997; SPIE-Int. Soc. Opt. Eng: San Jose, CA, USA, 1997; pp 53-60.

11. Hutter, J. L.; Bechhoefer, J., Calibration of atomic-force microscope tips. *Review of Scientific Instruments* **1993,** 64, (7), 1868-1873.

12. Sader, J. E.; Chon, J. W. M.; Mulvaney, P., Calibration of rectangular atomic force microscope cantilevers. *Review of Scientific Instruments* **1999,** 70, (10), 3967-3969.

13. Timoshenko, S., *Strength of Materials*. 2nd ed.; Van Nostrand: New York, 1940.

14. Li, L.; Bellan, L. M.; Craighead, H. G.; Frey, M. W., Formation and properties of nylon-6 and nylon-6/montmorillonite composite nanofibers. *Polymer* **2006,** 47, (17), 6208.

15. Nie, H. Y.; Motomatsu, M.; Mizutani, W.; Tokumoto, H., Local Modification Of Elastic Properties Of Polystyrene-Polyethyleneoxide Blend Surfaces. *Journal Of Vacuum Science & Technology B* **1995,** 13, (3), 1163-1166.

16. Warfield, R. W.; Barnet, F. R., Elastic-Constants Of Bulk Polymers. *Angewandte Makromolekulare Chemie* **1972,** 27, (DEC19), 215-217.

17. Song, K.; Krimm, S., Elastic-Modulus Of Poly(Ethylene Oxide) Determined From The Raman Longitudinal Acoustic Mode. *Journal Of Polymer Science Part B-Polymer Physics* **1990,** 28, (1), 63-69.

18. Dror, Y.; Salalha, W.; Khalfin, R. L.; Cohen, Y.; Yarin, A. L.; Zussman, E., Carbon nanotubes embedded in oriented polymer nanofibers by electrospinning. *Langmuir* **2003,** 19, (17), 7012-7020.

19. Kameoka, J.; Verbridge, S. S.; Liu, H. Q.; Czaplewski, D. A.; Craighead, H. G., Fabrication of suspended silica glass nanofibers from polymeric materials using a scanned electrospinning source. *Nano Letters* **2004,** 4, (11), 2105-2108.

20. Timoshenko, S.; Young, D. H.; Weaver, W., *Vibration problems in engineering*. 4th ed.; Wiley: New York,, 1974; p xiii, 521.

21. Tanenbaum, D. M.; Olkhovets, A.; Sekaric, L., Dual exposure glass layer suspended structures: A simplified fabrication process for suspended nanostructures on planar substrates. *Journal Of Vacuum Science & Technology B* **2001,** 19, (6), 2829-2833.

22. Liou, H.-C.; Dehate, E.; Duel, J.; Dall, F. In *Curing study of hydrogen silsesquioxane under H_2/N_2 ambient*, San Francisco, CA, USA, 2001; Mater. Res. Soc: San Francisco, CA, USA, 2001; p 1.

23. Neat Resin Properties. In *Technical Data Sheet for PDCPD*, Materia Incorporated.

24. Shivashankar, G. V.; Libchaber, A., Single DNA molecule grafting and manipulation using a combined atomic force microscope and an optical tweezer. *Applied Physics Letters* **1997,** 71, (25), 3727-3729.

25. Gevorkian, S. G.; Khudaverdian, E. E., Mechanical properties of DNA films. *Biopolymers* **1990,** 30, (3-4), 279-285.

26. Bennink, M. L.; Schärer, O. D.; Kanaar, R.; Sakata-Sogawa, K.; Schins, J. M.; Kanger, J. S.; Grooth, B. G. d.; Greve, J., Single-molecule manipulation of double-stranded DNA using optical tweezers: Interaction studies of DNA with RecA and YOYO-1. *Cytometry* **1999,** 36, (3), 200-208.

27. Cluzel, P.; Lebrun, A.; Heller, C.; Lavery, R.; et al., DNA: An extensible molecule. *Science* **1996,** 271, (5250), 792.

28. Husale, S.; Grange, W.; Hegner, M., DNA Mechanics Affected by Small DNA

Interacting Ligands. *Single Molecules* **2002,** 3, (2-3), 91-96.

29. Smith, S. B.; Finzi, L.; Bustamante, C., Direct mechanical measurements of the elasticity of single DNA molecules by using magnetic beads. *Science* **1992,** 258, (5085), 1122-1126.

30. Baumann, C. G.; Smith, S. B.; Bloomfield, V. A.; Bustamante, C., Ionic effects on the elasticity of single DNA molecules. *PNAS* **1997,** 94, (12), 6185-6190.

CHAPTER 5

ELECTROSPINNING JETS AS A TOOL TO ORIENT AND STRETCH MOLECULES[5]

Introduction

There has been much work investigating techniques to stretch DNA molecules in order to both better understand the molecular dynamics and develop single molecule genomic analysis techniques. In many of these techniques, one end of the DNA molecules is bound to a surface while the other is manipulated with a controllable force using, for example, magnetic tweezers,[1] optical tweezers,[2-4] or an atomic force microscope (AFM) probe.[5, 6] The DNA molecules may also be stretched by immobilizing one end and allowing the molecule to experience a hydrodynamic flow.[1, 7] Other methods for stretching DNA molecules include forcing them into nanochannels,[8, 9] molecular combing,[10] and causing them to experience elongational flow.[11-15] The majority of these techniques do not result in molecules that remain stretched after the experiment or can only stretch a few molecules at a time. None of these techniques produce stretched DNA molecules encapsulated in a protective medium that can be subsequently manipulated and analyzed optically or mechanically. In the present study we utilize the elongational flow of an electrospinning jet to simultaneously stretch DNA molecules and encapsulate them in a polymeric nanofiber for subsequent investigation and manipulation.

[5] Reproduced in part with permission from Bellan, L. M.; Cross, J. D.; Strychalski, E. A.; Moran-Mirabal, J.; Craighead, H. G., Individually Resolved DNA Molecules Stretched and Embedded in Electrospun Polymer Nanofibers. *Nano Letters* **2006,** 6, (11), 2526-2530. Copyright 2006 American Chemical Society.

Because of the wide variety of biocompatible polymers that can be electrospun into fibers and the lack of harsh chemical processes involved, there is interest in using the electrospinning technique for biological applications such as tissue scaffolding[16] and drug delivery.[17] Biological entities such as viruses[18] and enzymes[19] have been incorporated into electrospun nanofibers. Due to the large strain rates in electrospinning jets, the resulting fibers are thought to contain highly oriented polymer molecules,[20] and previous studies have shown that electrospinning can be used to orient anisotropic particles such as carbon nanotubes[21, 22] and CdS nanowires[23] embedded in the resulting polymer fiber.

Two previous studies have demonstrated the ability to electrospin nanofibers of DNA[24] and single partially-stretched large (200-900 kbp) DNA molecules.[25] In the first study, the fibers consisted only of DNA and were much larger than single molecules. In the second study, extremely large single DNA molecules were deposited on a mica surface. A third study has shown that DNA molecules incorporated into electrospun nanofiber membranes can be released and can be structurally intact and bioactive.[26] Here we demonstrate the ability to produce polymeric nanofibers containing isolated stretched λ DNA molecules. This is the first direct observation of orientation and elongation of individual polymer molecules in an electrospun nanofiber.

Theory

Consider a polymer molecule of N monomers each of length a, existing in three dimensions with end-to-end vector of $\vec{R}$. As each dimension (x,y, and z) is independent, the probability distribution function for this polymer can be approximated (in the large N limit) by the product of three one-dimensional Gaussian probability distributions[27]

$$P_{3d}(N,\vec{R}) = P_{1D}(N,x)P_{1D}(N,y)P_{1D}(N,z) = \frac{1}{(2\pi)^{3/2}(\langle x^2\rangle\langle y^2\rangle\langle z^2\rangle)^{1/2}}\exp(\frac{-1}{2}(\frac{x^2}{\langle x^2\rangle}+\frac{y^2}{\langle y^2\rangle}+\frac{z^2}{\langle z^2\rangle})) \quad (5.1)$$

where $\langle \mathrm{x}^2\rangle = \langle \mathrm{y}^2\rangle = \langle \mathrm{z}^2\rangle = \langle \vec{\mathrm{R}}^2\rangle/3 = Na^2/3$ are the random walk mean-square displacements in each of the three directions. Because $\mathrm{x}^2 + y^2 + z^2 = |\vec{R}|^2$, the probability distribution function in 3D can be written as

$$P_{3d}(N,\vec{R}) = (\frac{3}{2\pi Na^2})^{3/2}\exp(\frac{-3|\vec{R}|^2}{2Na^2}) \quad (5.2)$$

This probability distribution can be written in terms of the number of configurations $\Omega(N,\vec{R})$ for a given $\vec{R}$, i.e. $P_{3d}(N,\vec{R}) = \Omega(N,\vec{R})/\int\Omega(N,\vec{R})d\vec{R}$. Thus the entropy associated with a particular configuration is given by

$$S = k_b \ln\Omega = \frac{3}{2}k_b \ln(\frac{3}{2\pi Na^2}) - \frac{3k_b|\vec{R}|^2}{2Na^2} + k_b \ln\int\Omega(N,\vec{R})d\vec{R} \quad (5.3)$$

Because the entropy is a function of the end-to-end vector, there is an entropic force associated with each configuration given by $\vec{f} = -T\nabla S = 3k_bT\vec{R}/Na^2$ This force "pulls" the molecule back to the $\vec{R} = 0$ state, and is proportional to $\vec{R}$; thus one can think of this system as a Hookean spring with spring constant $k = 3k_bT/Na^2$. This derivation for an ideal chain holds for small extensions ($|\vec{R}| < Na$, when the Gaussian approximation is good). For double-stranded DNA (dsDNA), for which the worm-like chain model is appropriate, the behavior for both large and small extensions can be approximated by the asymptotic expression[27-29]

$$\frac{fa}{k_bT} \approx 2\frac{|\vec{R}|}{Na} + \frac{1}{2}(\frac{Na}{Na-|\vec{R}|})^2 - \frac{1}{2} \quad (5.4)$$

There are different models of polymer systems that allow the calculation of a characteristic relaxation time for the polymer chain. The Rouse model[30] may be used to describe a molecule under "freely draining" conditions, under which the

hydrodynamic interactions are small. This model is used for longer length scales. The Zimm model[31] takes into account hydrodynamic interactions between sections of the polymer chain ("nondraining"). This model is more appropriate for molecules that are in relatively unextended configurations. For entangled polymer solutions, the reptation model of deGennes[32] applies. The relaxation times for the three models are:

$$\tau_{Rouse} = \frac{6M\eta_s[\eta]}{\pi^2 RT} \qquad \tau_{Zimm} = \frac{0.422M\eta_s[\eta]}{RT} \qquad \tau_{deGennes} \approx \tau_{Rouse} * \frac{N}{N_e} \quad (5.5abc)$$

where M is the polymer molar mass, η_s is the solvent viscosity, $[\eta]$ is the intrinsic viscosity of the polymer, R is the universal gas constant, N is the number of Kuhn monomers, and N_e is the number of Kuhn monomers per entanglement.

There has been significant work studying the intrinsic viscosity of DNA, which allows the calculation of the relaxation time of a polymer molecule in a solution of known viscosity.[15, 33-36] The typical experiment performed to obtain this value involves measuring the viscosity of various dilute concentrations of the polymer and extrapolating to zero concentration according to

$$[\eta] = \lim_{c \to 0} \frac{\eta / \eta_s - 1}{c} \quad (5.6)$$

where η is the solution viscosity. For linearized λ dsDNA in simple buffers, the values in the literature range from ~13200 mL/g to ~16000 mL/g, depending on the buffer, salt concentration, and how closely to $c = 0$ the experimenters got. Once the intrinsic viscosity is known, one can calculate the relaxation modes for the polymer according to one of the relaxation time equations given above (eq. 5.5).

Given the relaxation behavior described above, one can predict the behavior of a single polymer molecule in various fluid dynamic environments. An elongational flow, such as an electrospinning jet, has a time scale described by the strain rate $\dot{\varepsilon}$ which may vary as a function of position and time. For example, consider the uniaxial elongational flow described by $\vec{v} = (-\dot{\varepsilon}x, -\dot{\varepsilon}y, 2\dot{\varepsilon}z)$ where $\dot{\varepsilon} > 0$. Along the axis of

elongation $\hat{z}$, $\vec{v} = 2\dot{\varepsilon}z\hat{z} = (dz/dt)\hat{z}$, and so $z = Ce^{\dot{\varepsilon}t}$ describes the flow, where C is set by initial conditions. A pair of particles on the z axis, initially at points $l/2$ and $-l/2$ (initial separation *l*) will move according to $z_{\pm} = \pm(l/2)e^{\dot{\varepsilon}t}$, and thus the separation $s = z_+ - z_- = le^{\dot{\varepsilon}t}$ increases exponentially.[37] Larson and Magda have shown that a polymer molecule will transition from a coiled state to a stretched state when the timescale of the flow, $\dot{\varepsilon}$, is comparable to the longest relaxation time τ of the polymer molecule. More specifically, this transition should occur when the Deborah number $De = \dot{\varepsilon}\tau \approx 0.5$.[12, 38]

Methods

The solution used for electrospinning was produced in several steps described below. First, 15 μL of stock λ bacteriophage DNA (New England BioLabs) solution was added to a solution of 1500 μL of buffer (10mM HEPES, 10mM NaCl) and 1.5 μL of stock YOYO-1 fluorescent dye solution (Molecular Probes), yielding a nominal labeling ratio of 7.6:1. This solution was incubated at 65 ºC for 15-20 minutes to linearize the DNA and then filtered through BioSpin 6 spin columns (Bio-Rad) to remove unincorporated dye. We added 100 μL of this solution to 900 μL of buffer (10mM HEPES, 10mM NaCl), 20 mg poly-L-aspartic acid (Sigma P6762) and 20-100 mg DABCO (Sigma). The poly-L-aspartic acid was added to prevent the DNA from collapsing into bundles.[39] The DABCO was added to reduce photobleaching.[40] This solution was gently mixed for several minutes. Finally, 200 mg of polyethylene oxide (PEO) (MW 100,000, Sigma) was added and the solution was gently mixed overnight to allow the polymer to fully dissolve. PEO is one of the most common polymers used in electrospinning experiments due to its biocompatibility, solubility in water, and ease of electrospinning. The above procedure yields a DNA concentration of roughly 3.7×10^{10} molecules per cm^3 of solid, corresponding to a linear density of

approximately 1 molecule/mm for 200nm diameter fibers. We also made control solutions that were identical to the above solution except that they lacked a) labeled DNA or b) poly-L-aspartic acid.

Nanofibers were deposited using the scanned electrospinning method[41] (Figure 3.2), allowing us to orient and isolate the fibers. The electrospinning tip was a microfabricated silicon chip coated with a thin gold layer. Drops of the solution were manually placed on the electrospinning tip before turning on the electrospinning voltage source. The electrospinning was performed for only a short period of time (less than a minute) in order to collect isolated fibers, and thus the droplet did not require a continuous flow of solution. We used a voltage of 7-10 kV over a distance of about 4 cm to form the electrospinning jet. The resulting fiber diameters varied from approximately 100-350 nm as measured by AFM.

Results and Discussion

The water-soluble fibers were spun on glass coverslips so that they could be imaged from below with a 60x 1.20 NA water-immersion objective. The resulting fibers were imaged using an inverted fluorescence microscope (Olympus IX70, EXFO X-cite 120 illuminator, Omega XF100-2 filter cube) using a Cascade 512b EMCCD camera (Roper Scientific). Examples of the resulting images are shown in Figure 5.1 a)-c). We also electrospun fibers from two control solutions that were identical to the sample solution except that they lacked a) labeled DNA (Figure 5.1d) or b) poly-L-aspartic acid (Figure 5.1e). Because the fibers formed from the solution lacking DNA showed no isolated discrete fluorescent lines (other than uniform background fluorescence from the PEO fibers themselves), we conclude that the fluorescent lines represent labeled DNA molecules. As expected, the fibers formed from the solution lacking poly-L-aspartic acid contained highly fluorescent blobs (large DNA bundles),

but showed few fluorescent lines. We also prepared fibers containing λ DNA molecules that were not fluorescently labeled and as expected observed no fluorescence above that of the PEO fiber autofluorescence. Sometimes the electrospinning jet became particularly unstable and spurted, depositing a large ribbon of material on the glass substrate. These large ribbons contain several stretched aligned DNA molecules, as is shown in Figure 5.1f.

The lengths of the DNA strands were measured manually using the image processing software *ImageJ*.[6] A histogram of the resulting data for 54 images (129 molecules, 1 experiment) from one coverslip is shown in Figure 5.2. Similar histograms were observed for other experiments. The lengths were measured from one end of a molecule to the other, including any small dark regions between the ends in which the molecule may have fragmented. Molecules that exhibited dark regions that were of the same size or larger than the fluorescent regions were not counted. It is possible that some of the shorter measured lengths were actually fragments of a larger molecule, or that some of the longer lengths counted as individual molecules were actually DNA concatomers. Brighter spots on the molecule may be due to bunching or folding. The full contour length of λ DNA (nominally 16.3 μm) labeled with YOYO-1 at a base pair to dye labeling ratio of approximately 4:1 has been reported as 22 μm.[7, 10] Given that each YOYO-1 dye molecule extends the chain by 0.4 nm,[42] we expect a contour length of 18.8 μm for the labeling ratio we used. The electrospinning process is chaotic, and so variation in elongation is expected. Another cause for the variation in elongational behavior is the random initial conformation of the coiled DNA molecule in the polymer solution.[13] We note that, along the length of a given fiber (corresponding to a section of the jet that solidified in a very short

[6] Rasband, W.S., ImageJ, U. S. National Institutes of Health, Bethesda, Maryland, USA, http://rsb.info.nih.gov/ij/, 1997-2006

Figure 5.1- Fluorescence microscopy images of stretched DNA molecules embedded in PEO nanofibers, including high-contrast insets at the bottom right of several images. The inset scale bars indicate 10 microns. Images a)-c) were formed from the standard solution containing 20mg DABCO. Image d) shows an image of fibers formed from solution lacking DNA, set to the same contrast settings as image a). The inset in image d) (bottom right) shows the same image with increased contrast, revealing high background noise and autofluorescence from the PEO but no significant fluorescence signal. Image e) shows fibers formed from solution lacking poly-L-aspartic acid. Image f) is of two overlapping "ribbons" formed (from 100mg DABCO solution) when the electrospinning jet became unstable and spurted.

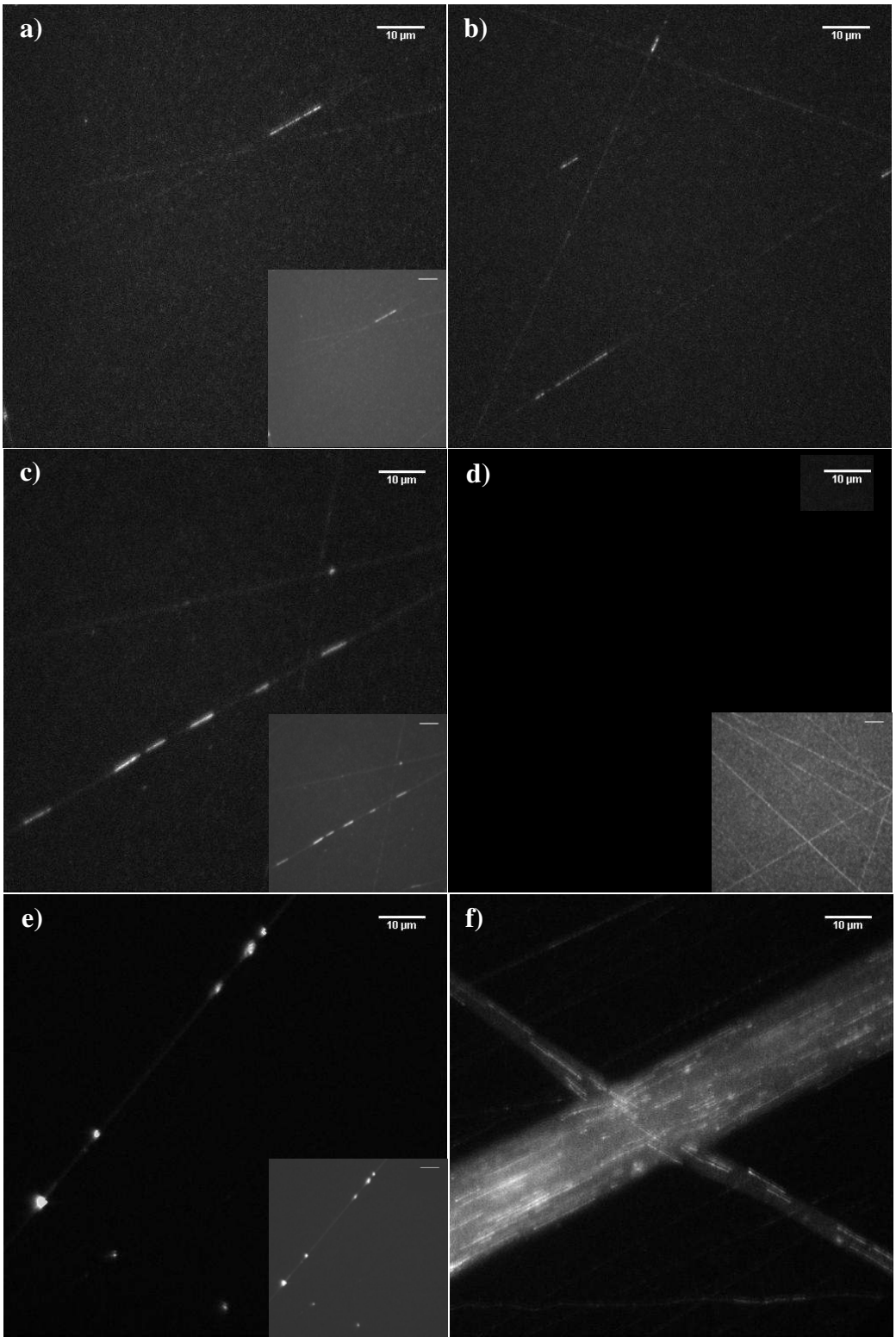
a)
10 µm
b)
10 µm
c)
10 µm
d)
10 µm
e)
10 µm
f)
10 µm

time period), the stretched length is often roughly constant (Figure 5.1c). Variations between fibers are likely due in part to variations in the fluid jet behavior in our electrospinning setup, manifested in the variation in the fiber diameter and jet velocity. Variations in the fiber diameter are seen during AFM imaging of electrospun nanofibers (Figure 5.3). Variation in the jet velocity is seen in that, while spinning fibers over trenches moving with a constant velocity, some fibers are suspended over the trench while others sag to the bottom.[43] Further optimization of the electrospinning parameters and jet stability should allow for more consistent stretching behavior.

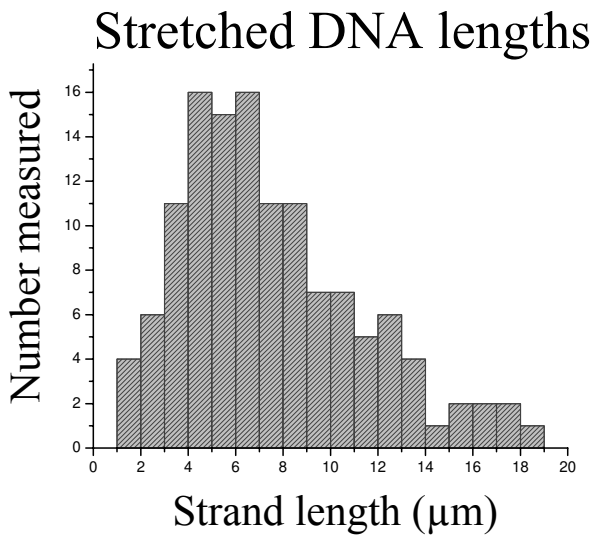

Figure 5.2 - Histogram showing the lengths of stretched DNA molecules (or fragments or concatomers) as measured from 54 images of one coverslip of fibers from the 20mg DABCO solution.

To better understand the fluid dynamic behavior of the DNA in the PEO solution while in the electrospinning jet, we also measured the relaxation time of the labeled DNA molecules in the bulk PEO solution. The viscous electrospinning solution was introduced into a fused-silica microchannel device (50 μm wide and 750

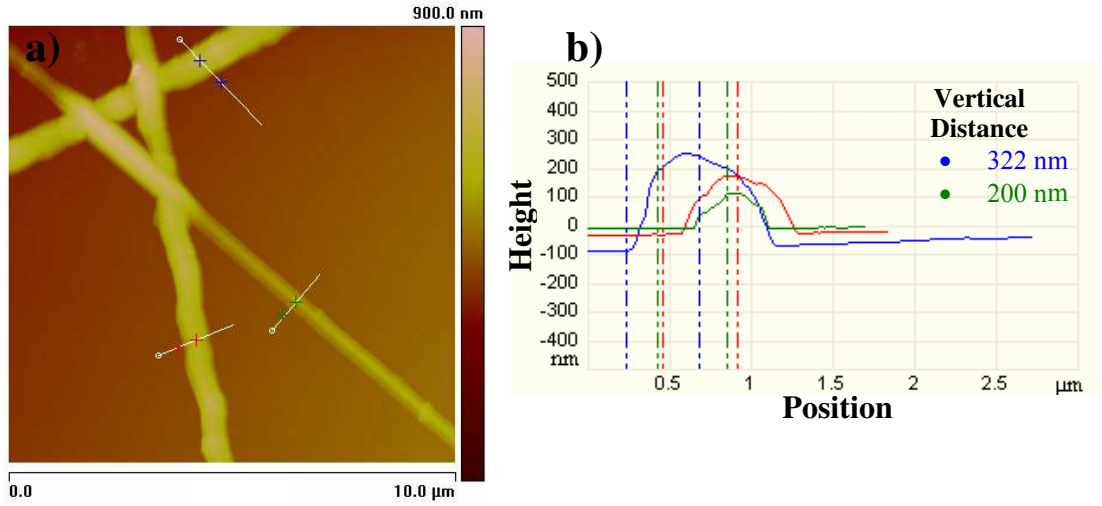

Figure 5.3 - a) AFM image of three PEO nanofibers and b) cross sectional plots of each fiber, illustrating the variation in fiber diameter.

nm deep) and the DNA was driven with an electric field (100-200 V/cm), causing it to experience a sheer force and elongate. The field was then turned off and videos were recorded of the elongated DNA relaxing into a blob. Previous studies have used similar methods to study the relaxation behavior of DNA in a viscous solution[13] and calculated relaxation times of 4-17 seconds (depending on the solution viscosity) using an exponential decay model.[12] Our videos were processed with homemade routines in *Matlab* (The Mathworks) and the DNA length vs. time data was fit to a decaying exponential using *Origin 7.5* (OriginLab) (Figure 5.4), yielding a time constant ranging from 2.1 to 19 sec (mean 8 ± 5 sec) over 20 samples, depending on whether the DNA was sticking to a surface.

The relaxation time constant can also be calculated using the equations above. For λ DNA, with a molecular weight of 31.5×10^6 g/mol and an intrinsic viscosity of ~15000 mL/g, relaxing in a solution of PEO which has a viscosity of 0.87 Pa sec (at

25°C) measured using an AR2000 rheometer (TA Instruments), the Rouse model (equation 5.5a) results in a relaxation time of 101 seconds, roughly an order of magnitude above the measured value. Though these models are overly-simplistic for the current situation, moving to a more complex model such as the reptation model can only cause the theoretical value to move further than the calculated value of ~8 seconds. There are several possible explanations for this lack of agreement; the most likely are shear-thinning, that the viscous solution never fully penetrated the microchannel and thus the DNA was actually observed in a much more dilute concentration of PEO (and thus much lower η_s), or that the DNA was relaxing near the walls of the channel, where the solution would exhibit a lower η_s due to slip effects.[44] Moreover, the use here of literature values of intrinsic viscosity measured in other solvent systems is likely inappropriate. Other techniques such as birefringence analysis, dynamic light scattering, or rheometry may allow a more correct determination of the DNA relaxation time in this solution, though the 10^7 difference in concentration between the PEO and DNA may render these measurements difficult, as much of the signal will be due to the PEO.

As mentioned earlier, a polymer molecule will undergo a coil-stretch transition at $De \approx 0.5$.[12, 38] If we calculate the Deborah number using previously published order-of-magnitude estimates of the overall strain rate in a whipping electrospinning jet,[20] 10^5 sec^{-1}, the resulting value (using measured relaxation times) of $De \approx 10^5$-10^6 suggests that we should expect to see the DNA molecules elongate in the jet. Even in the straight section of the jet, the order-of-magnitude estimated strain rate of 10 sec^{-1} yields $De \approx$10-100. The overall strain rates in the electrospinning jet are on or above the order of magnitude necessary for DNA chain scission in an elongational flow.[11] Consequently, observation of fragmented molecules in the resulting fibers is expected. Figure 5.1b shows an example of what could be a DNA molecule that has

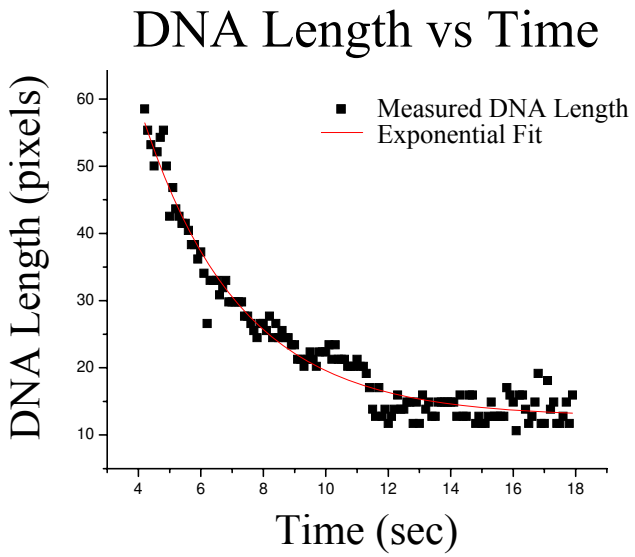

Figure 5.4 - Plot of DNA length vs. time for relaxation of a DNA molecule in bulk PEO solution. The relaxation time for this data was 3.1 seconds.

broken into two pieces, one much longer than the other (bottom left of image). Other possible scenarios that could cause this image include strongly non-uniform labeling of this particular DNA molecule (the dark gap between the two bright regions would then indicate an undyed section of the molecule) or a small fragment of another DNA molecule extremely close to a full molecule. However, the dilute concentrations of DNA used and the high uniformity (over long spans) of the fluorescent labeling render these possibilities unlikely.

Electrospun nanofibers may be mechanically manipulated using an AFM,[43] thereby reorienting and possibly further stretching the polymer molecules composing the fiber. Thus it may be possible to further stretch the embedded DNA molecules linearly in the nanofibers while preventing any fragments from drifting out of the initial sequence. Chemical access to the stretched DNA molecule may be possible by embedding the DNA in a porous water-insoluble electrospun nanofiber,[19, 45]

allowing for interrogation of specific sites on the stretched DNA molecule by various biological tags using techniques such as Fiber-FISH.[46-48]

The results presented here are interesting not only from a biological perspective, but may also offer insight into the behavior of electrospinning jets. To our knowledge, this is the first direct observation of individual aligned polymer molecules in an electrospun nanofiber. In the current work, we have examined a heterogeneous system consisting of PEO molecules and a smaller number of labeled DNA molecules. Future studies may examine homogeneous systems consisting entirely of DNA (or another polymer that can be fluorescently labeled) molecules of a given length, with a small fraction labeled with a fluorescent tag. Direct observation of the degree to which these molecules have been stretched can give information on the fluid dynamic behavior of the jet and the mechanical properties of the nanofibers.

Conclusion

By incorporating a dilute concentration of fluorescently labeled DNA molecules into an electrospinning process, we have produced PEO nanofibers containing isolated stretched DNA molecules. This technique is both rapid and simple. Because the DNA molecules are embedded in fibers that may be subsequently analyzed, this technique opens up possibilities in novel sequencing techniques and characterization of elastic properties of sections of DNA molecules. Moreover, the ability to directly observe individual polymer molecules that have been stretched and oriented in an electrospinning jet may provide new insight into the dynamics of electrospinning.

REFERENCES

1. Smith, S. B.; Finzi, L.; Bustamante, C., Direct mechanical measurements of the elasticity of single DNA molecules by using magnetic beads. *Science* **1992,** 258, (5085), 1122-1126.

2. Chu, S., Laser Manipulation of Atoms and Particles. *Science* **1991,** 253, (5022), 861-866.

3. Perkins, T. T.; Smith, D. E.; Chu, S., Direct Observation of Tube-Like Motion of a Single Polymer Chain. *Science* **1994,** 264, (5160), 819-822.

4. Smith, S. B.; Cui, Y.; Bustamante, C., Overstretching B-DNA: The Elastic Response of Individual Double-Stranded and Single-Stranded DNA Molecules. *Science* **1996,** 271, (5250), 795-799.

5. Rief, M.; Clausen-Schaumann, H.; Gaub, H. E., Sequence-dependent mechanics of single DNA molecules. *Nature Structural Biology* **1999,** 6, (4), 346-349.

6. Shivashankar, G. V.; Libchaber, A., Single DNA molecule grafting and manipulation using a combined atomic force microscope and an optical tweezer. *Applied Physics Letters* **1997,** 71, (25), 3727-3729.

7. Perkins, T. T.; Smith, D. E.; Larson, R. G.; Chu, S., Stretching of a Single Tethered Polymer in a Uniform Flow. *Science* **1995,** 268, (5207), 83-87.

8. Mannion, J. T.; Reccius, C. H.; Cross, J. D.; Craighead, H. G., Conformational analysis of single DNA molecules undergoing entropically induced motion in nanochannels. *Biophysical Journal* **2006,** 90, (12), 4538-4545.

9. Reccius, C. H.; Mannion, J. T.; Cross, J. D.; Craighead, H. G., Compression and free expansion of single DNA molecules in nanochannels. *Physical Review Letters* **2005,** 95, (26).

10. Bensimon, A.; Simon, A.; Chiffaudel, A.; Croquette, V.; Heslot, F.; Bensimon,

D., Alignment and Sensitive Detection of DNA by a Moving Interface. *Science* **1994,** 265, (5181, Genome Issue), 2096-2098.

11. Atkins, E. D. T.; Taylor, M. A., Elongational Flow Studies On Dna In Aqueous-Solution And Stress-Induced Scission Of The Double Helix. *Biopolymers* **1992,** 32, (8), 911-923.

12. Perkins, T. T.; Smith, D. E.; Chu, S., Single Polymer Dynamics in an Elongational Flow. *Science* **1997,** 276, (5321), 2016-2021.

13. Smith, D. E.; Chu, S., Response of Flexible Polymers to a Sudden Elongational Flow. *Science* **1998,** 281, (5381), 1335-1340.

14. Shrewsbury, P. J.; Liepmann, D.; Muller, S. J., Concentration effects of a biopolymer in a microfluidic device. *Biomedical Microdevices* **2002,** 4, (1), 17-26.

15. Shrewsbury, P. J.; Muller, S. J.; Liepmann, D., Effect of Flow on Complex Biological Macromolecules in Microfluidic Devices. *Biomedical Microdevices* **2001,** 3, (3), 225-238.

16. Buchko, C. J.; Chen, L. C.; Shen, Y.; Martin, D. C., Processing and microstructural characterization of porous biocompatible protein polymer thin films. *Polymer* **1999,** 40, (26), 7397.

17. Kenawy, E. R.; Bowlin, G. L.; Mansfield, K.; Layman, J.; Simpson, D. G.; Sanders, E. H.; Wnek, G. E., Release of tetracycline hydrochloride from electrospun poly(ethylene-co-vinylacetate), poly(lactic acid), and a blend. *Journal Of Controlled Release* **2002,** 81, (1-2), 57-64.

18. Lee, S. W.; Belcher, A. M., Virus-Based Fabrication of Micro- and Nanofibers Using Electrospinning. *Nano Letters* **2004,** 4, (3), 387-390.

19. Patel, A. C.; Li, S.; Yuan, J. M.; Wei, Y., In Situ Encapsulation of Horseradish Peroxidase in Electrospun Porous Silica Fibers for Potential Biosensor Applications. *Nano Lett.* **2006,** 6, (5), 1042-1046.

20. Reneker, D. H.; Yarin, A. L.; Hao, F.; Koombhongse, S., Bending instability of electrically charged liquid jets of polymer solutions in electrospinning. *Journal of Applied Physics* **2000,** 87, (9, pt.1-3), 4531-4547.

21. Dror, Y.; Salalha, W.; Khalfin, R. L.; Cohen, Y.; Yarin, A. L.; Zussman, E., Carbon nanotubes embedded in oriented polymer nanofibers by electrospinning. *Langmuir* **2003,** 19, (17), 7012-7020.

22. Salalha, W.; Dror, Y.; Khalfin, R. L.; Cohen, Y.; Yarin, A. L.; Zussman, E., Single-walled carbon nanotubes embedded in oriented polymeric nanofibers by electrospinning. *Langmuir* **2004,** 20, (22), 9852-9855.

23. Bashouti, M.; Salalha, W.; Brumer, M.; Zussman, E.; Lifshitz, E., Alignment of Colloidal CdS Nanowires Embedded in Polymer Nanofibers by Electrospinning. *ChemPhysChem* **2006,** 7, (1), 102-106.

24. Fang, X.; Reneker, D. H., DNA fibers by electrospinning. *Journal Of Macromolecular Science-Physics* **1997,** B36, (2), 169-173.

25. Takahashi, T.; Taniguchi, M.; Kawai, T., Fabrication of DNA nanofibers on a planar surface by electrospinning. *Japanese Journal Of Applied Physics Part 2-Letters & Express Letters* **2005,** 44, (24-27), L860-L862.

26. Luu, Y. K.; Kim, K.; Hsiao, B. S.; Chu, B.; Hadjiargyrou, M., Development of a nanostructured DNA delivery scaffold via electrospinning of PLGA and PLA-PEG block copolymers. *Journal Of Controlled Release* **2003,** 89, (2), 341-353.

27. Rubinstein, M.; Colby, R. H., *Polymer physics*. Oxford University Press: Oxford New York, 2003; p xi, 440 p.

28. Marko, J. F.; Siggia, E. D., Stretching DNA. *Macromolecules* **1995,** 28, (26), 8759-8770.

29. Bustamante, C.; Marko, J. F.; Siggia, E. D.; Smith, S., Entropic Elasticity Of Lambda-Phage DNA. *Science* **1994,** 265, (5178), 1599-1600.

30. Rouse, J. P. E., A Theory of the Linear Viscoelastic Properties of Dilute Solutions of Coiling Polymers. *The Journal of Chemical Physics* **1953,** 21, (7), 1272-1280.

31. Zimm, B. H., Dynamics of Polymer Molecules in Dilute Solution: Viscoelasticity, Flow Birefringence and Dielectric Loss. *The Journal of Chemical Physics* **1956,** 24, (2), 269-278.

32. De Gennes, P. G., Reptation Of A Polymer Chain In Presence Of Fixed Obstacles. *Journal of Chemical Physics* **1971,** 55, (2), 572-&.

33. Dawson, J. R.; Harpst, J. A., Light Scattering And Hydrodynamic Properties Of Linear And Circular Bacteriophage Lambda DNA. *Biopolymers* **1971,** 10, (12), 2499-&.

34. Douthart, R. J.; Bloomfie.Va, Intrinsic Viscosities Of Cyclic And Linear Lambda DNA. *Biopolymers* **1968,** 6, (9), 1297-&.

35. Liu, Y. G.; Jun, Y. G.; Steinberg, V., Longest relaxation times of double-stranded and single-stranded DNA. *Macromolecules* **2007,** 40, (6), 2172-2176.

36. Schmitz, K. S.; Pecora, R., Quasi-Elastic Light-Scattering By Calf Thymus DNA And Lambda-DNA. *Biopolymers* **1975,** 14, (3), 521-542.

37. Morrison, F. A., *Understanding rheology*. Oxford University Press: New York, 2001; p xiii, 545 p.

38. Larson, R. G.; Magda, J. J., Coil-stretch transitions in mixed shear and extensional flows of dilute polymer solutions. *Macromolecules* **1989,** 22, (7), 3004-3010.

39. Tang, J. X.; Wen, Q.; Bennett, A.; Kim, B.; Sheils, C. A.; Bucki, R.; Janmey, P. A., Anionic poly(amino acid)s dissolve F-actin and DNA bundles, enhance DNase activity, and reduce the viscosity of cystic fibrosis sputum. *Am J Physiol Lung Cell Mol Physiol* **2005,** 289, (4), L599-605.

40. Valnes, K.; Brandtzaeg, P., Retardation of immunofluorescence fading during microscopy. *J. Histochem. Cytochem.* **1985,** 33, (8), 755-761.

41. Kameoka, J.; Orth, R.; Yang, Y. N.; Czaplewski, D.; Mathers, R.; Coates, G. W.; Craighead, H. G., A scanning tip electrospinning source for deposition of oriented nanofibres. *Nanotechnology* **2003,** 14, (10), 1124-1129.

42. Johansen, F.; Jacobsen, J. P., H-1 NMR studies of the bis-intercalation of a homodimeric oxazole yellow dye in DNA oligonucleotides. *Journal Of Biomolecular Structure & Dynamics* **1998,** 16, (2), 205-222.

43. Bellan, L. M.; Kameoka, J.; Craighead, H. G., Measurement of the Young's moduli of individual polyethylene oxide and glass nanofibres. *Nanotechnology* **2005,** 16, (8), 1095-1099.

44. Degré, G.; Joseph, P.; Tabeling, P.; Lerouge, S.; Cloitre, M.; Ajdari, A., Rheology of complex fluids by particle image velocimetry in microchannels. *Applied Physics Letters* **2006,** 89, (2), 024104-3.

45. Bognitzki, M.; Czado, W.; Frese, T.; Schaper, A.; Hellwig, M.; Steinhart, M.; Greiner, A.; Wendorff, J. H., Nanostructured Fibers via Electrospinning. *Advanced Materials* **2001,** 13, (1), 70-72.

46. van de Rijke, F. M.; Florijn, R. J.; Tanke, H. J.; Raap, A. K., DNA Fiber-FISH Staining Mechanism. *J. Histochem. Cytochem.* **2000,** 48, (6), 743-746.

47. Heiskanen, M.; Hellsten, E.; Kallioniemi, O.-P.; Makela, T. P.; Alitalo, K.; Peltonen, L.; Palotie, A., Visual Mapping by Fiber-FISH. *Genomics* **1995,** 30, (1), 31.

48. Raap, A. K.; Florijn, R. J.; Blonden, L. A. J.; Wiegant, J.; Vaandrager, J.-W.; Vrolijk, H.; den Dunnen, J.; Tanke, H. J.; van Ommen, G.-J., Fiber FISH as a DNA Mapping Tool. *Methods* **1996,** 9, (1), 67.

CHAPTER 6

FABRICATION OF NANOCHANNELS USING SACRIFICIAL ELECTROSPUN FIBERS[7]

Introduction

As the technology required to observe single molecules has developed, so have methods to isolate and manipulate single molecules in fluid. Microfluidics and nanofluidics have allowed enhanced control over individual biomolecules, enabling new methods for biomolecular analysis that exploit phenomena unique to miniaturized fluidic devices.[1-3] As fluidic technology moves towards smaller volumes, there is an increased need for rapid and inexpensive methods to fabricate micro- and nanofluidic devices. Several recent studies have demonstrated techniques to fabricate micro- and nanochannels without using high-resolution lithography.[4-7]

PDMS remains one of the most popular materials used to fabricate micro- and nanofluidic structures.[8, 9] It is relatively inexpensive, easily and quickly molded, non-toxic, and transparent. The mechanical flexibility of PDMS lends itself to the construction of integrated valves and pumps, [10] as well as the controlled and reversible deformation of device channels using external forces.[11]

Past work has demonstrated the use of electrospun nanofibers as nonlithographic masks for patterning features in silicon wafers and thin films.[12, 13] A previous study has demonstrated the use of sacrificial heat-decomposable electrospun nanofibers to form nanochannels using spin-on-glass as a capping layer.[4] In this chapter we describe the formation of nanochannels in PDMS using electrospun PEO nanofibers. This nanochannel fabrication technique requires no cleanroom processes, heat treatment, or specialized equipment. The resulting device is contained in a flexible substrate and may be capped by either another flexible

[7] Submitted to JVST B.

PDMS layer or a stiff glass coverslip. Moreover, the PDMS layer is reusable, given that it is not bonded irreversibly to a capping layer. Using this technique, it is possible to fabricate a complex random mat of interlinked nanochannels or an aligned array of nanochannels. The nanochannel pattern depends solely on the pattern of the electrospun nanofibers. By depositing fibers on patterned silicon templates, devices incorporating both microfluidic and nanofluidic structures can be produced easily.

Device Fabrication

The fibers used to form sacrificial nanochannel templates were produced by electrospinning a mixture of polyethylene oxide (Acros Organics, Mw 100,000) mixed in 50/50 (v/v) water/ethanol at a concentration of approximately 20%. To produce oriented nanofiber arrays, we used the scanned electrospinning method whereby the collecting substrate is rotated quickly through the jet (Figure 3.2).[14] The solution was electrospun onto silicon chips that had been treated with Sigmacote (Sigma) non-stick coating. To integrate the nanochannels with microscale device features, several of these chips were patterned with large reservoirs using contact photolithography and deep reactive ion etching. Isolated aligned fibers or fiber mats were deposited over the entire chip, and water-soaked swabs were used to wipe away undesired polymeric material. Then PDMS (Sylgard 184, Dow Corning) was mixed at a 1:5 hardener-to-resin ratio, degassed, poured over the fiber-coated silicon, and degassed again. The PDMS was allowed to cure at room temperature overnight; the devices were not cured at an elevated temperature to avoid melting the PEO. Figure 6.1a shows an optical image of a device at this stage of the fabrication process consisting of two large reservoirs connected by a fiber mat. Any fibers present in the reservoirs formed features embedded in the reservoir ceiling and did not result in enclosed nanochannels after bonding. After the PDMS cured, a scalpel was used to release devices from the

silicon chips. These sections were peeled off of the silicon chip, sonicated in deionized water for 30 minutes, and allowed to soak in water overnight in order to dissolve away the PEO fibers inside the PDMS bulk. The PDMS was then dried and access holes were created using a metal punch. Finally, the PDMS was exposed to an oxygen plasma for ~30 s and bonded irreversibly to a glass coverslip used as a device capping layer. The entire fabrication process is outlined in Figure 6.1b.

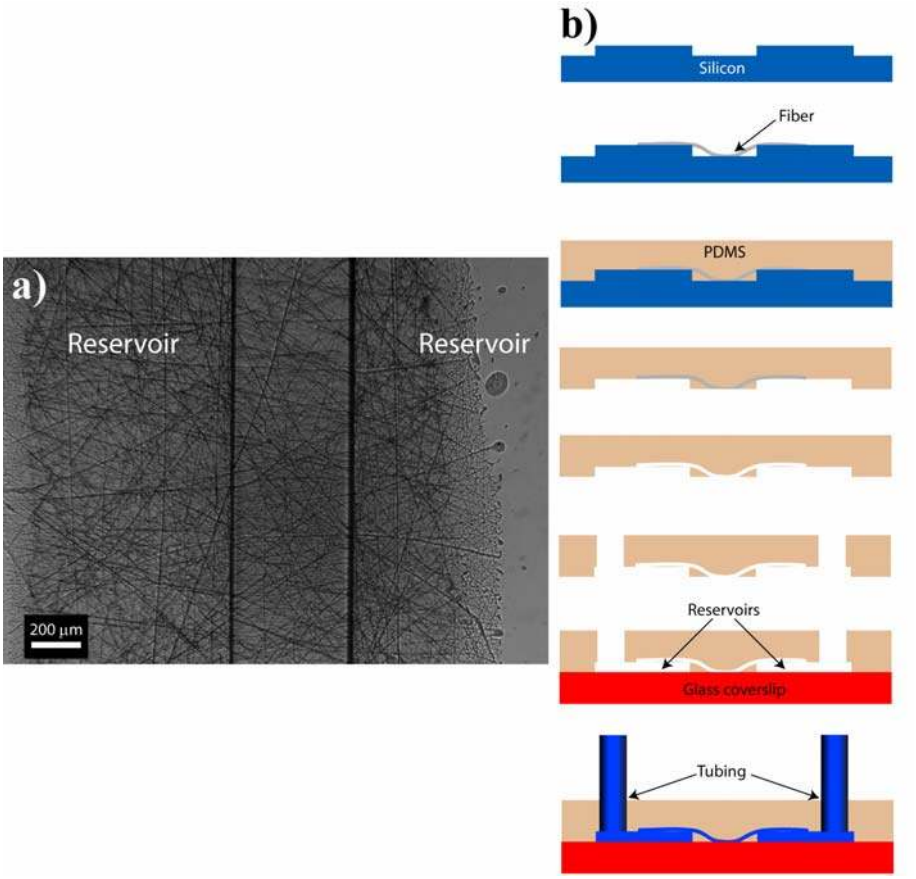

Figure 6.1- a) Optical image of a device consisting of two reservoirs connected by a random fiber mat, taken at the third process step after the PDMS has been poured over the template and cured. b) Schematic of a typical fabrication process.

Multiple device geometries were fabricated. Initially, we deposited fiber mats on unpatterned silicon chips. These devices consisted solely of a large network of nanochannels accessed by tubing attached to holes punched in the PDMS. In order to demonstrate that these nanochannel networks could be easily integrated with standard microfluidics, we then deposited nanofiber mats onto silicon chips containing etched features, resulting in devices (such as the device shown in Figure 6.1) that incorporate both microfluidic and nanofluidic structures. In this way, a multi-level PDMS fluidic structure was created without the need for multiple layers of lithography.

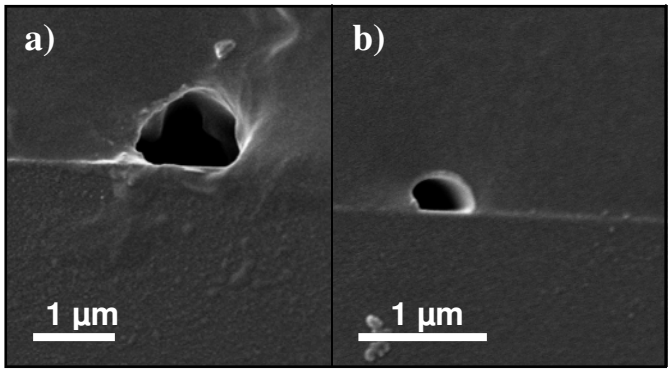

Figure 6.2- SEM images of nanochannel cross-sections. In both images, the glass coverslip is below the interface and the PDMS layer is above the interface. Images a) and b) show larger and smaller diameter channels, respectively.

Device Characterization

In order to determine the cross-sectional sizes of the nanochannels formed from the sacrificial PEO nanofibers, several devices were frozen in liquid nitrogen, fractured, sputter coated with Au/Pd, and imaged with a scanning electron microscope (SEM) (LEO 1550). Examples of the resulting cross-sectional SEM images are shown in Figure 6.2. Because electrospinning produces fibers with a range of sizes (diameters varying up to ~50% from the average value),[15, 16] we expect the nanochannels to exhibit a similarly broad range of diameters. We took SEM images

of a random mat of fibers deposited with the same parameters as those used to create the sacrificial template mats. We measured the diameter of 50 fibers and obtained an average diameter of 455 ± 146 nm. By tuning properties of the electrospinning solution (such as polymer concentration, polymer molecular weight, and solvent), the resulting fiber diameters can be influenced. Tuning the parameters of the electrospinning system may also yield fibers with a narrower diameter distribution. Electrospinning is able to produce nanofibers with diameters below 30nm; these ultrafine fibers could potentially be used to create similarly sized channels limited by the mechanical stability of the PDMS itself. Channels produced from sacrificial fibers are roughly circular in cross-section, as opposed to those with rectangular cross-sections made using standard lithographic techniques.

In order to test nanochannel accessibility, we used a syringe pump (KD Scientific model 230) to fill devices with a solution of 100 μM fluorescein (Sigma) and imaged them using an optical microscope (Olympus IX-70 microscope, EXFO X-cite 120 illuminator, Omega XF100-2 filter set, Olympus 60x 0.9 NA objective, Roper Scientific Cascade 512B EMCCD camera). Initially, we filled devices consisting solely of randomly oriented channels (Figure 6.3). We also filled channels that were integrated with microfluidic features such as reservoirs and fabricated using aligned fibers (Figure 6.4).

To demonstrate that single molecules could be introduced into the channels, we imaged individual DNA molecules in solution passing through the channels. The devices consisted of two large reservoirs (1cm x 0.5cm x 26 μm deep) connected by nanochannels formed from sacrificial electrospun nanofibers (Figure 6.1a). The channels were first filled with filtered 5x tris-borate EDTA (TBE) buffer (Sigma) that was introduced through one of the reservoirs. After we observed buffer exiting the opposite reservoir, we introduced a 50 ng/mL solution of λ bacteriophage DNA

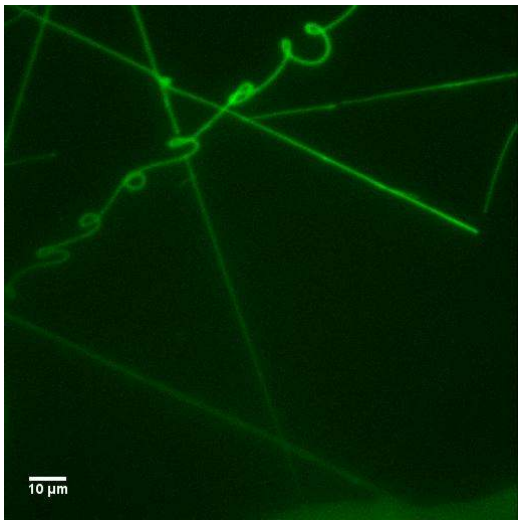

Figure 6.3-Fluorescence image of randomly aligned channels filling with a solution of the fluorescent dye fluorescein.

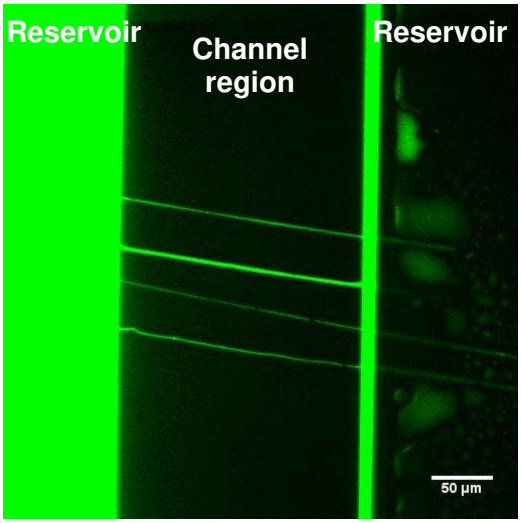

Figure 6.4- Fluorescence image of aligned channels connecting two reservoirs. The reservoir on the left has already filled with dye, and the dye has flowed through the channels and has begun to fill the reservoir on the right.

(New England Biolabs) that had been labeled with YOYO-1 (Molecular Probes) at a nominal labeling ratio of 7.6:1 using the syringe pump. We then imaged the

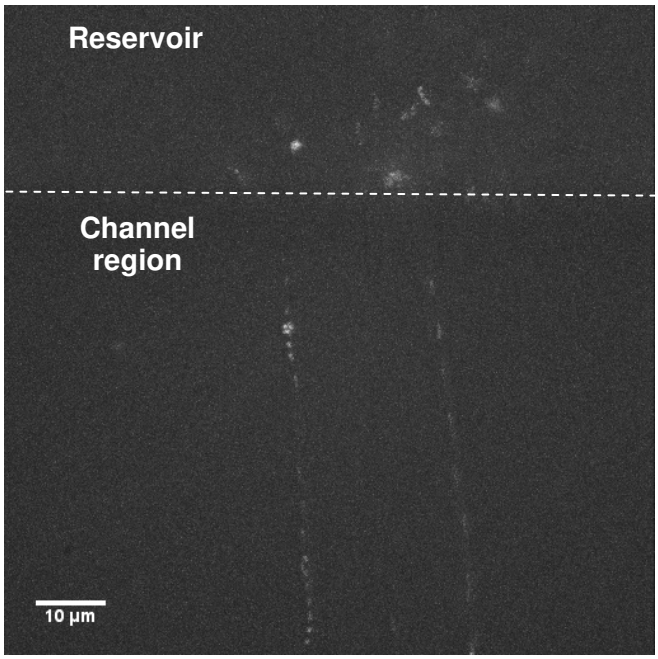

Figure 6.5- Fluorescence image indicating the paths of single molecules of DNA through fluidic channels. Several frames from a video of the DNA in the device were superimposed to create this image. Both the exposure time and the temporal gap between each of the DNA images were 75 ms.

nanochannel region of the device and observed DNA molecules as they traversed the channels. Figure 6.5 illustrates the motion of the DNA molecules in the channels.

Results and Discussion

PDMS is an established, versatile, and easy-to-use material for the construction of miniaturized fluidic structures. PEO is a similarly popular material to electrospin because it is non-toxic, water-soluble, easy to electrospin, and easy to work with. A fabrication process combining these two materials to form fluidic structures in PDMS is advantageous because the materials systems involved are standard for the field and require no toxic solvents. These features render this fabrication technique potentially

suitable for fabricating fluidic structures for instructional purposes. Moreover, the process described herein could easily be scaled up for mass production of PDMS substrates containing nanochannels. Several studies have investigated multi-source electrospinning systems to increase nanofiber deposition rates.[17-19] The fabrication technique described in this study could also be readily adapted for use with other polymeric materials.

The channels produced by the technique described in this article form paths determined by the layout of the deposited fibers. The "inverse mat" resulting from using a random fiber mat template provides a tortuous path for fluid and molecules to follow, as indicated in Figure 6.3. These random branching paths would be difficult and time-consuming to produce using standard lithographic techniques but may be useful for sensing, biomolecular separation, and mixing applications. Isolated nanochannels have been used for analysis of single molecules such as DNA,[20-22] and the technique described above, when combined with a oriented deposition of nanofibers, can produce such isolated, straight channels (Figure 6.4).

Conclusion

Using sacrificial electrospun PEO nanofibers as templates, we have formed nanofluidic channels in PDMS that are easily integrated with microfluidic features. These channels can be defined as random intersecting paths or as a set of aligned structures, depending on the deposited fiber template used. We have shown that fluid and single molecules can be driven into these channels and observed. This high-throughput, soft-lithographic technique may be used to form nanochannels easily in a wide range of materials, and thus renders several micro- and nanofluidic technologies previously confined to the research laboratory potentially commercially viable.

REFERENCES

1. Inglis, D. W.; Davis, J. A.; Austin, R. H.; Sturm, J. C., Critical particle size for fractionation by deterministic lateral displacement. *Lab on a Chip* **2006,** 6, (5), 655-658.

2. Han, J. Y.; Fu, J. P.; Schoch, R. B., Molecular sieving using nanofilters: Past, present and future. *Lab on a Chip* **2008,** 8, (1), 23-33.

3. Mannion, J. T.; Craighead, H. G., Nanofluidic structures for single biomolecule fluorescent detection. *Biopolymers* **2007,** 85, (2), 131-143.

4. Czaplewski, D. A.; Kameoka, J.; Mathers, R.; Coates, G. W.; Craighead, H. G., Nanofluidic channels with elliptical cross sections formed using a nonlithographic process. *Applied Physics Letters* **2003,** 83, (23), 4836-4838.

5. Liang, X.; Morton, K. J.; Austin, R. H.; Chou, S. Y., Single Sub-20 nm Wide, Centimeter-Long Nanofluidic Channel Fabricated by Novel Nanoimprint Mold Fabrication and Direct Imprinting. *Nano Lett.* **2007,** 7, (12), 3774-3780.

6. Verbridge, S. S.; Edel, J. B.; Stavis, S. M.; Moran-Mirabal, J. M.; Allen, S. D.; Coates, G.; Craighead, H. G., Suspended glass nanochannels coupled with microstructures for single molecule detection. *Journal Of Applied Physics* **2005,** 97, (12), 124317.

7. Wang, M.; Jing, N.; Su, C. B.; Kameoka, J.; Chou, C.-K.; Hung, M.-C.; Chang, K.-A., Electrospinning of silica nanochannels for single molecule detection. *Applied Physics Letters* **2006,** 88, (3), 033106-3.

8. Quake, S. R.; Scherer, A., From micro- to nanofabrication with soft materials. *Science* **2000,** 290, (5496), 1536-1540.

9. Love, J. C.; Anderson, J. R.; Whitesides, G. M., Fabrication of three-dimensional microfluidic systems by soft lithography. *Mrs Bulletin* **2001,** 26, (7), 523-

528.

10. Unger, M. A.; Chou, H. P.; Thorsen, T.; Scherer, A.; Quake, S. R., Monolithic microfabricated valves and pumps by multilayer soft lithography. *Science* **2000,** 288, (5463), 113-116.

11. Huh, D.; Mills, K. L.; Zhu, X.; Burns, M. A.; Thouless, M. D.; Takayama, S., Tuneable elastomeric nanochannels for nanofluidic manipulation. *Nature Materials* **2007,** 6, (6), 424-428.

12. Czaplewski, D.; Kameoka, J.; Craighead, H. G., Nonlithographic approach to nanostructure fabrication using a scanned electrospinning source. *Journal Of Vacuum Science & Technology B* **2003,** 21, (6), 2994-2997.

13. Czaplewski, D. A.; Verbridge, S. S.; Kameoka, J.; Craighead, H. G., Nanomechanical oscillators fabricated using polymeric nanofiber templates. *Nano Letters* **2004,** 4, (3), 437-439.

14. Kameoka, J.; Orth, R.; Yang, Y. N.; Czaplewski, D.; Mathers, R.; Coates, G. W.; Craighead, H. G., A scanning tip electrospinning source for deposition of oriented nanofibres. *Nanotechnology* **2003,** 14, (10), 1124-1129.

15. Li, L.; Bellan, L. M.; Craighead, H. G.; Frey, M. W., Formation and properties of nylon-6 and nylon-6/montmorillonite composite nanofibers. *Polymer* **2006,** 47, (17), 6208.

16. Li, D.; Xia, Y., Fabrication of titania nanofibers by electrospinning. *Nano Letters* **2003,** 3, (4), 555-560.

17. Theron, S. A.; Yarin, A. L.; Zussman, E.; Kroll, E., Multiple jets in electrospinning: experiment and modeling. *Polymer* **2005,** 46, (9), 2889-2899.

18. Yarin, A. L.; Zussman, E., Upward needleless electrospinning of multiple nanofibers. *Polymer* **2004,** 45, (9), 2977-2980.

19. Jirsak, O.; Sanetrnik, F.; Lukas, D.; Kotek, V.; Martinova, L.; Chaloupek, J. A

Method of Nanofibres Production from a Polymer Solution Using Electrostatic Spinning and a Device for Carrying out the Method. WO 2005/024101 A1, 17 March, 2005.

20. Mannion, J. T.; Reccius, C. H.; Cross, J. D.; Craighead, H. G., Conformational analysis of single DNA molecules undergoing entropically induced motion in nanochannels. *Biophysical Journal* **2006,** 90, (12), 4538-4545.

21. Reccius, C. H.; Mannion, J. T.; Cross, J. D.; Craighead, H. G., Compression and free expansion of single DNA molecules in nanochannels. *Physical Review Letters* **2005,** 95, (26).

22. Stavis, S. M.; Edel, J. B.; Li, Y.; Samiee, K. T.; Luo, D.; Craighead, H. G., Single-molecule mobility and spectral measurements in submicrometer fluidic channels. *Journal of Applied Physics* **2005,** 98, (4), 044903-5.

CHAPTER 7

CONTROL OF AN ELECTROSPINNING JET USING ELECTRIC FIELDS[8]

Introduction

One of the major features of the electrospinning process is that it is able to directly deposit nanofibers consisting of a wide range of materials. Polymer nanofibers containing small active particles can be produced by adding the particles to the solution before deposition.[1-3] Biosensors produced with electrospun nanofibers can be fabricated in direct deposition processes that avoid the use of harsh solvents typical of most lithography processes.[4] Electrospinning is a simple and inexpensive method to produce nanodevices that exploit the material properties of the active polymer nanofiber or encapsulated molecules. For example, Liu et al. have reported using an electrospun polyaniline nanofiber as an ultrasensitive NH_3 detector.[5] Electrospun glass fibers were deposited over trenches by Kameoka et al. and used as doubly clamped beam oscillators which could be used for detection.[6] Verbridge et al. have used electrospun nanofibers as templates for fabricating suspended nanochannels that could be used for both mechanical and optical measurements of the solution contained therein.[7] To be able to produce these devices with high yield, one must be able to position the deposited fibers relative to other features (such as electrodes or trenches) to within 1-100 μm, depending on the device. Current standard electrospinning processes do not have such control. In this chapter we discuss a method to deposit fibers in a more controlled fashion.

The fluid dynamic behavior of electrospinning jets is complex, and the jet will often enter a "whipping mode" where charge-charge repulsion and surface tension

[8] Reproduced in part with permission from Bellan, L. M.; Craighead, H. G., Control of an electrospinning jet using electric focusing and jet-steering fields. *Journal of Vacuum Science & Technology B* **2006,** 24, (6), 3179-3183. Copyright 2006 American Vacuum Society.

cause chaotic bending of the jet. This produces a random mat of fibers (Figure 7.1a). Moreover, the deposited fibers are initially charged and there is some time constant for the charge to leak into the grounded substrate. This charging will also cause chaotic motion of the jet near the surface.

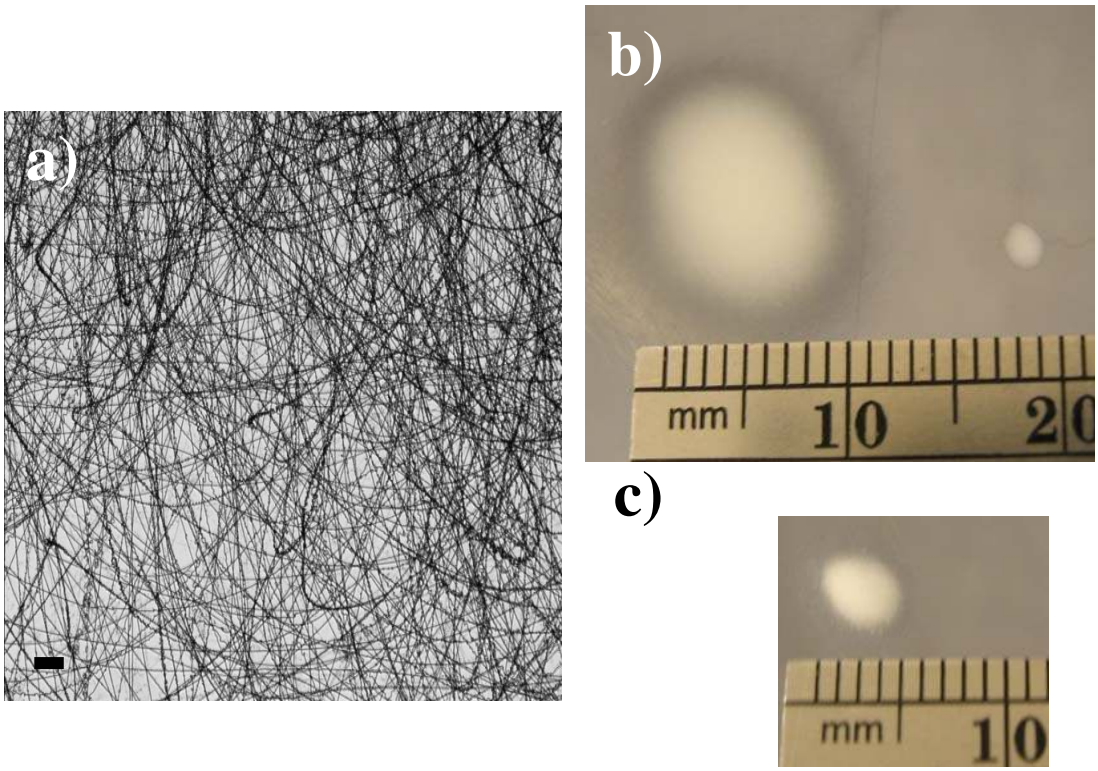

Figure 7.1- a) Optical microscope image for typical random mat produced by electrospinning (scale bar indicates 100 microns), b) picture of unfocused spot (left side) and spot produced by a jet in a focused, axisymmetric mode and c) picture of spot produced by focused jet in whipping mode.

It would be useful to deposit electrospun fibers with specific orientations in specific positions (i.e. to "draw" with the jet). However, depositing electrospun fibers in a controlled fashion is difficult due to the high jet velocity (1-10 m/sec) typical of most electrospinning systems. Moreover, the chaotic whipping mode that is

responsible for the final thinning of the fiber causes the jet to deposit fibers randomly over a large (~cm typically) characteristic "spot size" (Figure 7.1b, left spot). Several methods for electrospinning separate oriented fibers have been demonstrated, including depositing on a rotating substrate[8-10] and depositing on a substrate with electrodes that can attract or repel the fibers.[11, 12] However, these methods are generally limited to orientation in one dimension. The fluid jet in typical electrospinning setups flows too quickly to use common linear motion stages (with typical maximum velocities ranging from 10-50 cm/sec) for mechanical scanning in two dimensions, making it difficult to use such systems to draw out single straight dry fibers with arbitrary XY control. Only one recent study has demonstrated the ability to use fast XY stages with a near field electrospinning setup that produces a jet with a smaller velocity.[13]

Because electrospinning jets are charged, they can be manipulated by electric fields. This is an attractive idea for many reasons. Compared to the relatively slow speeds of linear mechanical stages, electric manipulation should allow for much quicker arbitrary manipulation of the charged jet. With the right electronics, very strong electric (or magnetic) fields can be switched very quickly. Scanned electron and ion beams are a mainstay of modern nanofabrication approaches. However, there has been relatively little work in the area of manipulating electrospinning jets with electric fields. A previous study demonstrated the ability to reduce the characteristic spot size of an electrospinning jet by using a series of focusing electrodes that suppressed the whipping mode to some extent.[14] The current study takes this idea one step further by using both a DC focusing field to reduce the characteristic spot size (Figure 7.1b and 7.1c) as well as a time-varying jet steering field. Figure 7.1b shows a spot produced with no focusing fields (left spot) and a spot produced with focusing fields that allowed the jet to enter an axisymmetric fluid dynamic mode (right spot).

Figure 7.1c shows a spot produced with focusing fields that did not completely suppress the whipping mode but did reduce the spot size.

Experimental Setup

An illustration and an image of the current experimental setup are shown in Figures 7.2a and 7.2b, respectively. The electrospinning tip consists of a needle fed with solution by a syringe pump (Harvard Apparatus syringe infusion pump 22) feeding at a rate of 2-3 μL/min. The polymer solution used in this study was 20% by weight polyethylene oxide (PEO) (100,000 MW, Aldrich) in 50/50 (by volume) deionized water and ethanol. We used a PEO solution because it is simple to electrospin, both the polymer and the solvents are non-toxic, and the deposited material is simple to clean up. The high voltage applied to the tip (~18kV) is provided by an Emco DX250 high voltage supply connected to an Agilent DC supply. At a distance of 3.5 cm below the tip, close to the collecting substrate, are the focusing and steering electrodes. These functions are performed by a short metal cylinder (copper gaskets 2 or 4 mm tall, 3.5 cm diameter) cut into quadrants. A constant voltage for focusing is applied to two sections, while time-varying steering voltage is applied to the other two sections. The jet is steered from its default position only when at least one of the steering voltages is different from the focusing voltage. The collecting substrate sits directly below these electrodes at a distance of 6 cm from the tip, on top of a grounded plate. We placed a small amount of water on the grounded plate so that, during initial setup of the jet without the substrate in place, polymer solution would not accumulate on the grounded plate. It is important to note that the steering and focusing electrodes must be placed close to the collecting substrate. Electrodes near the tip may manipulate the jet behavior far from the sample, but as the jet travels downstream it can resume the chaotic whipping mode, even if it had been suppressed

further upstream. All electrospinning was performed in air at room temperature, and thus it was necessary to ensure that all electrodes in the system, including the tip, were appropriately separated from each other so as to avoid arcs.

The electronics used to drive the focusing/steering electrodes were homebuilt. In the initial experimental setup, we used two high voltage relays (Gigavac G81C245) to switch the potential on two of the electrodes between the focusing voltage (~10kV) and ground. The relays were controlled by computer using digital outputs on a National Instruments PCI-6036E DAQ card. For this initial setup, the electrode thickness was 2mm. In the second experimental setup, we doubled the electrode thickness to increase the jet deflection and used a more complex electrode driving circuit. For this setup, arbitrary waveforms to steer both axes were generated with the DAQ card analog outputs. These two signals were amplified (gain of ~6.6x) by a simple op-amp circuit that acted not only as an amplifier but also as an extra electrical buffer between the high voltage section of the circuit and the computer output. The outputs of the op-amps were connected to the grids of two single ended triode (SET) amplifiers based on the 6BK4B vacuum tube. The resistor used between the high voltage supply and the plate of the tube was conservatively chosen to be 20MΩ taking into account the maximum current output of the high voltage supply (Emco F121 supply running at 10kV), 0.834 mA, and this limited the time response of the electrical system to a time constant of ~ 0.5 msec. Future versions of the driving electronics may incorporate higher power voltage supplies that would allow the amplifier to swing voltages more quickly and thus produce finer features. A “push-pull” configuration is another possible improvement. More optimized electrode geometries would also be beneficial.

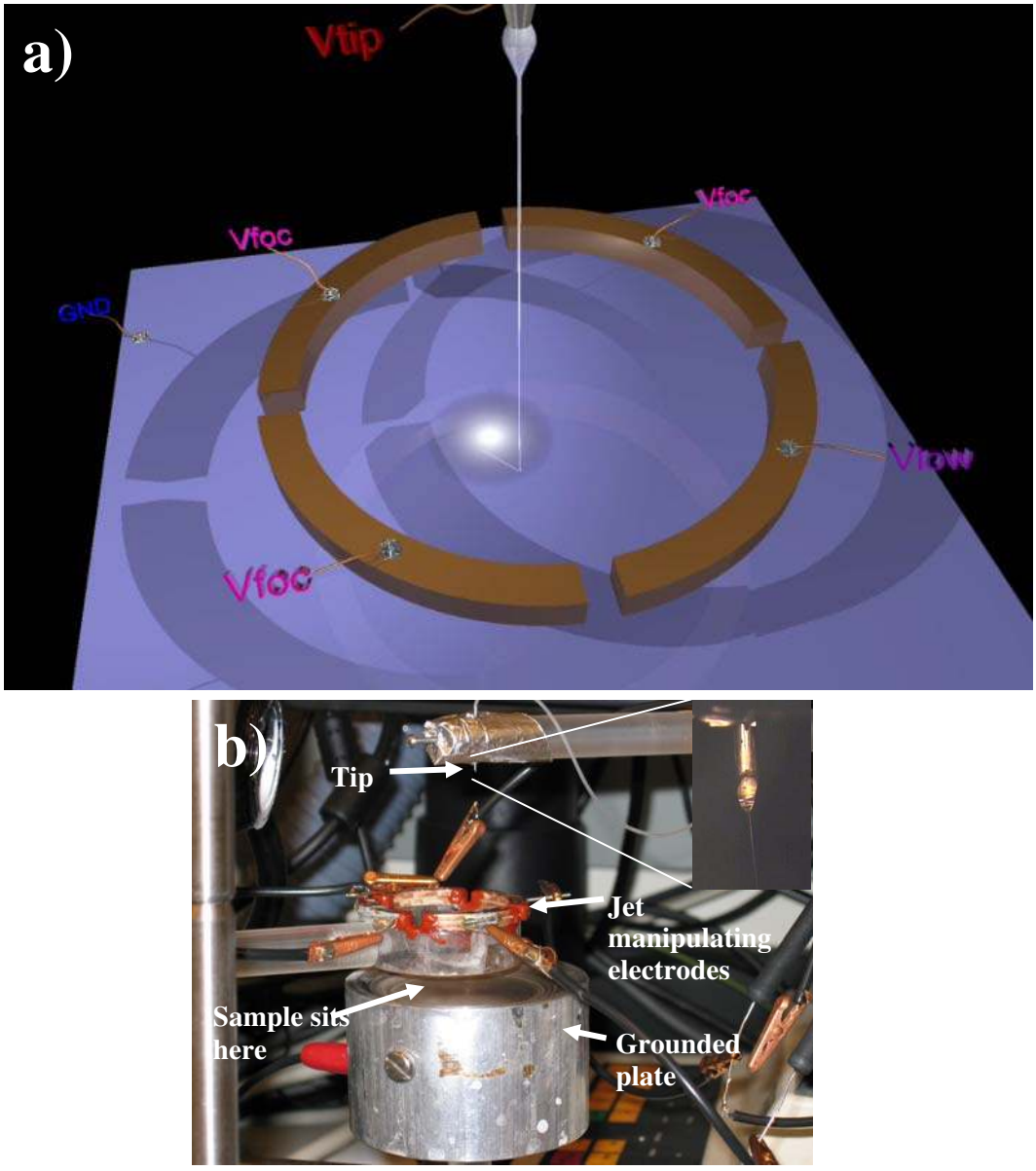

Figure 7.2- a) Schematic of controlled electrospinning system (not to scale) and b) picture of controlled electrospinning setup.

Results and Discussion

With the first controlled electrospinning setup we were able to deposit lines of nanofibers with linewidths of ~100 μm in a controlled fashion (Figure 7.3a). This system was unable to steer the jet quickly enough to deposit single straight fibers, but was still able to impart a pattern to the resulting deposition. Using the second system, we were able to draw single electrospun fibers in straight lines in a controlled fashion. The maximum deflected length of these single lines was ~1 cm. Some fibers were deposited over trenches etched in the Si substrate to demonstrate the speed of the transverse jet movement and that the fibers were in fact at least mostly dry when deposited. Figure 7.3b and 7.3c show optical microscope images of typical patterns produced by the system, and Figure 7.4 shows images from a scanning electron microscope (SEM) and atomic force microscope (AFM), which are useful for measuring the width and height of the fibers, respectively. The SEM images demonstrate that the deposition system was able to produce fibers that spanned trenches etched in the substrate. This indicates that the steering velocity is much larger than the jet velocity, as the fibers would otherwise sag to the bottom of the trench. Moreover, this also indicates that the fibers were fairly dry when deposited, since a wet fluid would not result in a suspended dry fiber. The first AFM image (Figure 7.4c) shows the height of two fibers, and this value roughly agrees with the width of similar fibers as measured with the SEM.

There are two mechanisms that cause the electrospinning jet to deposit fibers in a macroscopic "spot size." The first, and most often addressed, cause of the instability at the collector surface is the whipping mode of the jet caused by charge-charge repulsion on the surface of the jet. However, as one approaches the collecting surface, the effect of charge accumulation in previously-deposited fibers becomes more important and can contribute to the layout of the deposited fibers.[15, 16] The

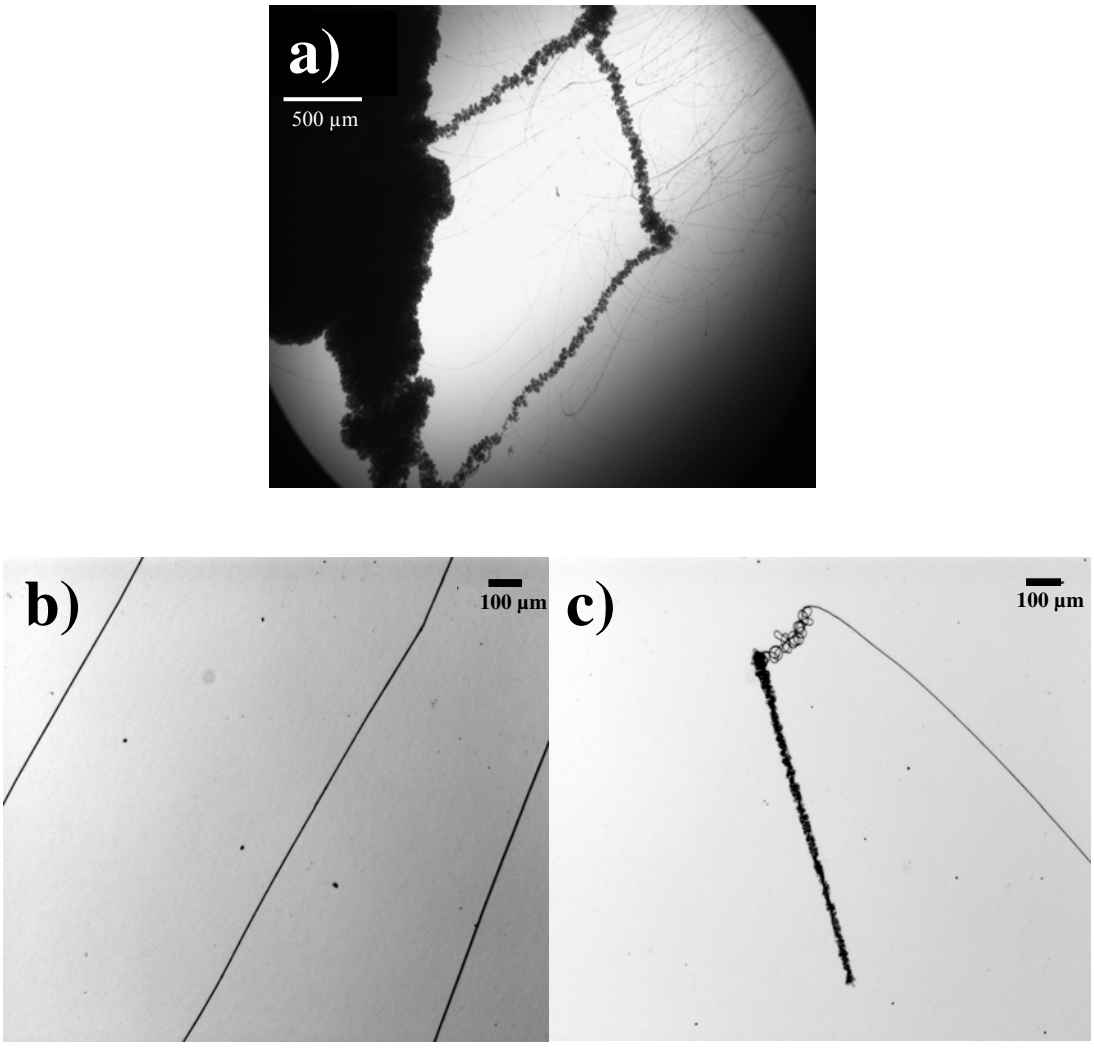

Figure 7.3- Optical microscope images of PEO fibers deposited by: a) first controlled electrospinning system using relays and b,c) second controlled electrospinning system using high voltage amplifier. In image a), the small chaotic fibers are due to initial setup of the jet, and the thick mat on the left of the image is the default position of the jet when it is not being steered. Image b) shows parallel lines produced by the second experimental setup, and image c) shows a terminated fiber produced by the second experimental setup.

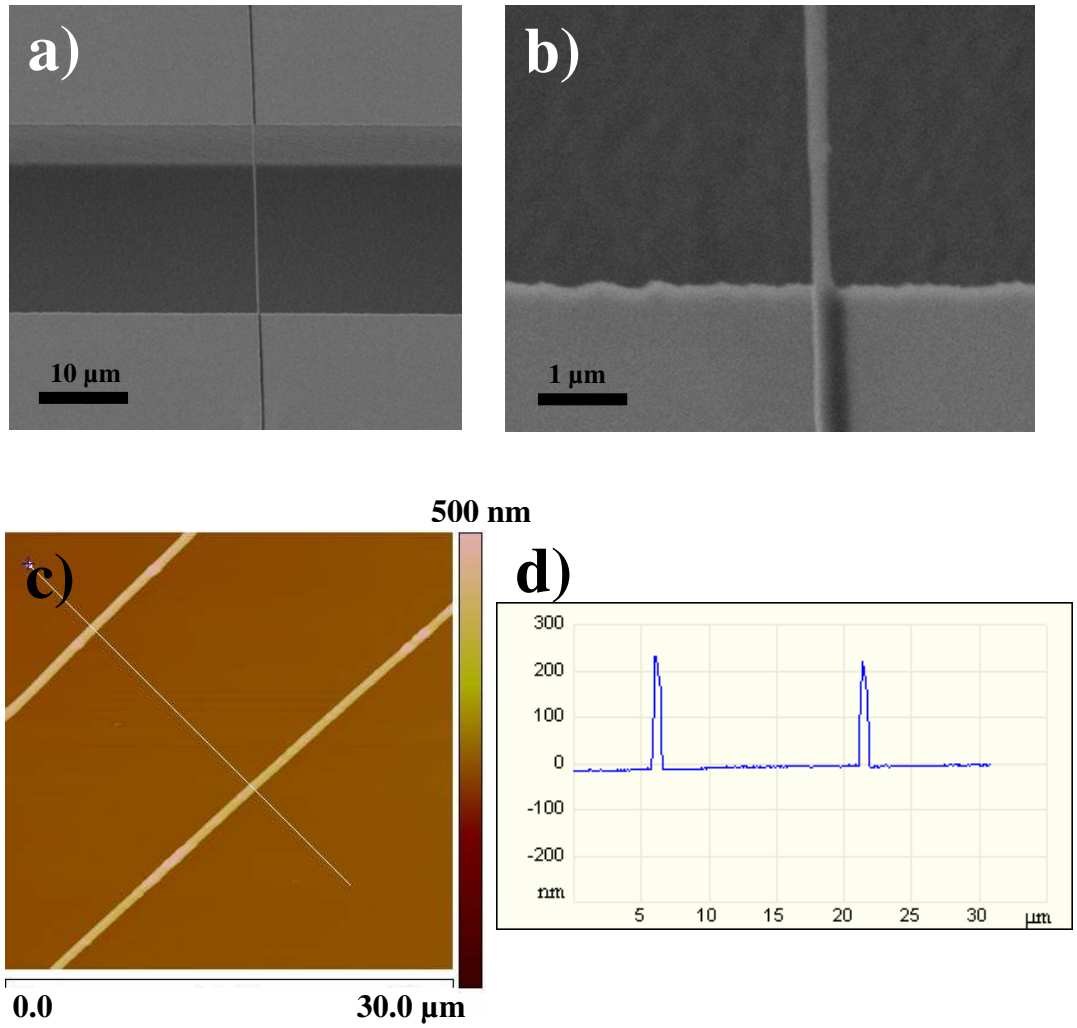

Figure 7.4- a,b) SEM images of suspended PEO nanofibers and c-d) AFM images and cross section of fibers on Si substrate.

system relaxation time constant for charge decaying out of the PEO into the grounded Si substrate is strongly dependant on the temperature and relative humidity of the system.[17] The system relaxation time is on the order of 0.01-1 seconds, much slower than the deposition rate.[18] Thus, if the jet is steered to a position on the substrate where polymer was recently deposited, it will be affected by the residual

charge and behave erratically.

Though these results are very encouraging, there are several limitations in the present setup that need to be addressed. First, the analog output electronics that drive the focusing/steering electrodes are not fast enough to produce small features. The DAQ card can produce square waveforms with frequencies up to ~1 kHz and the vacuum tube amplifiers have a time constant that is similarly limiting. A system consisting of fast arbitrary waveform generators coupled to high voltage amplifiers with a shorter time constant (implying a more powerful HV supply) should be able to manipulate the jet in a more controlled fashion and produce smaller features. A second important limitation of the system is the stability of the jet at the electrospinning tip. A stable Taylor cone at the tip is necessary for stable, consistent fiber deposition, as any instability at the tip will travel downstream and affect the fluid dynamic behavior of the jet. In our experimental setup, the tip was connected to a syringe on a syringe pump via thin silicone tubing. Because of the high viscosity and small tubing diameter, it took a long time for the system to settle to a steady solution feed rate. Moreover, the high voltage applied to the tip caused the solution and silicone tubing to become highly charged. We were able to hear corona around the tubing and near the syringe pump itself. If the tubing came too close to any metal (grounded) object, an arc formed between the two. Near where the arc formed, we observed bubbles form in the solution. This behavior was obvious when an arc formed, but is thought to occur to some extent near any corona as well. The bubbles traveled upstream in the solution until they reached the tip and caused instabilities in the Taylor cone. A more optimized system would have the syringe controlled by a pump and directly connected (without tubing) to the electrospinning tip. Microfabricated chip-based nozzles are another potential means to improve deposition uniformity; these are discussed in Chapter 8. High voltage insulation would also be

placed between the syringe and any nearby metal objects to prevent corona from forming.

When the jet is steered too far from its default position, it will jump from the substrate to the steering electrode with the lowest voltage, producing a terminated fiber on the substrate. An example of one of these terminated fibers is shown in Figure 7.3c. This behavior is essentially "blanking" the jet, similar to a beam blanker in electron and ion beam systems, although the jet blanker may only work near the deflection extremes. One might envision an electrode dedicated to this task. This electrode would essentially allow or prevent deposition of the fluid jet on the substrate. Presumably one would not want polymer to accumulate on the blanker electrode, and so the blanked position should cause the jet to deposit into a refreshed solvent bath.

Conclusion

We have shown that it is possible to focus and steer an electrospinning jet using static and time-varying electric fields. We have deposited PEO nanofibers in a pattern designated by a series of voltages applied to the steering electrodes. With our second experimental setup, we were able to steer the electrospinning jet quickly enough to produce single straight fibers. Finally, we have demonstrated that it is possible to controllably deposit terminated fibers using an electrospinning system with quickly varying steering electric fields. These results will allow for more complex geometries to be fabricated using electrospun nanofibers.

REFERENCES

1. Liu, H.; Edel, Joshua B.; Bellan, Leon M.; Craighead, H. G., Electrospun Polymer Nanofibers as Subwavelength Optical Waveguides Incorporating Quantum Dots. *Small* **2006,** 2, (4), 495-499.

2. Dror, Y.; Salalha, W.; Khalfin, R. L.; Cohen, Y.; Yarin, A. L.; Zussman, E., Carbon nanotubes embedded in oriented polymer nanofibers by electrospinning. *Langmuir* **2003,** 19, (17), 7012-7020.

3. Salalha, W.; Dror, Y.; Khalfin, R. L.; Cohen, Y.; Yarin, A. L.; Zussman, E., Single-walled carbon nanotubes embedded in oriented polymeric nanofibers by electrospinning. *Langmuir* **2004,** 20, (22), 9852-9855.

4. Patel, A. C.; Li, S.; Yuan, J. M.; Wei, Y., In Situ Encapsulation of Horseradish Peroxidase in Electrospun Porous Silica Fibers for Potential Biosensor Applications. *Nano Lett.* **2006,** 6, (5), 1042-1046.

5. Liu, H. Q.; Kameoka, J.; Czaplewski, D. A.; Craighead, H. G., Polymeric nanowire chemical sensor. *Nano Letters* **2004,** 4, (4), 671-675.

6. Kameoka, J.; Verbridge, S. S.; Liu, H. Q.; Czaplewski, D. A.; Craighead, H. G., Fabrication of suspended silica glass nanofibers from polymeric materials using a scanned electrospinning source. *Nano Letters* **2004,** 4, (11), 2105-2108.

7. Verbridge, S. S.; Edel, J. B.; Stavis, S. M.; Moran-Mirabal, J. M.; Allen, S. D.; Coates, G.; Craighead, H. G., Suspended glass nanochannels coupled with microstructures for single molecule detection. *Journal Of Applied Physics* **2005,** 97, (12), 124317.

8. Kameoka, J.; Craighead, H. G., Fabrication of oriented polymeric nanofibers on planar surfaces by electrospinning. *Applied Physics Letters* **2003,** 83, (2), 371-373.

9. Kameoka, J.; Orth, R.; Yang, Y. N.; Czaplewski, D.; Mathers, R.; Coates, G.

W.; Craighead, H. G., A scanning tip electrospinning source for deposition of oriented nanofibres. *Nanotechnology* **2003,** 14, (10), 1124-1129.

10. Jong-Sang Kim, D. H. R., Polybenzimidazole nanofiber produced by electrospinning. *Polymer Engineering & Science* **1999,** 39, (5), 849-854.

11. Li, D.; Wang, Y.; Xia, Y., Electrospinning of polymeric and ceramic nanofibers as uniaxially aligned arrays. *Nano Letters* **2003,** 3, (8), 1167-1171.

12. Li, D.; Wang, Y. L.; Xia, Y. N., Electrospinning nanofibers as uniaxially aligned arrays and layer-by-layer stacked films. *Advanced Materials* **2004,** 16, (4), 361-366.

13. Sun, D.; Chang, C.; Li, S.; Lin, L., Near-Field Electrospinning. *Nano Letters* **2006,** 6, (4), 839 -842.

14. Deitzel, J. M.; Kleinmeyer, J. D.; Hirvonen, J. K.; Beck Tan, N. C., Controlled deposition of electrospun poly(ethylene oxide) fibers. *Polymer* **2001,** 42, (19), 8163-8170.

15. Deitzel, J. M.; Kleinmeyer, J.; Harris, D.; Tan, N. C. B., The effect of processing variables on the morphology of electrospun nanofibers and textiles. *Polymer* **2001,** 42, (1), 261-272.

16. Theron, A.; Zussman, E.; Yarin, A. L., Electrostatic field-assisted alignment of electrospun nanofibres. *Nanotechnology* **2001,** 12, (3), 384-390.

17. Wagner, A.; Kliem, H., Dispersive ionic space charge relaxation in solid polymer electrolytes. I. Experimental system polyethylene oxide. *Journal of Applied Physics* **2002,** 91, (10), 6630-6637.

18. Kliem, H.; Wagner, A. In *High dielectric permittivity by ionic space charge polarization in polyethylene oxide*, Conference on Electrical Insulation and Dielectric Phenomena, Kitchener, Ont., Canada, 2001; IEEE: Kitchener, Ont., Canada, 2001; p 648.

CHAPTER 8

A CHIP-BASED MICROFABRICATED ELECTROSPINNING NOZZLE[9]

Introduction

As the field of electrospinning grows, there is increased interest in investigating the effects of nozzle geometry on both the behavior of the electrospinning jet and the properties of the resulting fibers. Because the electrospinning process uses an electrically forced jet to produce fibers from solution, both the nozzle material and geometry can play an important role in defining the fluidic cone and jet. Typical electrospinning systems utilize a standard syringe needle to provide a constant supply of solution to an electrically formed fluid cone at the sharp end of the needle. Other systems have used solid sharp tips to which a small droplet of solution is applied;[1] though a constant supply of solution is not practical with such designs, they are useful for quick deposition of a small number of fibers. Several multi-jet systems have been described that allow for increased mass throughput.[2-4] Multicomponent fibers have been produced using electrospinning systems with modified spinnerets that combine multiple solutions in either a coaxial[5] or side-by-side configuration.[6] However, there has been little investigation into the limits of a nozzle-based design.

In this chapter we describe the use of extremely small (5 μm) diameter nozzles as electrospinning sources and compare them to standard electrospinning sources such as needles and sharp tips. The microfabricated nozzle source produces a smaller, more uniform mat of fibers than the other sources, and can be produced in large arrays on a silicon chip. This layout is convenient for automated access by a robotic system, as well as integration with other chip-based components (such as charged jet optics) and

[9] Submitted to JVST B.

microfluidic devices. We demonstrate that these nozzles can deposit fibers of various shapes, including short sections of fiber deposited by a self-chopping jet.

Experimental Setup

As an electrospinning source we used the robotic NanoMate system (Advion Biosciences) (Figure 8.1a) typically used to introduce samples into mass spectrometers using electrospray ionization (ESI-MS). To define the nozzle geometry, we used a standard silicon ESI chip containing a large array of microfabricated 5 μm nozzle sources with a SiO_2 passivating layer (Figures 8.1b and 8.1c). To our knowledge, this is the smallest electrospinning source demonstrated that incorporates a nozzle, allowing a continuous feed of solution. Because the ESI chip is grounded in the NanoMate system, we used a floating high voltage supply (Emco High Voltage F121) to apply a voltage of 5-7kV between the electrospinning solution behind the nozzle and a collecting surface placed ~1-3 cm from the front of the ESI chip.

Results

For our initial attempts to electrospin with the modified NanoMate system, we used solutions of 5%-7% polyethylene oxide (Arcos Organics, 100,000 Mw) in 50/50 v/v water/ethanol, typically used in electrospinning experiments. We were unable to force this fluid through the nozzles, and SEM imaging (not shown) indicated that the nozzles were clogging. By adding formic acid to the PEO solution, we were able to form a jet, but it produced droplets as opposed to fibers. The PEO solution had previously been used with standard electrospinning system configurations and, at higher polymer concentrations, produced fibers. However, using a solution of 240 mg PMMA (996,000 Mw) dissolved in a mixture of 4.5mL acetonitrile and 1mL ethanol we were able to produce a fiber-forming electrospinning jet from a single 5 μm

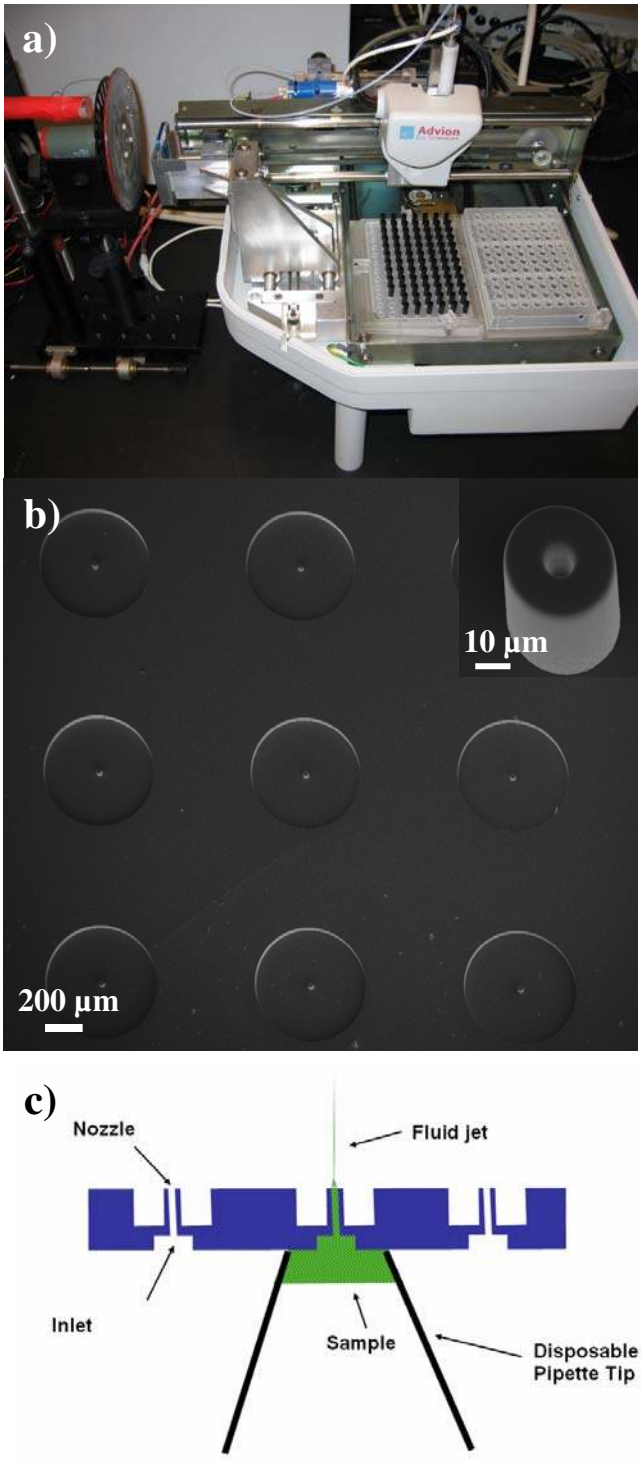

Figure 8.1- a) NanoMate automated ESI-MS system, b) SEM images of ESIChip nozzles, and c) schematic showing nozzle cross-section.

nozzle. A solution with only 20mg of PMMA in 2mL acetonitrile and 0.5 mL ethanol formed a jet but deposited droplets, and another solution containing 110 mg of PMMA in 2mL acetonitrile and 0.5 mL ethanol formed thick fibers. Using a solution of 67 mg PMMA in 2mL anisole, we were able to produce fibers with the "beads-on-a-string" geometry, though the solution at times produced only droplets. SEM images of these samples are shown in Figure 8.2. Fibers were collected both on a stationary substrate and on a substrate that was rotated through the jet to help isolate the fibers. In several situations, while examining the resulting fibers, we observed short isolated lengths of fiber as well as the typical single non-woven strand (Figure 8.2). When the substrate was stationary, instead of observing the typical circular mat produced by standard electrospinning systems, we often observed a starburst pattern due to short isolated sections of fiber being deposited radially at the perimeter of the mat (Figure 8.2d). We believe this is due to the accumulated charge in the deposited mat radially deflecting the path of a broken section of the jet in flight.[7] In order to confirm that the jet was breaking in flight, we imaged the electrospinning source using a high speed camera (Vision Research Phantom v7, ~30,000 fps, 10μs exposure). Several frames from the resulting video are shown in Figure 8.3, indicating that the jet was indeed breaking close to the nozzle.

Though there are several theoretical treatments of electrospinning jets,[8-16] there have been relatively few experimental investigations into how the fibers resulting from an electrospinning jet depend on the radius of the nozzle forming the jet. While some work has shown fiber diameter dependence on nozzle diameter (using diameters ranging from 580 μm to 1190 μm),[17] other work (using diameters ranging from 100 μm to 830 μm) has shown no dependence.[18] A recent numerical treatment investigating the effects of various parameters on electrospinning jets showed that the resulting fiber diameters depending strongly on the initial jet radius, which may

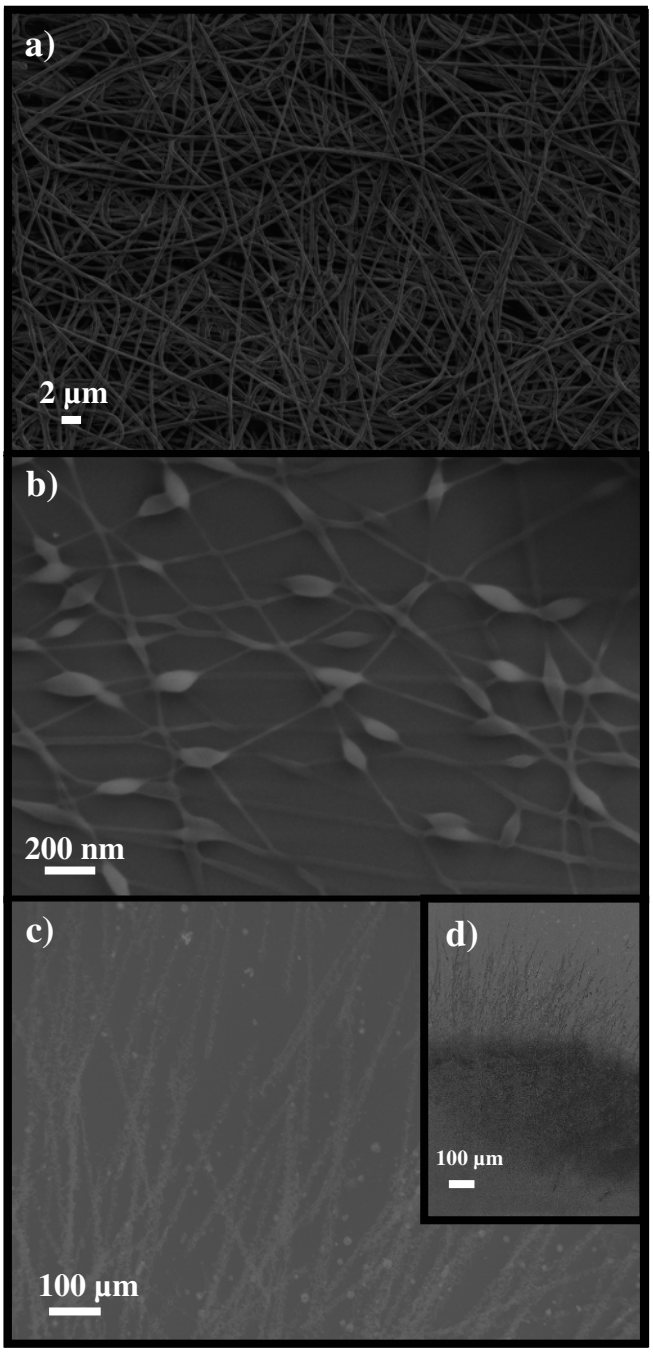

Figure 8.2- SEM images of a) PMMA fibers from acetonitrile/ethanol , b) PMMA fibers from anisole, showing beads-on-a-string geometry, c) PMMA fibers from acetonitrile/ethanol, showing broken fiber deposition near edge of mat and d) a different place on the same sample as shown in c), showing the edge of the mat with radial broken fiber deposition (pointing upwards in this image).

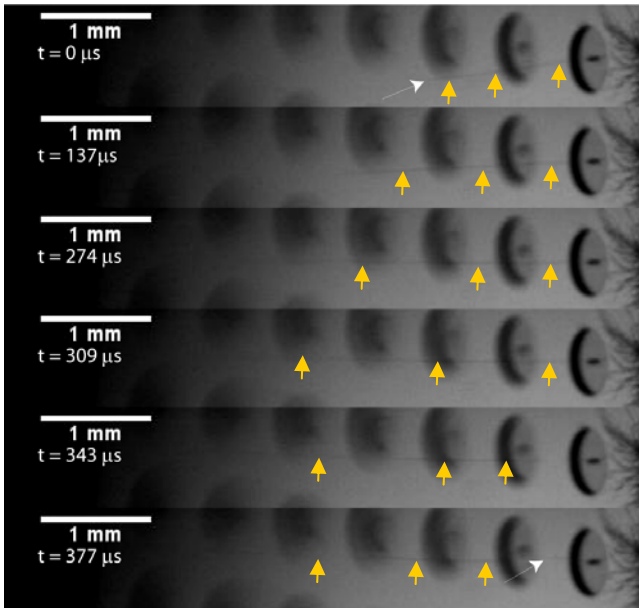

Figure 8.3- Frames from high speed video indicating breaking of the jet in flight. Yellow arrows indicate the fluid jet, and white arrows indicate where the jet broke.

depend on the nozzle diameter as well as other parameters.[19] Recent work by Helgeson et al. has produced an empirical relationship to predict fiber diameter from solution properties and electrospinning parameters.[20] Future work with a chip-based electrospinning system would allow for a systematic study of the dependence of fiber properties on nozzle diameter.

To compare the behavior of the microfabricated nozzles to other electrospinning sources, we electrospun a solution of 50 mg PMMA (996,000 Mw) in 2ml acetonitrile and .5mL ethanol, using the NanoMate system, a microfabricated silicon tip[1] coated with gold, and a 22 gauge syringe needle. For each system, we applied an accelerating voltage of 7.3 kV over a source-sample separation distance of 2.5 cm. The resulting fiber mats are shown in Figure 8.4. Each of the white spots is a mat of fibers (as verified using optical microscopy). While the silicon tip and needle sources produced relatively large, uneven mats, the NanoMate source produced a

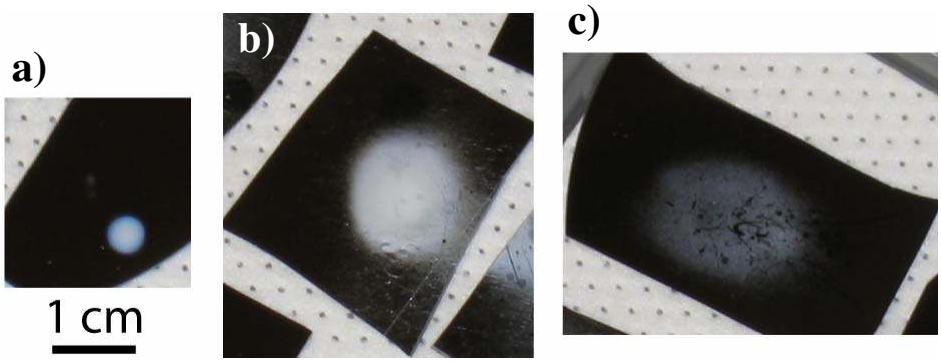

Figure 8.4- Images of fiber mats produced by a) microfabricated chip-based nozzle, b) microfabricated silicon tip, and c) hypodermic needle source. All images are shown at the same magnification.

smaller, more uniform spot.

Conclusion

Though we have only used one nozzle at a time in this study, it is likely that multiple nozzles could easily be operated simultaneously by simply feeding them solution, allowing a high throughput. To operate the system for longer periods of time, a syringe pump could be used to feed solution to the backside of the ESI Chip instead of the robotic pipettor on the NanoMate. One could also integrate the ESI Chip with microfluidic devices placed behind the nozzles to develop an automated sample preparation system for single biomolecule analysis.[21] Microfabricated electrospinning nozzles also offer much promise for integration with systems using electric fields to steer the charged jet.[22] Technology and electrode geometries similar to those developed for electron beam microcolumn systems could be applied.[23, 24] Chip-based microfabricated electrospinning nozzles offer a new approach to potentially improve deposition uniformity, reduce spot size, increase the throughput of electrospinning systems and decrease the resulting fiber diameter.

REFERENCES

1. Kameoka, J.; Orth, R.; Yang, Y. N.; Czaplewski, D.; Mathers, R.; Coates, G. W.; Craighead, H. G., A scanning tip electrospinning source for deposition of oriented nanofibres. *Nanotechnology* **2003,** 14, (10), 1124-1129.

2. Theron, S. A.; Yarin, A. L.; Zussman, E.; Kroll, E., Multiple jets in electrospinning: experiment and modeling. *Polymer* **2005,** 46, (9), 2889-2899.

3. Yarin, A. L.; Zussman, E., Upward needleless electrospinning of multiple nanofibers. *Polymer* **2004,** 45, (9), 2977-2980.

4. Jirsak, O.; Sanetrnik, F.; Lukas, D.; Kotek, V.; Martinova, L.; Chaloupek, J. A Method of Nanofibres Production from a Polymer Solution Using Electrostatic Spinning and a Device for Carrying out the Method. WO 2005/024101 A1, 17 March, 2005.

5. Li, D.; Xia, Y., Direct fabrication of composite and ceramic hollow nanofibers by electrospinning. *Nano Letters* **2004,** 4, (5), 933-938.

6. Liu, Z.; Sun, D. D.; Guo, P.; Leckie, J. O., An Efficient Bicomponent TiO_2/SnO_2 Nanofiber Photocatalyst Fabricated by Electrospinning with a Side-by-Side Dual Spinneret Method. *Nano Lett.* **2006**.

7. Zussman, E.; Theron, A.; Yarin, A. L., Formation of nanofiber crossbars in electrospinning. *Applied Physics Letters* **2003,** 82, (6), 973-975.

8. Reneker, D. H.; Yarin, A. L.; Hao, F.; Koombhongse, S., Bending instability of electrically charged liquid jets of polymer solutions in electrospinning. *Journal of Applied Physics* **2000,** 87, (9, pt.1-3), 4531-4547.

9. Yarin, A. L.; Koombhongse, S.; Reneker, D. H., Taylor cone and jetting from liquid droplets in electrospinning of nanofibers. *Journal of Applied Physics* **2001,** 90, (9), 4836-4846.

10. Yarin, A. L.; Koombhongse, S.; Reneker, D. H., Bending instability in electrospinning of nanofibers. *Journal of Applied Physics* **2001,** 89, (5), 3018-3026.

11. Hohman, M. M.; Shin, M.; Rutledge, G.; Brenner, M. P., Electrospinning and electrically forced jets. II. Applications. *Physics of Fluids* **2001,** 13, (8), 2221-2236.

12. Hohman, M. M.; Shin, M.; Rutledge, G.; Brenner, M. P., Electrospinning and electrically forced jets. I. Stability theory. *Physics of Fluids* **2001,** 13, (8), 2201-2220.

13. Shin, Y. M.; Hohman, M. M.; Brenner, M. P.; Rutledge, G. C., Electrospinning: A whipping fluid jet generates submicron polymer fibers. *Applied Physics Letters* **2001,** 78, (8), 1149-1151.

14. Shin, Y. M.; Hohman, M. M.; Brenner, M. P.; Rutledge, G. C., Experimental characterization of electrospinning: the electrically forced jet and instabilities. *Polymer* **2001,** 42, (25), 9955.

15. Feng, J. J., The stretching of an electrified non-Newtonian jet: A model for electrospinning. *Physics of Fluids* **2002,** 14, (11), 3912-3926.

16. Carroll, C. P.; Joo, Y. L., Electrospinning of viscoelastic Boger fluids: Modeling and experiments. *Physics of Fluids* **2006,** 18, (5), 053102-14.

17. Katti, D. S.; Robinson, K. W.; Ko, F. K.; Laurencin, C. T., Bioresorbable nanofiber-based systems for wound healing and drug delivery: Optimization of fabrication parameters. *Journal of Biomedical Materials Research Part B: Applied Biomaterials* **2004,** 70B, (2), 286-296.

18. Macossay, J.; Marruffo, A.; Rincon, R.; Eubanks, T.; Kuang, A., Effect of needle diameter on nanofiber diameter and thermal properties of electrospun poly(methyl methacrylate). *Polymers for Advanced Technologies* **2007,** 18, (3), 180-183.

19. Thompson, C. J.; Chase, G. G.; Yarin, A. L.; Reneker, D. H., Effects of parameters on nanofiber diameter determined from electrospinning model. *Polymer*

2007, 48, (23), 6913-6922.

20. Helgeson, M. E.; Grammatikos, K. N.; Deitzel, J. M.; Wagner, N. J., Theory and kinematic measurements of the mechanics of stable electrospun polymer jets. *Polymer* **2008,** 49, (12), 2924-2936.

21. Bellan, L. M.; Cross, J. D.; Strychalski, E. A.; Moran-Mirabal, J.; Craighead, H. G., Individually Resolved DNA Molecules Stretched and Embedded in Electrospun Polymer Nanofibers. *Nano Letters* **2006,** 6, (11), 2526-2530.

22. Bellan, L. M.; Craighead, H. G., Control of an electrospinning jet using electric focusing and jet-steering fields. *Journal of Vacuum Science & Technology B* **2006,** 24, (6), 3179-3183.

23. Chang, T. H. P.; Thomson, M. G. R.; Kratschmer, E.; Kim, H. S.; Yu, M. L.; Lee, K. Y.; Rishton, S. A.; Hussey, B. W.; Zolgharnain, S., Electron-beam microcolumns for lithography and related applications. *Journal Of Vacuum Science & Technology B* **1996,** 14, 3774-3781.

24. Muray, L. P.; Spallas, J. P.; Stebler, C.; Lee, K.; Mankos, M.; Hsu, Y.; Gmur, M.; Chang, T. H. P., Advances in arrayed microcolumn lithography. *Journal Of Vacuum Science & Technology B* **2000,** 18, 3099-3104.

CHAPTER 9

SUMMARY

This thesis work has focused on both the application of novel measurement techniques to electrospinning jets and the resulting fibers, and the development of modifications to electrospinning to increase the range of applications. To characterize the electrospinning jet itself, particle image velocimetry was used to measure the fluid velocity in the jet directly. This experiment also indicated transverse fluid oscillations near the beginning of the jet; these oscillations could be related to the macroscopic whipping instability further down the jet. Future work may attempt to follow the paths of the tracer particles further down the jet into higher velocity straight jet regimes, or even into the whipping regime. Such measurements may yield information about the fluidic and material behavior of the jet that is difficult or impossible to extract from simply observing the jet shape and movement.

A significant amount of discussion has been dedicated to the elongational properties of electrospinning jets. In this work, polarized Raman spectroscopy and atomic force microscopy were used to characterize the molecular orientation and resulting mechanical properties of electrospun nanofibers, respectively. The elongational flow was also used as a tool to stretch DNA molecules in the electrospinning solution. The molecules remained stretched and embedded in the resulting nanofibers. This rapid, inexpensive technique could be used as a high-throughput sample preparation process for genomic analysis. Future work with this technique may demonstrate the resolution of sequence-specific labeling on individual DNA molecules stretched by electrospinning. Other encapsulating materials besides PEO could also be investigated and may offer improved results.

As an addition to the significant literature already demonstrating lithographic

processes utilizing electrospun fibers, a new fabrication process using sacrificial electrospun nanofibers to form nanochannels was developed. One of the major advantages of this technique is that it can be applied to a wide range of polymeric material. The two materials chosen to demonstrate this use of sacrificial nanofibers were PEO (for forming the nanofibers) and PDMS (for forming the encapsulating medium). As PEO is the most popular material to electrospin, and PDMS is one of the most popular materials used to form micro- and nanofluidic structures, a process that combines these two materials to form fluidic channels is highly advantageous. The ability to easily integrate nanofluidic and microfluidic structures is another benefit of this process. The channels produced by random mats of electrospun fibers may have applications as artificial vascular systems, fluidic mixers, filters, or high surface-area sensors. Channels produced by aligned fibers could be used for single-molecule sensing and biomolecule separations.

Two new modifications to electrospinning apparatus have been discussed. In the interest of developing a method to deposit electrospun fibers with controlled position and orientation (i.e. "draw" arbitrary single-fiber patterns), a system employing time-varying electric fields transverse to the jet was developed. While the results from this system are promising, there is much room for improvement. The electrode design is simplistic and may benefit from engineering efforts from those with experience in charged particle optics. The electronics driving the electrodes must be able to operate in a faster, more linear fashion in order to produce smaller features. The system may benefit from steering fields designed to operate in a push-pull configuration. Novel methods for confining the whipping instability are necessary to be able to deposit fibers in a given position reproducibly. Finally, a stable source must be developed that can continuously deliver a stable fluid jet for an extended period of time. With the improvements described above, a fully optimized controlled

electrospinning system may replace focused ion beams or electron beam lithography systems for some applications (specifically, for fabrication of thin lines of polymeric material). In order to address the need for new electrospinning sources, a microfabricated nozzle-based electrospray system was modified to electrospin material from 5 μm nozzles (the smallest electrospinning nozzle source to date, to my knowledge). These sources offer more uniform deposition, smaller spot sizes, and greater potential for integration with microfluidic systems and chip-based charged particle optics. Moreover, in a system with a large array of available sources, a new source is easily installed into the system when an older source becomes nonfunctional. There is also the possibility of investigating the dependence on nozzle diameter of the fiber diameter using nozzles of a range of diameters fabricated on the same chip.

Though electrospinning has been a practiced technique for several decades, it is only recently gaining the attention required to fully develop. Until quite recently, and perhaps still, the majority of electrospinning literature focuses on expanding the range of materials to which the technique can be applied, as opposed to developing new applications or modifications of the process itself. The majority of the significant theoretical work treating electrospinning has been published in the last decade. Moreover, there are few, if any, current commercially available products or services using the electrospinning process. I would argue that these facts signify that the technique is still in its infancy.